January 2016

INFLUENCES OF INTERFACES AND PROMOTERS ON THE WATER-GAS SHIFT REACTION OVER SUPPORTED NOBLE METAL CATALYSTS

Yanran Cui
Purdue University

PURDUE UNIVERSITY
GRADUATE SCHOOL
Thesis/Dissertation Acceptance

This is to certify that the thesis/dissertation prepared

By Yanran Cui

Entitled
INFLUENCES OF INTERFACES AND PROMOTERS ON THE WATER-GAS SHIFT REACTION OVER SUPPORTED NOBLE METAL CATALYSTS

For the degree of Doctor of Philosophy

Is approved by the final examining committee:

Fabio H. Ribeiro
Chair

W. Nicholas Delgass
Co-chair

Christopher Uyeda

Jeffrey P. Greeley

To the best of my knowledge and as understood by the student in the Thesis/Dissertation Agreement, Publication Delay, and Certification Disclaimer (Graduate School Form 32), this thesis/dissertation adheres to the provisions of Purdue University's "Policy of Integrity in Research" and the use of copyright material.

Approved by Major Professor(s): Fabio H. Ribeiro, W. Nicholas Delgass

Approved by: Sangtae Kim 12/7/2016

Head of the Departmental Graduate Program Date

INFLUENCES OF INTERFACES AND PROMOTERS ON THE WATER-GAS SHIFT REACTION OVER SUPPORTED NOBLE METAL CATALYSTS

A Dissertation

Submitted to the Faculty

of

Purdue University

by

Yanran Cui

In Partial Fulfillment of the

Requirements for the Degree

of

Doctor of Philosophy

December 2016

Purdue University

West Lafayette, Indiana

ACKNOWLEDGEMENTS

My graduate research for the past five years has been very rewarding and fulfilling. I have learned a lot about the catalysis science and various techniques to study a catalyst system. It also enables me to think from the fundamental and molecular level. What's more, research here has taught me how to critically and systematically think and solve problems, which will be very important in my future life. I'm really grateful for a lot of people who have generously given me great support and help during this journey.

First, I would like to thank my parents for their love and support for me. They supported my every decision and always stand by my side to give me hand. It is their love that makes me brave enough to pursue my dream here.

I'm highly grateful to my advisors, Prof. Fabio H. Ribeiro and Prof. W. Nicholas Delgass. Prof. Fabio H. Ribeiro always ensured the availability of resources and means to achieve the best possible results. His great expertise and abundant knowledge have given me a lot suggestions and make my projects progress in a good direction. The most important thing I learned from him is that a real scientist has to be meticulous and rigorous while performing experiments, which is the only way to ensure the quality of experiments and contribute useful information to the whole area. Prof. Ribeiro also funds me to present at many prestigious conferences and I have met a lot great people in our area. He also gives me great recommendations and help during my search for jobs. Prof. Delgass has taught

me to think outside the box and critically analyze the data in hand. He always gives me great suggestions and inspires me to think from a different aspect. He taught me how to properly design experiments and obtain the key information missing. His great passion towards science really inspires me and gives me a lot courage. Every discussion with him has always been a great pleasure for me. He is not only an advisor on academics, but also a great mentor on my life. I'm very fortunate to have such great advisors guiding me and showing me the beauty of catalysis. It feels proud to be the part of the 'Michel Boudart Academic Tree'.

I would also like to thank Prof. Jeffrey Greeley and Prof. Christopher Uyeda for being a part of my thesis committee. Prof. Greeley has provided great suggestions on my qualifying exam and preliminary exam. Also during the daily collaboration, Prof. Greeley has great theoretical knowledge and gives me a lot valuable advice from the fundamental aspect. Prof. Christopher Uyeda is a great expert on organic chemistry and his suggestions will give me a new understanding of my research. I would also like to thank Prof. Jeff Miller. He has spent a lot time teaching me the XAS techniques and helps us a lot on designing XAS experiments and analyzing the XAS data. I also want to thank Prof. Volkan Ortalan who has helped me a lot on the microscopy characterizations.

I would also like to extend my gratitude towards previous and current water-gas shift group members. I'm grateful to Dr. Mayank Shekhar and Dr. Damion Williams who have given me the initial training on the WGS project and opened the door to research for me. Special thanks would go to my great colleague and friend Dr. Kaiwalya Sabnis. We worked together for more than 3 years and he has given me a lot help on my research. He encourages me when I have failure and gives me valuable suggestions to solve the

problems. His knowledge, diligence and nice personality all make me feel proud to be his friend. Dr. Zhenglong Li and I have a very good collaboration on the Au/MgO project and I really learned a lot from him. Dr. Viktor Cybulskis helped me a lot on the IR experiments. Jamie Harris and Dr. Atish Parekh has helped me a lot on the Transmission IR and DRIFTS experiments. Dr. Cem Akatay and Dr. Chang Wan Han have given me a lot help on microscopy characterizations and the beautiful images they got are very important to get a deeper understanding of the catalysts. I would like to thank Dr. Wen-Sheng Lee for teaching me the catalyst synthesis methods used throughout my research. Dr. Fred Sollberger for collaboration on the PtCo bimetallic catalysts we have tested. Dr. Dhairya Mehta for helping me on the BET and Chemisorption experiments. I would like to thank Tej Choksi and Paulami Majumdar for their great work on the DFT calculations which elucidates the experimental observation results. Thanks to Shankali Pradhan for the valuable discussion and the help on the WGS unit. Also I thank Cory Milligan for his help on running the WGS kinetics and his discussion on XPS experiments. I also want to specially thank Dr. David Taylor and Dr. Yury Zvinevich for their help with troubleshooting in various experimental units. It would be impossible for me to progress without their help. I thank the rest of the Ribeiro group members for their help and support when needed.

There have been times when research has failure. I would like to thank my friends here for their support for me. Xiaohui Liu, Yung-Jih Yang, Lei Ling, Haoran Yang, Haiyu Fang, Yang Xiao, Silei Xiong, Danni Gao, Jianfeng Liu, Hanting Zeng, Zhe Li, Zheyu Jiang, Zhenwei Wu, Yelin Ni, etc.

Thank you very much to everyone!

TABLE OF CONTENTS

APPENDICES

LIST OF TABLES

Appendix Table

LIST OF FIGURES

ABSTRACT

Cui, Yanran. Ph.D., Purdue University, December 2016. Influences of Interfaces and Promoters on the Water-Gas Shift Reaction Over Supported Noble Metal Catalysts.
Major Professor: Fabio H. Ribeiro and W. Nicholas Delgass

The water-gas shift reaction (WGS) is an important reaction to produce high purity hydrogen for various industrial processes such as ammonia synthesis and hydrotreating of petrochemicals. Finding a catalyst with higher activity is desired to speed up the reaction at lower temperatures where the equilibrium conversion is higher. Supported noble metal catalysts have been identified as a class of active catalysts for this reaction. The interface sites between the metal and support play an important role in determining the overall activity and can be modified by properly tuning the metal-support interactions. On the other hand, WGS reaction can be used as a probe reaction to study the fundamental catalytic processes over various heterogeneous catalysts. The overall goal of this work is to develop a model based approach to catalyst design that we call *Discovery Informatics*, which involves building a database with sufficient chemical and information diversity to allow identification of active sites, modelling the kinetics and discovering descriptors of the kinetic parameters.

The first part of this work focuses on Fe promotion effects on a rutile supported Au catalyst. By properly adding Fe to the Au/rutile catalysts, WGS rate per mole of Au at 120 °C could be promoted to a maximum of about 4 times. As Fe loading increased, significant changes

in the WGS kinetics were observed, that is, a decrease in apparent reaction order with respect to CO (0.7 to -0.3) and an increase in apparent activation energy (53 kJ/mol to 98 kJ/mol). The changes in the WGS kinetics imply stronger binding of CO on the active sites. *Operando* FTIR experiments identified an increase in CO adsorbed on strongly backdonating Au sites as the Fe loading was increased. The results showed that Fe-doping can modify the CO adsorption properties of interface Au sites, which changes the WGS rates and the nature of the active sites.

Besides CO adsorption, H_2O dissociation is another important factor that influences the activity of WGS catalysts. The second part of this work focuses on studying the H_2O dissociation by using an Au/MgO catalyst as a model system. In this work, MgO and $Mg(OH)_2$ were adopted as supports and loaded with 2.5 wt% Au. WGS rates and kinetics were measured on these catalysts. Au/MgO showed higher WGS rates than Au/$Mg(OH)_2$ but a lower apparent order with respect to H_2O. This implies a higher H_2O/OH coverage over the Au/MgO compared with Au/$Mg(OH)_2$, which corresponds to a higher binding affinity for H_2O/OH on Au/MgO. A kinetic isotope effect (KIE), which is the ratio between the WGS rate with H_2/H_2O and WGS rate with D_2/D_2O, was measured for both catalysts and both showed the same KIE ratio of about 2.0±0.3. This similar KIE implies a similar reaction mechanism on both catalysts and that breaking of a hydrogen bond is involved in the rate-determining step. Density Functional Theory (DFT) calculations also revealed a decrease of about 0.7 eV in the energy barrier for H_2O dissociation at the Au/MgO interface compared with pure MgO and pure Au. Further experimental studies on other supports such as TiO_2, ZrO_2, Al_2O_3 etc. also shows that a lower apparent order with respect to H_2O

(about -0.3) results in a higher WGS rate. Thus the hydroxyl group participates in the rate-determining step and H_2O order can be used as a potential descriptor for the activity.

The last two studies focus on the active sites for WGS over supported Pt catalysts and the Na promotion effects on those catalysts. Multiple types of sites exist on supported Pt catalysts (single Pt atoms, Pt clusters and Pt nanoparticles) but it is still debated in the literature which kind of sites are more important for the WGS reaction. A Pt/TiO_2 catalyst with only Pt nanoparticles on the support was prepared by organic solvothermal method. It showed similar activity and WGS kinetics to the normal Pt/TiO_2 catalyst, which implies that single Pt atoms or small clusters of Pt atoms are not the dominant active sites. Variations of the rate with support imply the importance of the Pt-support interface in controlling activity. Na has been reported to promote supported Pt catalysts. In order to study the reason for promotion, a series of Pt-Na catalysts supported on multi-walled carbon nanotubes (MWCNT) was prepared with different Pt:Na ratio. Na was observed to promote the TOR of Pt/MWCNT catalysts by a factor of more than 20. The addition of Na changed the kinetic parameters of Pt/MWCNT (increase in apparent activation energy, decrease in CO and CO_2 orders) similarly to the modifications previously reported for Na-promoted Pt/Al_2O_3, Pt/TiO_2 and Pt/ZrO_2 catalysts. The independence of response of the apparent kinetic parameters to Na on the underlying parent support for Pt suggests that Na leads to a support-type effect of its own. As confirmed by *in situ* ΔXANES experiments, Na enhanced the binding of CO with Pt. XAS data showed that Pt remained in reduced or metallic state under the WGS conditions. It is suggested that Na forms islands over the Pt particles and forms a new type of Pt-NaOx interface as the active site. A washing procedure could remove the Na from the MWCNT and re-distribute it over the surface of Pt. The

washed catalysts showed much lower Na loadings but similar WGS TOR at 250°C compared to their as-prepared counterparts, which further supports the conclusion that the Pt-NaOx interfaces are the active sites.

CHAPTER 1. INTRODUCTION

'Water gas' is a mixture of hydrogen and carbon monoxide. It is used extensively in the industry for the manufacture of ammonia, methanol, hydrogen (for hydro-treating, hydrocracking of petroleum fractions and other hydrogenations in the petroleum refining and petrochemical industry), hydrocarbons (by the Fischer-Tropsch process) and metals (by the reduction of the oxide ore) [1, 2]. It is manufactured by the reaction of a carbonaceous material (coal, coke, natural gas, naphtha, etc.) with steam, oxygen or carbon dioxide.

The WGS reaction (Eq. 1) was first reported in 1888, but it came into popular usage later, as a source of hydrogen for the Haber process for the manufacture of ammonia. It is accompanied by methanation reaction (Eq. 2) as a side reaction.

$$CO(g) + H_2O(g) \leftrightarrow CO_2(g) + H_2(g)(\Delta H = -41.1 kJ/mol) \quad \text{Eq. 1}$$

$$CO(g) + 3H_2(g) \leftrightarrow CH_4(g) + H_2O(g) \quad \text{Eq. 2}$$

The WGS reaction is slightly exothermic and equilibrium controlled. Thus the lower temperature favors higher conversions for WGS reaction. The equilibrium constant is related with temperature according to Eq. 3.

$$K_p = \exp[(4577/T) - 4.33] \quad \text{Eq. 3}$$

The WGS reaction is not significantly affected by the pressure. The products, CO_2 and H_2, have strong inhibitive effects on the forward WGS reaction. In keeping with equ 3, as temperature increases, it will favor more on the reverse WGS reaction, while the reaction will have higher conversions at lower temperature. But at lower temperature, the reaction rates will be lowered and thus it will require large reactor volume to obtain the desired equilibrium conversion. Nowadays the industrial WGS process takes place in a series of adiabatic converters where the effluent from the reformer system is converted in two WGS reactors (High Temperature Shift and Low Temperature Shift converters, respectively), with the second WGS reactor at a significantly lower temperature in order to shift the equilibrium towards the favored hydrogen product.

There are four general types of WGS catalysts [1]. One of them is the promoted iron oxide catalyst. Catalysts of this type promote the shift reaction at moderately high temperatures (350–450^{o}C) and are therefore called high temperature shift (HTS) catalysts. The second type is copper-zinc oxide catalyst and is called the low temperature shift (LTS) catalyst because it is used at relatively low temperatures (190–250^{o}C). The third type employs cobalt and molybdenum sulfides as the active ingredients. Catalysts of this type are sulfur-tolerant and can be used in sulfur-containing 'sour gas' streams and are therefore called sour gas shift catalysts. There was interest in a fourth type of catalyst, medium temperature shift or MTS catalyst that operates at temperatures between the HTS and LTS catalysts. In addition to the above four, precious metal- based catalysts (mainly platinum and gold) have been under intensive investigation during the last decade for use in fuel cell applications. This is because the requirements of WGS catalysts for fuel cell applications are quite different from those of the traditional Fe_2O_3-Cr_2O_3 or Cu-ZnO based catalysts [1].

Although the Cu-ZnO-Al_2O_3 is very active LTS catalyst but they have the following disadvantages

1. They are sensitive to air (pyrophoric).
2. They require lengthy in situ pre-reduction.
3. They are sensitive to moisture and sulfur poison.

They can only be used in a narrow temperature range. It is still the main focus of the WGS research to find an active and stable catalyst at low temperatures. Among them, supported noble metal catalysts showed great advantages in solving the above problems of traditional LTS catalysts [3]. Thus they have gotten a lot of attention during the last decade and showed great potential in wide application for fuel cells and related clean energy issue. Among all the noble metal catalysts, supported Au and Pt catalysts are especially attractive due to their high activity at very low temperatures. The activity of the supported noble catalysts is strongly dependent on the support type [4, 5]. Usually the support will modify the active sites at the metal-support interfaces and it significantly influences the WGS activity. Thus understanding the influences of interfaces is very important for developing more active catalysts. However, the relationship between the metal-support interaction and the WGS activity is still not fully understood.

Furthermore, the WGS reaction can be used as a powerful probe reaction to study the fundamental processes on different model catalyst systems. It involves multiple reaction pathways and can be used to understand the structure activity relationship of heterogeneous catalysts [6]. This requires the study from a molecular level and can be further extended to other catalytic reactions. The overall goal of our research is called *Discovery Informatics*. By combining various techniques of controlled synthesis of catalysts, WGS kinetics

measurement, catalysts characterization and DFT modeling, we aim at constructing a sufficiently large data base to gain enough chemical information, to enable us to identify the active sites and discover critical descriptors and common trends for active catalysts. This will provide vital insights in the catalytic processes over a wide range of catalysts and help improve catalyst design in the future.

To be specific, this dissertation mainly focuses on studying the influences of noble metal-support interfaces as active sites for the WGS reaction and how we can utilize this interaction to improve the activity. The first two chapters mainly discuss supported Au catalysts. The first chapter discusses the promotion effects of Fe and its influences on the CO adsorption properties of supported Au. The second chapter studies the Au-MgO interfaces and its influences on the H_2O dissociation. Main kinetic parameters which may be used for describing active catalysts are identified.

The last two chapters describe studies of supported Pt catalysts and the influence of Na addition on the activity. Chapter 3 studies the active sites of supported Pt catalysts and identifies Pt nanoparticles to be the active sites instead of single Pt atoms. Chapter 4 further uses Pt-Na/MWCNT catalysts as a model catalyst system to study the promotion effect of Na. It is found that Na promotes the WGS activity by creating new Pt-NaOx interfaces and thus changes the adsorption properties of Pt. It challenges the report in the literature that the single Pt atoms are the active sites and Na promote the rate by making more single Pt atom sites.

CHAPTER 2. FE PROMOTED AU/RUTILE FOR THE WATER-GAS SHIFT REACTION

2.1 Introduction

Water-Gas Shift reaction (WGS) is the reaction of CO and H_2O to form CO_2 and H_2. It is an important reaction to produce clean hydrogen used for ammonia synthesis, hydrocarbon processing, methanol synthesis and fuel cell application [1]. Since it is an exothermic reaction, catalysts with good stability and high activity at lower temperature are strongly preferred. Since Haruta reported the high catalytic activity of supported Au for the preferential oxidation of carbon monoxide (in a mixture of CO and H_2) at low temperature [7], Au has attracted a lot of attention and found applications in many reactions. In the past decade, supported Au has been shown to be an excellent WGS catalyst with high activity at low temperatures [7, 8]. These catalysts are also non-pyrophoric and require no exceptional pre-treatment before use. These findings all make supported Au to be a very interesting and promising catalyst for application.

To explain the superior catalytic activity of supported Au catalysts, a lot of efforts have been made to elucidate the nature of the Au active sites. However, the results are complicated, and different Au active sites have been reported. Haruta used isotopic hydrogen to characterize the rate of HD formation on Au/TiO_2 and find the relationship

between the rate and Au particle sizes. Based on this relationship, they concluded that perimeter Au atoms at the interface between Au-TiO_2 are active sites for hydrogen dissociation [9]. Janssens et a1. combined DFT calculations, adsorption studies on single crystal surfaces and activity measurements on well-characterized supported Au particles. They found that the coordination number of Au atoms significantly influence the CO adsorption strength and thus becomes a crucial parameter for Au catalytic activity. They also concluded that the low-coordinated Au corner atoms are active sites for CO oxidation [10]. Fu et a1. used CO-TPR and XPS characterizations to reveal that cationic Au strongly associated with the surface cerium-oxygen groups are responsible for the activity of Au/CeO_2 towards WGS reaction [11]. Valden et a1. reported bilayer Au clusters supported on single crystal titania are most effective in catalyzing CO oxidation [12]. By finding the correlation between WGS rates and Au particle sizes, Ribeiro et. al. were able to determine that it is the corner Au atom and perimeter atoms are active for the WGS reaction [13, 14]. In all, Au active sites are diversified and varies according to different reaction conditions and various supports.

The metal-support interaction is also very important in determining the Au catalyst activity. The properties of the support surface (i.e., quality and number of nucleation sites) influence the size, dispersion and morphology of the Au nanoparticles, and, thereby, the concentration of active, low coordinated sites. Ceria and zirconia appear to stabilize ionic states of gold [15], and to increase their charge. Andreeva et al.[16] postulated the existence of gold in an ionic form at the interface between the Au and the TiO_2 phases, probably as Au ions inserted in the surface regions of the TiO_2 lattice. Andreeva's group firstly reported Au/Fe_2O_3 catalysts as a low temperature supported Au catalyst for WGS [17, 18]. The

activity of the Au/Fe_2O_3 can be significantly enhanced by adding some other noble metals. Venugopal et al. reported the use of Ru to improve the catalytic activity of Au/Fe_2O_3 [19, 20]. Hua et al. reported that certain types of metal oxides can also act as promoters for the Au/Fe_2O_3 catalyst [21]. Hutchings et. al. deduced that it is primarily the 0.5-nm bilayer clusters, rather than 0.2- to 0.3-nm monolayer Au clusters, that are active for CO oxidation on FeO_x supports [22]. But the detailed kinetics and CO adsorption properties on the Au/Fe_2O_3 are still not very clear. The active sites for the WGS reaction require more exploration. Besides single phase support, FeOx also promotes the activity of other supported Au catalysts. Recently Carretin et a1. has reported that the Fe can promote the activity of Au/rutile towards CO oxidation [23]. The promotion effect of Fe for the WGS reaction has not been well explored. In this paper, we explored the unique WGS kinetics of Au/Fe_2O_3 compared with other oxide supported Au catalysts. Based on the kinetics, we proposed the influence of Fe_2O_3 on the Au active sites and utilize the property to promote the WGS activity over Au/rutile. We attributed the promotion effects to electronic modification of Au atoms by Fe which will change the CO binding strength.

2.2 Experimental Methods

2.2.1 Catalyst Preparation

Au supported on Fe_2O_3 was prepared by deposition-precipitation method. $HAuCl_4 \cdot 3H_2O$ was purchased from Alfa Aesar and used as the precursor. Generally, 40 mg of $HAuCl_4 \cdot 3H_2O$ was mixed with 110 ml deionized water to form a clear solution. The pH was adjusted to 6.0 by adding 0.1N NaOH solution drop by drop at 35 °C. After the pH

reached 6.0, 1 gram of Fe_2O_3 support was added to the solution and the mixture was stirred and heated to 80 °C and kept for 2 hours. The mixture was finally cooled down and aged for 1.5 hour while kept being stirred. The final precipitates were centrifuged and washed with deionized water and dried in vacuum overnight at room temperature.

For Au supported on Fe promoted rutile, the rutile support was doped with Fe before loading Au. The synthesis method is borrowed from literature [23]. $Fe(NO_3)_3$ was purchased from Sigma Aldrich and used as the precursor. Certain amount of $Fe(NO_3)_3$ was dissolved in 1.5 mL deionized water to form a solution. 1 gram rutile support was added to the deionized water and stirred at 60 °C until a thickened slurry was obtained. The slurry was dried in vacuum overnight at room temperature before further treatment. The Fe doped rutile was transferred to a tubular reactor and calcined in air for 4 hours at 450 °C (flow rate: 50 sccm, temperature ramping rate: 5°C/min).

Au was loaded onto the Fe doped rutile following the same deposition-precipitation method as Au supported on Fe_2O_3. The as-prepared catalysts are denoted as Au/x%Fe-rutile catalysts, in which x is the weight loading of the Fe. All the Au catalysts were kept from light and tested within two weeks after preparation.

2.2.2 WGS Kinetic Measurements

The WGS kinetics were measured with a high throughput, fully automated setup of four parallel plug flow reactors, description of which can be found elsewhere [23, 24]. The WGS reaction rates were measured under differential conditions i.e. CO conversion was

maintained below 10% to avoid any diffusion limitations and the products of the WGS reaction (CO_2 and H_2) were also co-fed.

Before WGS kinetic measurement, Au/Fe_2O_3 and Au/Fe-rutile catalysts were reduced at 200 °C in 25% H_2/Ar for 2 hours (flow rate: 50 sccm, temperature ramping rate: 5 °C /min). After pretreatment, the catalysts were exposed to WGS mixture (standard condition, 6.8% CO, 21.9% H_2O, 8.5% CO_2, 37.4% H_2, and balance Ar) with a flow rate of 75.4 sccm. Au/Fe_2O_3 catalyst was stabilized at 140 °C. Since Au/Fe-rutile catalysts have higher activity, they were stabilized at 120 °C. The catalysts were stabilized for a period of ca. 20 hours, which was enough for the initial deactivation to occur and a stable CO conversion to be reached. The apparent reaction orders were measured over the stabilized catalysts by varying the partial pressures of one component at a time over the range of 4–21% CO, 5–25% CO_2, 11–34% H_2O, and 14–55% H_2. After the measurement of each apparent reaction order, WGS reaction rates were measured at the standard conditions, in order to measure the deactivation if there was any. This is an assessment of the stability of the catalyst with time and against the change in the feed compositions. To determine the apparent activation energy, the temperature was varied over a range of 30°C, with the concentrations maintained at the standard condition. After the measurements were complete, the catalysts were passivated at room temperature by 2% O_2 in inert gas flow before they were taken out from the reactors.

2.2.3 Catalyst Characterization

The bulk structure of the WGS used catalysts was determined using X-ray diffraction (XRD) with an AXS D8 Advance Bruker Instrument with Cu Kα radiation. Samples were scanned through 30-80^0 (2θ) with scanning rate 2° min^{-1}. The BET surface areas were measured using nitrogen adsorption isotherms (Micromeritics ASAP 2020). Samples were degassed at 150 °C for 5 to 6 hours before N_2 adsorption. Atomic Absorption (AA) was performed to determine the actual Au loading with a PerkinElmer AAnalyst 300 Atomic Absorption Spectrometer.

Transmission electron microscopy (TEM) and high-resolution transmission electron microscopy (HRTEM) were performed using an FEI Titan 80-300 keV Field Emission Environmental Transmission Electron Microscope–Scanning Transmission Electron Microscope at the Birck Nanotechnology Center in Purdue University. Samples for imaging were prepared by dispersing the catalysts in ethanol then spread onto a carbon coated copper grid. Au nanoparticle shapes and sizes were determined.

In order to observe the CO adsorption species under WGS reaction, *operando* Fourier Transform Infrared Spectroscopy (FTIR) was performed on the Au/Fe-rutile catalysts. The IR data were collected with a Bruker Vertex 70 FTIR. All spectra were collected at a resolution of 4 cm^{-1} and averaged over 100 scans for the background and 50 scans for the sample under steady state conditions. The catalysts were ground and sieved (125 micrometer-250 micrometer). About 100 mg catalyst powder was crushed into a pellet and loaded into the IR cell. 50 sccm 25% H_2/N_2 was flowed through the IR cell and the temperature was ramped to 200 °C with a ramping rate of 5 °C/min. The catalyst was kept

at 200 °C in 25% H_2/N_2 for 2 hours for reduction. Then the gas was switched to 50 sccm N_2 and the temperature was decreased to 120 °C. The spectra were collected as background. 50 sccm 6.8% CO/N_2 was flowed through the IR cell and transmission FTIR spectra were collected. Then 50 sccm WGS mixture (6.8% CO, 21.9% H_2O, 8.5% CO_2, 37.4% H_2, and balance N_2) was flowed through the cell and stabilized IR spectra were collected.

2.3 Results

2.3.1 Results of Au/Fe_2O_3 catalysts

2.3.1.1 WGS Kinetics Results

Due to the reversibility of the WGS reaction, the apparent activation energy and the reaction orders with respect to CO, H_2O, H_2 and CO_2 were fitted to a power rate law expression of the form:

$$r = Aexp\left(-\frac{E_{app}}{RT}\right)[CO]^a[CO_2]^b[H_2]^c[H_2O]^d(1-\beta)$$

Where r is the overall rate, $\beta = ([CO_2][H_2])/(K_{eq}[CO][H_2O])$ is the approach to equilibrium, A and E_{app} are the apparent pre-exponential factor and apparent activation energy for the forward rate. The numbers a, b, c and d are apparent reaction orders. K_{eq} is the equilibrium constant for the WGS reaction. The apparent activation energy was calculated by the Arrhenius plot. The apparent reaction orders were calculated from the slope of the log plot of the rate vs. the partial pressure of certain gas. Figure A2.1 shows typical plots used for measuring the WGS kinetics parameters. Table 2.1 shows the detailed

WGS kinetic data (apparent reaction orders, WGS rate per total moles of metal) of Au/TiO_2 and Au/Al_2O_3 compared with Au/Fe_2O_3. All the apparent activation energies reported are within ± 3kJ $(mol)^{-1}$ range. The reported orders with respect to each species are associated with a ± 0.03 error bar.

WGS Rates reported here are all compared at 120 °C by extrapolation of Arrhenius plot. The rates are normalized by total moles of Au loaded. WGS rates of supported Au catalysts showed a dependence on support. Au/Fe_2O_3 showed a rate between Au/TiO_2 and Au/Al_2O_3. Compared with similar loading Au/TiO_2 and Au/Al_2O_3, Au/Fe_2O_3 has very distinct kinetic features. One distinct feature is the negative CO order. This implies that Au/Fe_2O_3 has a much higher coverage of CO, which will be discussed in more detail later. It means the Au/Fe_2O_3 has a much stronger interaction with CO. The other distinct feature is the higher apparent activation energy. This high activation energy may be related with the strong interaction of Au/Fe_2O_3 with CO.

Table 2.1 WGS Kinetics comparison of Au/TiO_2, Au/Al_2O_3 and Au/Fe_2O_3

Catalyst	Temp. / °C	WGS Rate at 120 °C/10^{-3} mol H_2 (mol metal)$^{-1}$ s^{-1}	Ea /kJ$(mol)^{-1}$	H_2O	CO_2	CO	H_2
Au/TiO_2	120	14.6	55	-0.24	-0.12	0.72	-0.12
Au/Al_2O_3	180	2.9	12	0.81	-0.09	0.87	-0.36
Au/Fe_2O_3	130	8.0	106	0.95	-0.04	-0.70	-0.06

To confirm the special kinetics of Au/Fe_2O_3 catalysts with different loadings, a set of Au/Fe_2O_3 was prepared and tested. Their kinetics is summarized in Table 2.2. All the

catalysts were reduced and stabilized at 140 ^{o}C. They were tested between 130 ^{o}C and 140 ^{o}C. The CO orders tend to increase with Au loading. Correspondingly, the apparent activation energy tends to decrease. An interesting transition of CO order appeared between 2.4% and 6.2% Au loading. The CO order changed from negative to positive. The activation energy looks more like Au/TiO_2 for the high-loading Au/Fe_2O_3. This transition implies the change in chemical nature of the Au sites adsorbing CO.

Table 2.2 WGS Kinetics of Au/Fe_2O_3 samples with different Au loadings

Au Loading /wt%	WGS Rate at 120°C/10^{-3} mol H_2 (mol metal)$^{-1}$ s^{-1}	Ea /kJ(mol)$^{-1}$	H_2O	CO_2	CO	H_2
0.5	8.0	106	0.95	-0.04	-0.70	-0.06
1.0	6.4	91	0.91	-0.07	-0.56	-0.02
2.4	1.9	78	1.06	-0.23	-0.43	-0.19
6.2	0.9	55	0.84	-0.1	0.21	-0.21
8.1	1.2	44	0.67	-0.09	0.35	-0.12

2.3.1.2 XRD Results on the Support

Since FeOx has different possible phases including α-Fe_2O_3, γ-Fe_2O_3 and Fe_3O_4. There is a possibility that the support phase may be changed during reduction and it resulted in the transition of CO order. So in order to determine whether there is support phase change in the Au/Fe_2O_3 as Au loading increases, XRD was performed on the 1.0% and 6.2% Au/Fe_2O_3 samples. The XRD results are shown in Figure A2.2. The comparison with the

standard peaks is shown in Figure A2.3 and Figure A2.4. From the XRD results, we can see that the peaks are quite similar. But for the 6.2% Au/Fe_2O_3 samples, there are two additional peaks at around 38°and 45°. These are assigned to the Au since the Au particles are much larger on these high loading samples (3~4nm vs. 1~2nm). Other peaks are more like γ-Fe_2O_3 peaks. The XRD results of the two samples confirmed that there is no bulk phase change in the support. This implies that the CO order transition from negative to positive may not be due to the support phase change. Instead, a more plausible explanation is that as the Au loading increases, the Au particles tend to be bigger, resulting in less interaction with the Fe_2O_3 support. Thus the chemical nature and CO adsorption properties may be changed, resulting in lower CO coverage and positive CO order.

2.3.1.3 TEM Results of the Au/Fe_2O_3 Catalysts

The activity of supported Au catalysts is strongly dependent on the Au particle size. So the information on the Au particle size distribution is necessary in order to compare the activity fairly. Thus TEM was performed on the Au/Fe_2O_3 catalysts and Fe promoted Au/rutile catalysts. These results are shown in Figure 2.1. The Au average diameters and standard deviations are shown in Table 2.3.

Table 2.3 Average Au diameters of Au/Fe_2O_3 with different Au loadings

Au Loading / wt %	0.5	1.0	2.4	6.2	8.1
Au Average Diameter/nm	1.2±0.5	1.5±0.4	2.1±0.4	2.7±0.9	3.3±1.1

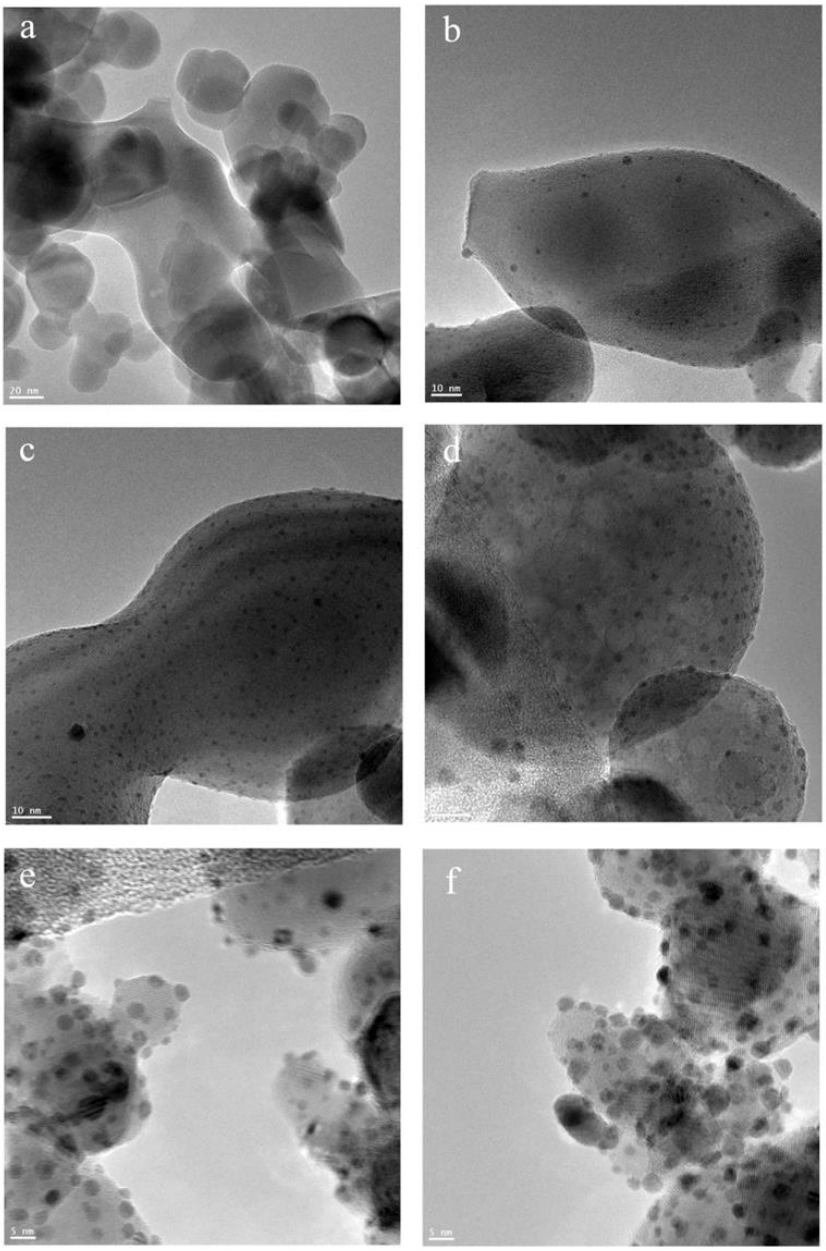

Figure 2.1 TEM of Au/Fe-rutile samples a) Au/rutile, b) Au/0.25% Fe-rutile, c) Au/0.5% Fe-rutile, d) Au/1% Fe-rutile, e) Au/2% Fe-rutile, f) Au/5% Fe-rutile.

TEM results reveal that the particle sizes increase with the Au loading. The low loading samples showed quite small particle sizes with small particle size standard deviation. This

may imply that the Au has strong interaction with the Fe_2O_3 support, preventing Au from sintering. Also for the high loading Au samples, Au particles increase to 3~4 nm and the particle size standard deviation also becomes larger. These may reduce the interaction between Au and Fe_2O_3 support. The rate relationship with Au particle sizes is shown in Figure 2.2. Compared with our previous Au model, the rates are correlated with average Au particle size by a power law of -2.3 order, which is similar to that for Au/Al_2O_3. So the possible active sites should be both the perimeter and corner sites. The CO order vs. Au particle sizes is shown in Figure 2.3. It is clearly shown that there is a trend for CO order to increase with Au particle sizes. This may imply that Au particle sizes plays a role in determining the Au-support interaction, which consequently electronically modifies the chemical nature of Au atoms and CO adsorbing property.

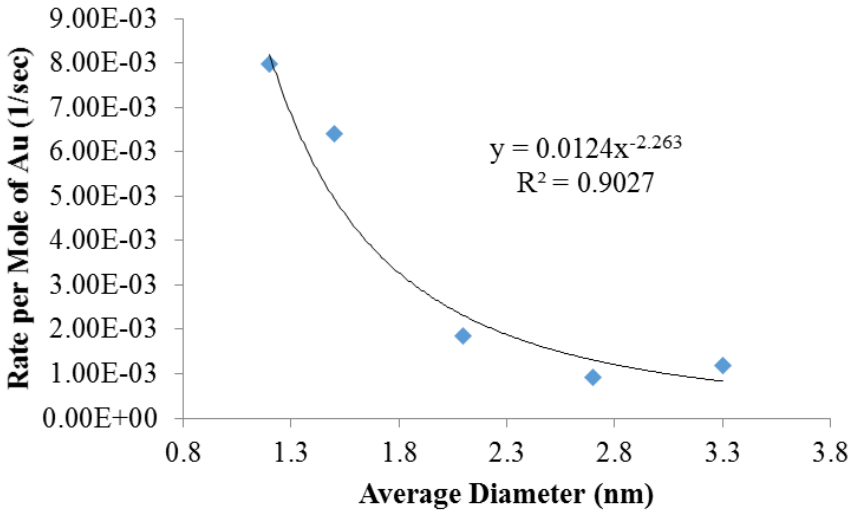

Figure 2.2 WGS Rate vs. Au Average Diameter

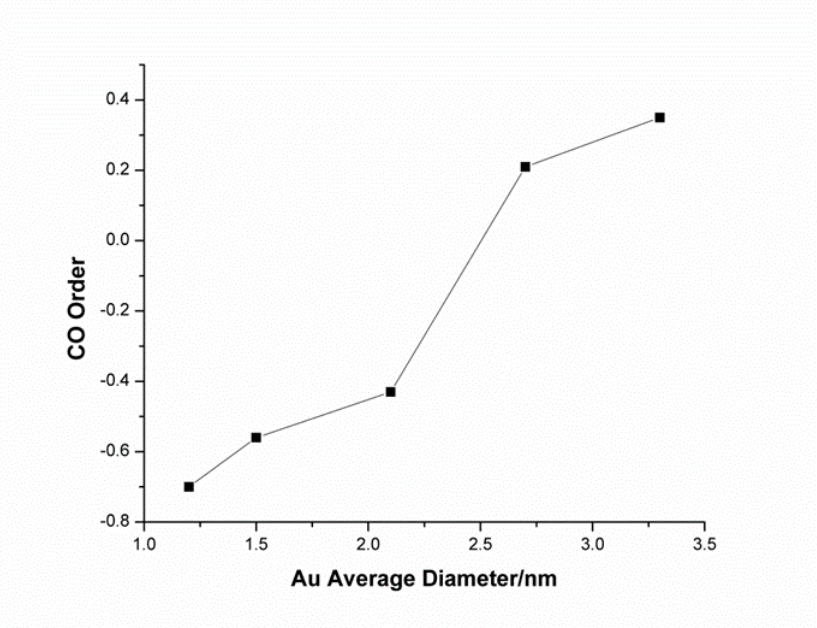

Figure 2.3 CO order vs. Au average diameter

2.3.2 Results of Au/Fe-rutile catalysts

2.3.2.1 WGS kinetics results of the Au/Fe-rutile

The Fe influences on the Au active sites was further studied by using Fe as a promoter to Au/rutile catalyst for the WGS reaction. The Au loadings were kept the same for all the Au/Fe-rutile catalysts while the Fe loadings were varied from 0.25wt% to 5wt%. All the catalysts were pretreated and stabilized following the same procedure as described in the experimental part. The WGS rates are summarized in Table 2.4. The Au loadings were all kept around 1 wt%. The WGS rates were normalized by the total moles of Au and to a temperature of 120 ^{o}C. The rate results showed that Fe can promote the activity of Au/rutile. As Fe loading increases, the WGS rate first increased and then decreased. The maximum

appeared at about 1 wt% Fe loading. The maximum promotion is about 4 times of the Au/rutile sample. But as Fe loading approaches 5 wt%, the rate decreased and became similar to that for Au/Fe_2O_3. Also the kinetics showed a trend with Fe loading. The apparent activation energy increases from about 53 kJ $(mol)^{-1}$ to about 98 kJ $(mol)^{-1}$. On the contrary, apparent CO order decreases from ~0.7 to -0.3 as Fe loading increases. Also as the Fe loading increases, the kinetics approaches the kinetics of Au/Fe_2O_3. The significant changes in kinetics implies modification of the reaction process and active sites on the Au/rutile samples by adding Fe.

Table 2.4 WGS kinetics of Au/TiO_2 catalysts with different Fe loadings

Catalyst (1wt%Au)	WGS Rate at 120°C/10^{-2} mol H_2 (mol metal)-1 s-1	Ea /kJ$(mol)^{-1}$	H_2O	CO_2	CO	H_2
Au/TiO_2	3.8	53	-0.21	-0.09	0.68	-0.06
$Au/0.25\%Fe\text{-}TiO_2$	7.8	56	-0.09	-0.14	0.50	-0.10
$Au/0.5\%Fe\text{-}TiO_2$	12	50	0.03	-0.14	0.56	-0.09
$Au/1\%Fe\text{-}TiO_2$	13.3	64	0.19	-0.11	0.30	-0.17
$Au/2\%Fe\text{-}TiO_2$	7.9	80	0.53	-0.09	0.03	-0.11
$Au/5\%Fe\text{-}TiO_2$	4.2	98	0.38	-0.03	-0.33	-0.17
Au/Fe_2O_3	0.6	91	0.91	-0.07	-0.56	-0.02

2.3.2.2 XRD results of the Au/Fe-rutile

XRD was also performed on the Fe promoted Au/rutile catalysts to determine the bulk phases. The results are shown in Figure 2.4. As the Fe loading increases, the XRD spectra

showed no change in the spectra compared with bare Au/rutile catalyst. All the peaks are assigned to rutile phases. No FeOx related peaks were found. This result indicates that the Fe was well-dispersed on the rutile surface and no chunk FeOx was formed during the preparation.

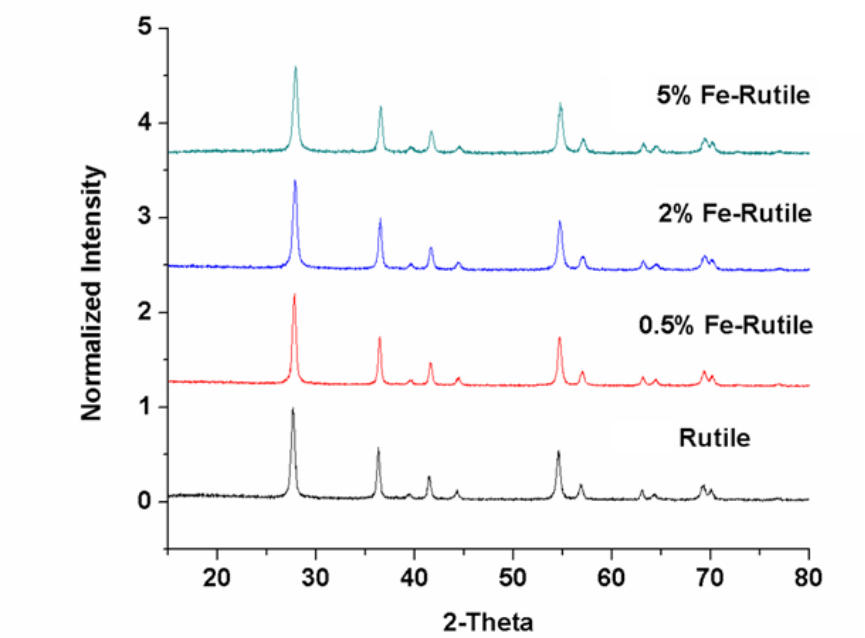

Figure 2.4 XRD of Au/Fe-rutile catalysts with different Fe loadings.

2.3.2.3 TEM results of the Au/Fe-rutile

In order to make a fair comparison between different Au/Fe-rutile samples, the Au particles should have similar average Au particle sizes. So TEM was performed to obtain the particle sizes, which is shown as Figure 2.5. The statistic results are summarized in Table 2.5. The TEM results confirmed the similar particle size distribution (Figure A2.5) and the same

average particle sizes. So the promotion effect is not because of particle size difference. Instead, the Fe addition is responsible for the promotion.

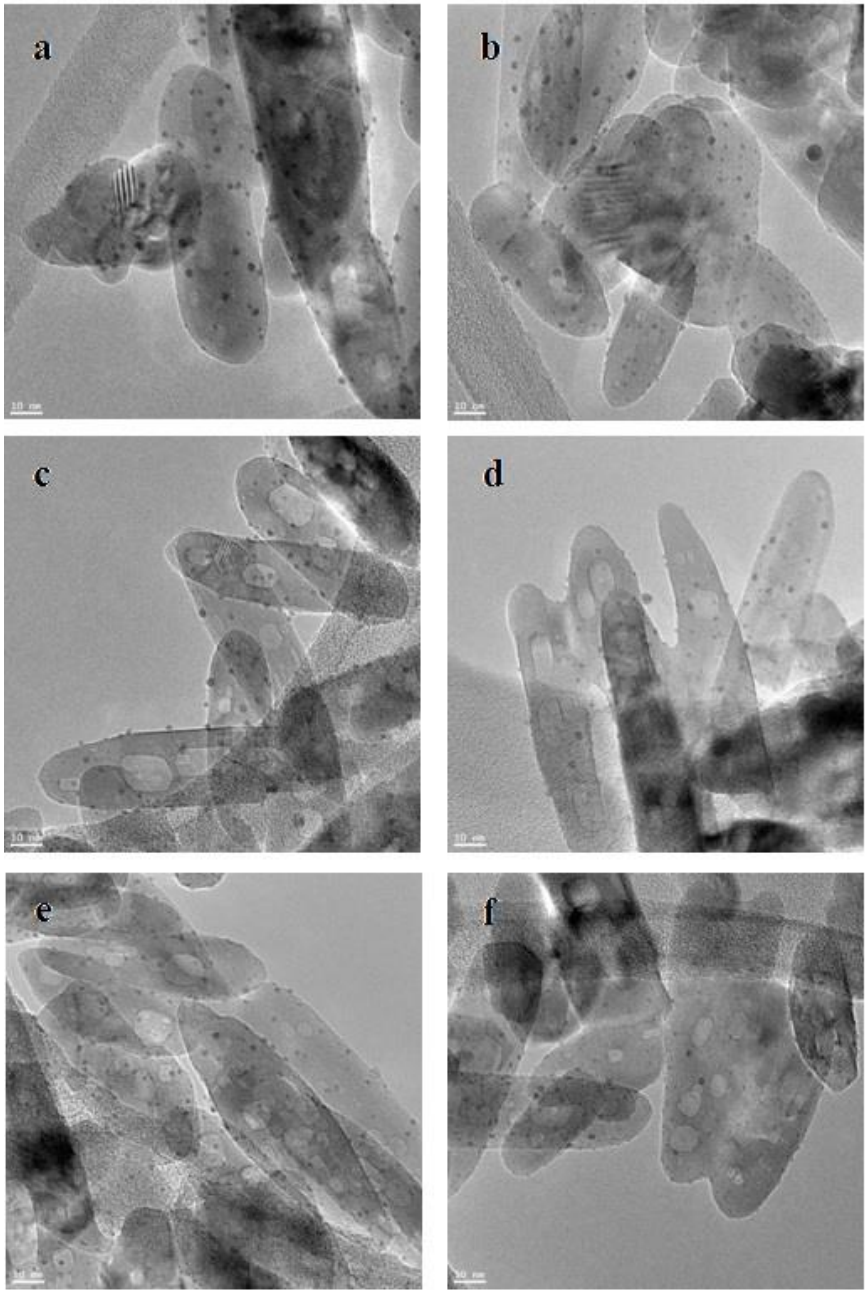

Figure 2.5 TEM of Au/Fe-rutile samples a) Au/rutile, b) Au/0.25% Fe-rutile, c) Au/0.5% Fe-rutile, d) Au/1% Fe-rutile, e) Au/2% Fe-rutile, f) Au/5% Fe-rutile.

Table 2.5 Average Au particle sizes for Au/Fe-rutile catalysts

Fe Loading /wt%	**0**	**0.25**	**0.5**	**1**	**2**	**5**
Number Average Au Particle Size /nm	2.1±0.5	2.1±0.5	2.0±0.3	2.1±0.3	1.9±0.3	1.9±0.3

2.3.2.4 *Operando* FTIR results of the Au/Fe-rutile

In order to better observe the adsorption species changes on the surface of Au/rutile by adding Fe, *operando* FTIR was performed on the 1 wt% Fe promoted sample. The results are compared with the *operando* FTIR results of Au/rutile as shown in Figure 2.6. The peak at around 2100 cm^{-1} was assigned to CO adsorbed on metallic Au atoms. When the Au is electron rich and gets slightly negatively charged, it will back-donate more electrons to the C-O anti π^* bond and weaken the C-O bond. So the CO adsorption peak will red-shift to a lower wave-number, which is shown as the peaks at around 2040 cm^{-1} and 1970 cm^{-1}. Au/Fe-rutile samples showed more CO peaks at lower wave-numbers compared with Au/rutile. IR peaks at wavenumbers of 2097 cm^{-1}, 2044 cm^{-1} and 1967 cm^{-1} were observed while for Au/rutile only peak at 2097 cm^{-1} was observed. The IR bands at lower frequencies were stronger than the corresponding peaks of Au supported on un-doped rutile and thus suggest a participation of Fe in the neighborhood of the site. Thus, the results showed that Fe-doping can modify the CO adsorption properties of Au/Rutile and that WGS rates can be correspondingly promoted with appropriate Fe content. Another interesting feature here is that the peak due to CO adsorbed on metallic Au (2100 cm^{-1}) was first promoted as Fe

loading increases from 0% to 1wt%. However, when the Fe loading is higher than 1 wt%, the peak due to CO adsorbed on metallic Au was decreased as Fe loading continues to increase. For the Au/5%Fe-rutile, the 2100 cm^{-1} peak has the lowest intensity and was shifted to a frequency about 2100 cm^{-1}. On the other hand, the peaks of lower frequencies continue to increase as Fe loading increases. Finally the low frequency peaks below 2075 cm^{-1} were the dominant peaks on Au/5%Fe-rutile catalysts.

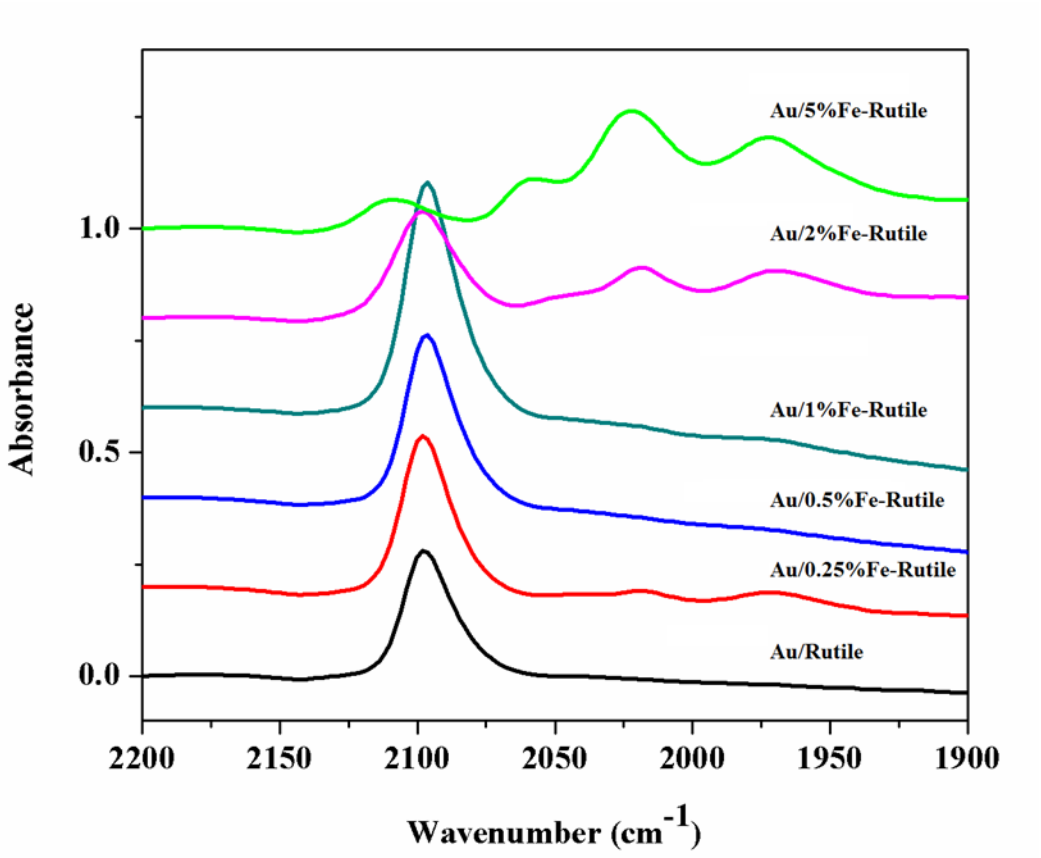

Figure 2.6 *Operando* FTIR of Au/Fe-Rutile catalysts under WGS conditions

To further measure the CO adsorption differences, *operando* transmission IR was performed on the Au/rutile catalysts with different Fe loadings. All the catalysts were pretreated the same way as in the WGS kinetics measurement. Then the temperature was

decreased to 120 °C. 50 sccm 6.8% CO/N_2 was flowed through the IR cell and the IR spectra was recorded after a stabilized IR spectroscopy was obtained. The results are shown in Figure 2.7. The IR peak at 2100 cm^{-1} under WGS condition was blue-shifted slightly compared under the 6.8% CO/N_2 flow. The blue shift may be due to the higher CO coverage under the CO/N_2 mixture compared with WGS mixture. Under the 6.8% CO/N_2 condition, as the Fe loading increases, the peak intensity will also tend to increase first and then decrease as the Fe loading increases further. At the same time, as Fe loading increases, the IR peaks at lower frequencies increased. Multiple peaks around 2000 cm^{-1} were observed at Fe loading larger than 1%. This is in consistent with the *operando* FTIR results under WGS condition.

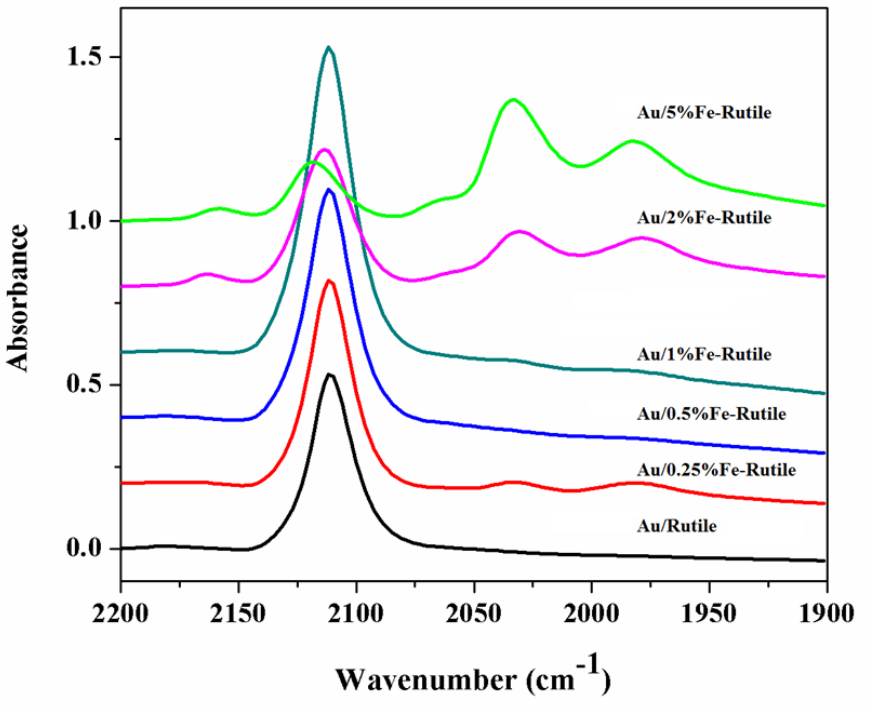

Figure 2.7 Transmission IR on a series of Au/Fe-rutile catalysts under 6.8% CO/N_2 at 120 °C

2.4 Discussion

2.4.1 Au supported on Fe_2O_3 catalysts

Based on our previous results for the Au particle size effects on Au/TiO_2 and Au/Al_2O_3, the WGS rates obtained for different loadings of Au could also be correlated with the average Au particle sizes (Figure 2.2). Generally, we modelled the supported Au nanoparticle as a truncated-cubooctahedral model (Figure A2.6). The Au atoms could be categorized as three types based on the coordination numbers: corner atom, perimeter atom and general surface atoms. As the Au particle sizes increase, the fraction of the three types of Au atoms will decrease following a different power law. So if we correlate the rate with the Au particle size, based on the trend, we could deduce the dominant active sites for the WGS reaction. We have concluded that for Au/TiO_2, the dominant active sites are corner atoms ($d^{-2.7}$) while for the Au/Al_2O_3, the dominant active sites are both corner and perimeter Au atoms ($d^{-2.2}$) as shown in Figure A3.2 [13, 14]. Here for the Au/Fe_2O_3, the correlation implies that it behaves similar as Au/Al_2O_3. Corner and perimeter Au atoms here showed similar activity toward WGS.

On the other hand, the apparent activation energy and apparent reaction orders could give us further implications of the surface species. If a catalytic reaction follows a Langmuir-Hinshelwood type of mechanism, the intrinsic reaction rate is a direct function of the relative surface concentrations of the adsorbed species that are actively involved in the reaction mechanism. The measured apparent kinetic parameters (activation energy and reaction orders) are hence dependent on the relative surface concentrations of the adsorbed

reactive species. The relative surface concentrations are often related to the gas phase concentrations of the reaction mixture components through Langmuir isotherm equations. For a mixture of reactant A and B

$$A + B \rightarrow P$$

$$\theta_A = \frac{K_A C_A}{1 + K_A C_A + K_B C_B}$$

Where θ_A is the fraction of the available surface covered by species A at equilibrium, K_i is the adsorption equilibrium constant for species i and C_i is the gas phase concentration of species i. The dependence of K_i on temperature makes θ_A temperature dependent. θ_A also depends on the heat of adsorption of species A and B. In turn, the apparent reaction order with respect to such species involved in the reaction depends not only on the gas phase concentration but also on the reaction temperature. It is therefore necessary to measure the kinetic data over different catalysts at same temperature for objective comparison of relative surface concentrations of reactive species. The reaction rate is directly proportional of θ_A and θ_B if these species are adjacently adsorbed. An apparent reaction order of ~1 for a particular reactant entails that the relative surface concentration is near zero; whereas the apparent reaction order of -1 implies that the reactant is strongly bonded to the surface. In the latter case, the reaction rate is dependent upon the number of sites left free by this strongly adsorbed reactant. Therefore, any fractional orders measured in between these extremes can paint a quantitative picture of relative surface concentrations and heats of adsorption of different surface intermediates. A simple estimation of the relative surface concentrations by using apparent reaction order is

$$\theta_A = 1 - 2n_A$$

In case of WGS reaction, the apparent CO and CO_2 orders can be used to gauge the relative size of the carbon pool while the apparent H_2O and H_2 orders yield similar information about the hydroxyl pool (generated due to adsorption and dissociation of water on the catalytic surface). Most importantly, since the measured reaction rate directly depends on the number of 'dominant' active sites on the catalyst surface, the apparent reaction orders are related to the relative surface concentrations over these dominant active sites.

As shown in the kinetic results, Au/Fe_2O_3 showed distinct kinetic features compared with other oxide supported Au catalysts, that is, high apparent activation energy and negative CO order. Also as the Au loading increased, CO order tended to increase while apparent activation energy decreased. The unusual CO order of Au/Fe_2O_3 may be explained by the different interaction of Au with the Fe_2O_3 support. Au on Fe_2O_3 tended to have more strong interaction with the support, which may result in more negatively charged Au atoms. The low-coordinated Au atoms have high-lying metal d states, which are in a better position to interact with the adsorbed CO valence state. The transition of CO order from negative to positive is also unusual. One possible reason is that as Au loading increased, the support undergoes phase changes. But this hypothesis is rejected by the XRD results. The XRD showed that the bulk phase of Fe_2O_3 didn't change much after reaction. Another possible explanation for the CO order may be the Au particle size changes. As the Au loading increased, Au nanoparticles tended to increase. In the small Au particles, there is a larger fraction of unsaturated Au atoms which have stronger interaction with Fe_2O_3 support. These Au atoms will easily be modified by the support, probably getting some electron

donation from the reducing support. So when the Au nanoparticles are small, they have higher CO affinity. But as Au particle size increases, the modification effects get weaker because there are more saturated Au. Finally, the adsorbing ability of Au towards CO decreased, consequently the CO order increased. From the results of the TEM, we can also plot the relationship between the CO order and particle sizes. Clearly we see the trend of CO order increasing with Au particle size. This can partially support the CO order relationship with the Au-support interaction. The interaction between the Au and Fe is very interesting and could be possibly to be utilized to modify other supported Au catalysts.

2.4.2 Au supported Fe-rutile catalysts

As an application of the Au-Fe interaction shown by the Au/Fe_2O_3 catalysts, Fe was added to Au/rutile catalyst to check its influences on the activity of Au/rutile catalyst. The WGS rates per mole of Au over Au/rutile could be promoted by Fe to a maximum of 4 times at 120 °C. However, since the Au particle sizes have significant influence on the WGS rates, Au particle size information is critical in order to compare the WGS rates fairly. From the TEM results, the Fe addition didn't change the average Au particle size. All the samples showed number average diameter of ~2 nm. Based on our previous results for the WGS rates correlation with Au particle size, the WGS rate for Au/rutile is proportional to $d^{-2.7}$, where d is the number average Au diameter. So if we assume Fe has no effect on the WGS activity of Au/rutile, in order to increase the WGS rate by 3.5 times, the Au nanoparticles should have a 1.2 nm average diameter. Obviously this is not the case here. So particle

sizes influence is ruled out from the reasons for rate promotion. The promotion is due to the presence of Fe.

The BET surface area for the rutile support is around 50 m^2/g. The 1 wt% Fe will cover 30% of the total surface area by assuming a mono-layer formation. Fe may form some patches on the surface. It is possible that the promotion effect is just a combination of Au/FeOx and Au/rutile. However, the XRD results confirmed that the Fe is well-dispersed on the rutile surface. This implies that no patches of FeOx were formed. Furthermore, Au/FeOx has an even lower WGS than Au/rutile. The promoted WGS rate is higher than both catalytic systems. So it ruled out the possibility that the promotion is due to a physical averaging between the WGS rates on Au/FeOx and Au/rutile. The significant changes in the WGS kinetics imply that the chemical nature of the active sites has been modified by addition of Fe.

Besides the activity, the Fe addition also changes the kinetics significantly. The apparent reaction orders were plotted with respect to the Fe loading in Figure 2.8. The apparent activation energy was increased monotonically from 50 kJ $(mol)^{-1}$ to about 100 kJ $(mol)^{-1}$. On the contrary, the apparent reaction order with respect to CO decreased from 0.7 to -0.3. From the discussion of the Au/Fe_2O_3 samples above, the apparent reaction orders were related with the relative surface concentration of the corresponding species. Thus the changes in the CO order imply a stronger CO adsorption on the Au/rutile surface. This is similar to what we observe for the Au/Fe_2O_3 system as the Au particle decreases and the Au has a strong interaction with the support, resulting in a higher CO affinity. We could correlate the WGS rate with the CO order changes, and this is shown in Figure 2.9. The

trend is very similar to the so-called Sabatier's rule. Here in this case, the CO binding strength affects the overall WGS rates. The CO binding shouldn't be either too weak or too strong in order to obtain a maximum rate. Proper addition of Fe could modify the binding strength. The increase in apparent activation energy also correlated with the CO order decreasing. Based on the Tempkin's rule, the apparent activation energy can be determined by

$$E_{app} = E_{rds} - n_{CO}\Delta H_{CO}$$

Where E_{app} is the apparent activation energy, E_{rds} is the activation energy for the rate-determining step, n_{CO} is the apparent reaction order with respect to CO, ΔH_{CO} is the adsorption heat of CO. Since the adsorption heat is a negative value, as CO order decreases, correspondingly the apparent activation energy will increase.

One possible explanation for the Fe promotion could be the electronic interaction between Au and Fe. Under the reducing WGS conditions, Fe could be partially reduced. For the Au in close contact with Fe, Fe could donate some electrons to the adjacent Au atoms and make them electron rich. The electron-rich Au atoms ($Au^{\delta-}$) will have a higher CO affinity, which makes the CO to react more easily on the surface. However, as more and more Fe was added, the Au begins to bind CO too strongly. This could stabilize the carboxyl species formed from CO and OH and lower its rate of decomposing to the CO_2 products.

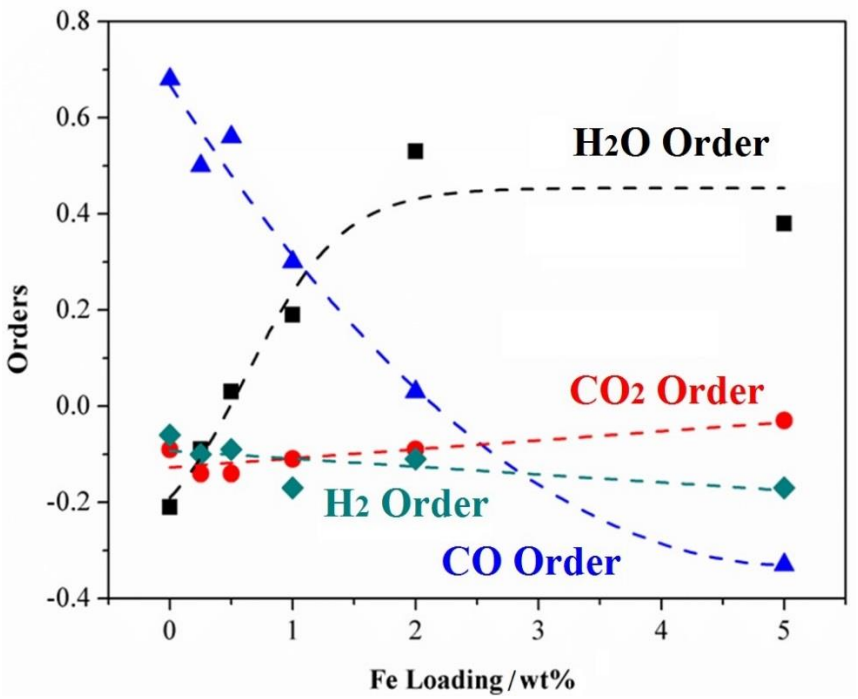

Figure 2.8 Apparent reaction orders changes with different Fe loadings

Another feature here is the apparent reaction order with respect to H_2O, which increased from -0.2 to 0.4 as Fe was loaded. But at about 2 wt% Fe loading, the H_2O order saturated and stayed the same for higher Fe loadings. The final H_2O order is similar to what we observe for the Au/Fe_2O_3. This behavior is in consistent with most of the H_2O adsorption and dissociation happening on the support. This gives another proof to the conclusion from the XRD that the well-dispersed Fe is covering the surface. As more and more Fe was loaded, the surface is all covered by FeOx species (it is estimated that ~5wt% Fe will form a monolayer on the rutile surface, BET surface area ~55 m^2/g), and the H_2O adsorption is the same as on the Au/Fe_2O_3 surface. Also from our previous results, the Au catalysts which have a higher apparent H_2O order (Au/Al_2O_3, Au/ZnO etc) tend to have a lower rate than the Au catalysts with a lower apparent H_2O order (Au/TiO_2, Au/CeO_2 etc), this is shown

in Figure A2.7. So the increase in H_2O order couldn't be an explanation for the promotion of the rate. On the contrary, it could make negative contributions to the promotion. But here the CO affinity change is larger enough to out-weigh the negative influences of the H_2O order change, resulting in promotion of the overall WGS rate.

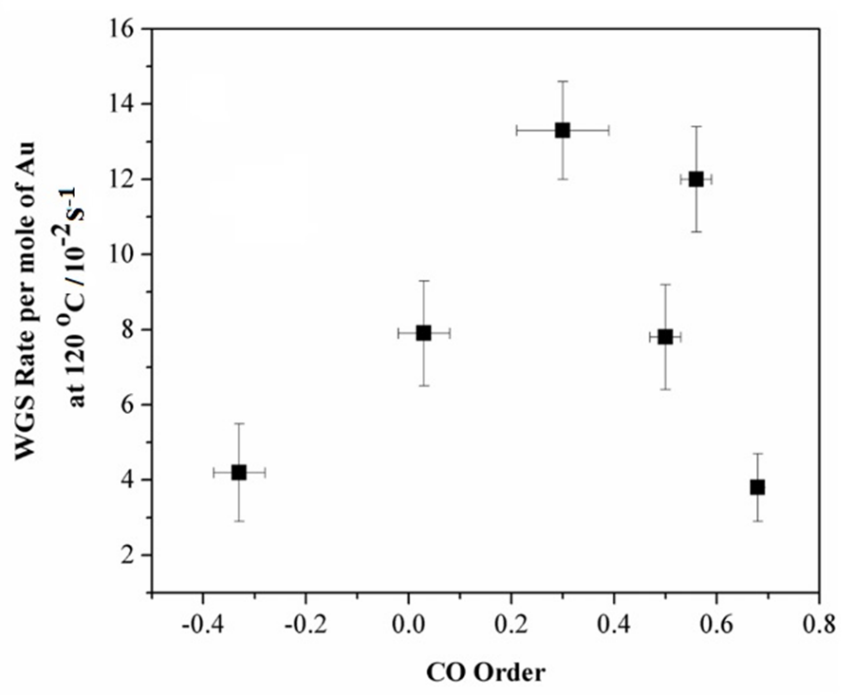

Figure 2.9 WGS rate changes with respect to CO order

The adsorption properties changes were further confirmed from the *operando* FTIR results. Here the Au/Fe-rutile catalysts were tested following the same procedure as described for WGS. For the sample with larger than 1wt% Fe loading, there are more CO peaks at lower wavenumbers compared with the Au/rutile results. The CO peak at ~2100 cm^{-1} could be assigned to CO adsorbed on metallic Au atoms. The CO peaks at 2040 cm^{-1} and 1967cm^{-1}, however, are hardly detectable for Au/Fe-rutile catalysts with Fe loading no larger than 1%. These peaks are at much lower wave-numbers, which imply a much stronger

adsorption of CO. Based on the *operando* FTIR results, the Fe promoted Au/rutile does show more and stronger CO adsorption peaks at lower wave-number. In other words, the CO binds more strongly on the Fe promoted Au/rutile compared with pure Au/rutile. This supports our conclusion from the kinetics.

Further experiments with CO/N_2 mixture on different Fe loading Au/rutile catalysts are shown in Figure 2.7. For Au/rutile catalyst, CO adsorbed on metallic Au is observed (2100 cm^{-1}). As Fe loading increases, CO adsorbed on metallic Au peak intensity increases with Fe loading. But further increases in Fe loading above 1% will decrease the peak intensity of CO adsorbed on metallic Au. At the same time, low wave-number peaks at around 2000 cm^{-1} begin to appear and increase the intensity as more Fe is loaded. This implies that the Au atoms at the interfaces are more negatively charged as more Fe is loaded. This is in consistent with the *operando* FTIR experiments under WGS condition that Fe could increase the CO binding strength of Au/rutile. However, further increase in the binding strength of CO is not beneficial for WGS activity. From the kinetics and IR experiments here, a proper CO binding strength is required to realize an optimum promotion.

2.5 Conclusion

WGS rate correlation with average Au particle sizes on Fe_2O_3 revealed that both corner and perimeter Au atoms are dominant active sites for WGS on Fe_2O_3. Also we observed unique kinetic features for Au/Fe_2O_3. The Au/Fe_2O_3 showed a significantly higher apparent activation energy and a negative apparent reaction order with respect to CO. Also the

apparent activation energy decreases and CO order increases as the Au loading increases. Support phases didn't change during this process but the Au particle sizes changes. This may be due to the less interaction between Au and the Fe_2O_3 support as Au particle size increases. DRIFTS results revealed that Au/Fe_2O_3 has a stronger CO affinity compared with Au/TiO_2. This implies that Fe_2O_3 tends to have stronger interaction with Au and could possibly modify the electron charges of the Au active sites.

The interaction between Au and FeOx could also be adopted to promote the activity of Au/rutile. When Fe was added to Au/rutile, the WGS rate was promoted by a maximum of 4 times compared with pure Au/rutile. But as Fe loading increased further, the rate decreased and finally approached the same as that of Au/Fe_2O_3. The kinetic parameters are also influenced by the Fe loading. When Au loading was fixed, as more and more Fe was added, the apparent CO order decreased from 0.7 to -0.3. On the contrary, the apparent activation energy increased from 50 kJ $(mol)^{-1}$ to 100 kJ $(mol)^{-1}$. This trend is similar to what we observed for Au/Fe_2O_3 as Au particle size decreased. The changes in the kinetics imply modification of active sites, which could possibly be due to the electron donation from Fe to Au, which will make Au atom more electron rich and negatively charged. From the findings here, the charge status of the Au will be influenced by the promoter and this will cause significant changes in the kinetics and adsorption ability. The negative charged Au may be more active here than the metallic Au atoms. This modification method could be possibly to apply for other supported noble metal systems.

CHAPTER 3. IDENTIFYING THE PARTICIPATION OF HYDROXYL GROUP IN THE WATER-GAS SHIFT REACTION BY USING AU/MGO CATALYST

3.1 Introduction

Supported gold catalysts, as LTS catalysts, have attracted extensive research in the last few years and have been identified as a class of active and important catalysts [24-28]. Flytzani-Stephanopoulos et a1. have reported preparation of single atom Au atoms supported on various supports (KLTL-zeolites, MCM-4 silica, titania etc.) and effects of adding Na or K [27, 28]. On the other hand, Williams et al. and Shakhar et al. have shown a clear relationship between WGS rate and Au particle size and concluded that the corner atoms of Au particles are the active sites of Au/TiO_2 for the WGS reaction [13, 14]. Also, the activity of Au catalysts is strongly dependent on the support. For example, Au/TiO_2 has about two orders of magnitude higher WGS rate per mole of Au than Au/Al_2O_3 at the same Au particle size [13, 14]. The reason behind the influence of the supports is still not clearly illustrated, but the current working hypothesis is that the source is the difference in H_2O activation ability between the various oxide supports. In order to get an in-depth understanding of the support influence and the hydroxyl group participation in the water-gas shift reaction, we have combined experiments with theoretical modelling.

For this purpose, MgO was selected as a model system due to its simple structure for DFT calculations [29, 30]. Although there are reports on Au/MgO for the CO oxidation reaction

[31, 32], the WGS reaction over the Au/MgO catalyst has not been well studied. In this paper, we will show the details of catalyst synthesis and demonstrate the feasibility of using MgO and its hydroxide counterparts, $Mg(OH)_2$, as supports for the WGS. On the other hand, the role of water dissociation in the WGS reaction mechanism is not well understood on supported gold catalysts. Motivated by these questions, we carried out experimental research combined with the computational DFT studies on Au/MgO, which is adopted as a model catalyst. Based on both experimental and computational studies, we will show our findings on WGS reaction mechanism and the role of water dissociation over Au/MgO catalyst.

3.2 Experimental Methods

3.2.1 Catalyst Preparation

The Au/MgO catalyst was prepared by a two-step deposition precipitation method with urea, slightly modified from the method used by Milone et al.[33] MgO was obtained from US Research Nanomaterials, Inc. in nanoparticle form (MgO, 99+%, 20 nm). The as-received MgO was steamed in a flow of 66.5 sccm of ~22% H_2O in air at 450°C for 12 hours before using for catalyst preparation. To add gold to the MgO support, 40 mg of Au precursor (99.99% $HAuCl_4 \cdot 3H_2O$ from Alfa Aesar) was added to 110 mL millipore water to give a 0.0024 M gold solution. The solution was kept being stirred at 950 rpm and heated to 85°C. Once the solution reached the target temperature, 1 g of MgO support was added to the solution, and the mixture was kept at 85°C for 30 min. Urea was then added to the mixture, and to gain a concentration of urea of 1.26 M. The final mixture was kept at 85°C

for 15.5 hours and stirred at 950 rpm in the absence of light. After cooling, the mixture was centrifuged to separate the solids from solution, washed with millipore water, and dried under vacuum overnight at room temperature.

Due to the reaction of MgO with H_2O, the as-prepared catalyst has a bulk support phase of $Mg(OH)_2$. In order to obtain Au/MgO, the fresh catalyst needs to be reduced at 150 ℃ in 25% H_2/Ar for 2 hours (flow rate: 50 sccm, temperature ramping rate: 2 ℃/min) followed by annealing in Ar flow at 400 ℃. The phase change will be proved by the XRD results.

3.2.2 WGS Kinetics Measurements

The WGS reaction was measured with a high throughput, fully automated setup of four parallel plug flow reactors, the full description of which can be found elsewhere [13,14]. The WGS reaction rates were measured under differential conditions i.e. CO conversion was maintained below 10% to avoid any diffusion limitations and the products of the WGS reaction (CO_2 and H_2) were also co-fed [34].

Before WGS kinetics measurement, Au on $Mg(OH)_2$ was reduced at 150 ℃ in 25% H_2/Ar for 2 hours (flow rate: 50 sccm, temperature ramping rate: 2 ℃/min). Further annealing in Ar flow at 400 ℃ will convert the reduced Au/$Mg(OH)_2$ to Au/MgO, which will be proved by XRD in the following discussion. After pretreatment, the catalysts were exposed to WGS mixture (standard conditions, 6.8% CO, 21.9% H_2O, 8.5% CO_2, 37.4% H_2, and balance Ar) with a flow rate of 75.4 sccm. Both Au/$Mg(OH)_2$ and Au/MgO were stabilized at 200 ℃ for a period of c.a. 20 hours, which was enough for the initial deactivation to occur and a stable CO conversion to be reached. The apparent reaction orders were

measured over the stabilized catalysts by varying the partial pressures of one component at a time over the range of 4–21% CO, 5–25% CO_2, 11–34% H_2O, and 14–55% H_2. After the measurement of each reaction order, WGS reaction rate was measured at the standard conditions, in order to measure the deactivation if there was any. This is an assessment of the stability of the catalyst with time and against the change in the feed compositions with time and no significant deactivation was observed (Figure A3.1). To determine the apparent activation energy, the temperature was varied over a range of 30°C, with the concentrations maintained at standard conditions. After measuring the kinetics, the H_2 and H_2O were switched to D_2 and D_2O and kept at the same flow rates as H_2 and H_2O. The WGS rates per mole of Au were measured at 220 °C with D_2 and D_2O at the same standard condition. The ratio between the WGS rates by D_2 and D_2O and WGS rates by H_2 and H_2O was calculated and is defined as the kinetic isotope effect ratio (KIE).

After the measurements were complete, the catalysts were passivated at room temperature in 30 sccm 2% O_2/Ar gas flow for 4hs before they were taken out from the reactors.

3.2.3 Catalyst Characterizations

Atomic Absorption (AA) was performed to determine the actual Au loading with a PerkinElmer AAnalyst 300 Atomic Absorption Spectrometer. About 50 mg catalysts were completely dissolved in 5 mL aqua regia and then diluted with millipore water to a total volume of 50 mL. The Au concentration of the diluted solution was measured by AA and the Au loading was calculated.

Powder XRD patterns were collected in air on a Rigaku SmartLab X-ray diffractometer. The patterns were collected from 2θ angles of 10 to 80 degrees in 0.01 degree steps. The collection time per step was 0.25 s.

Z-contrast high angle ADF scanning TEM (HAADF-STEM) imaging was performed to clearly visualize distributions of Au nanoparticles on the lower Z supports (i.e., MgO or $Mg(OH)_2$) and to determine particle size distributions. The catalysts were characterized by an FEI Titan 300 kV S/TEM equipped with a Gatan Imaging Filter (GIF) and a Fischione Model 3000 annular dark field (ADF) detector. ADF images were collected at the camera length of 195 mm. Image collection time and dwell time for ADF-STEM images were 25 second and 24 μsec, respectively. To determine the average Au particle diameter, about 300 Au nanoparticles were counted and the Au particle distribution is calculated. To investigate morphologies and atomic structures of Au nanoparticles, high-resolution transmission electron microscopy (HRTEM) imaging was performed. HRTEM images were collected with excluding inelastic scattered electrons using energy filtering TEM (EFTEM) mode (slid width: 20 eV) to improve image contrast and the exposure time was 1 second.

Operando Fourier Transform Infrared Spectroscopy (FTIR) was performed on the Au/MgO catalyst with a Bruker Vertex 70 FTIR. About 100 mg as-prepared $Au/Mg(OH)_2$ catalyst was sieved (125 micrometer-250 micrometer) and crushed into a pellet and loaded into an IR cell. The same reduction pretreatment was performed followed by annealing in Ar at 400 °C for 2 hours. The IR background spectra were taken with 50 sccm N_2 flow in an empty cell. The catalyst was stabilized at the standard WGS condition for 12 hours. During the stabilization, WGS rates and IR spectra were collected together to check the

adsorption species changes with time. All spectra were collected at a resolution of 4 cm^{-1} and averaged over 100 scans for the background and 50 scans for the sample under steady state conditions. Integration of the IR peak band areas were completed with Casa XPS version 2.3.12. Mixed Gaussian-Lorentzian line-shape curves (30% Gaussian, 70% Lorentzian) were used for peak band fitting.

CO Temperature-programmed reduction (TPR) experiments were also performed in the IR cell to check the reactivity of the adsorbed hydroxyl group of Au/MgO and MgO support. About 80 mg of freshly prepared $Au/Mg(OH)_2$ catalyst was loaded in the IR cell. $Au/Mg(OH)_2$ was reduced in 50 sccm 25% H_2/Ar at 200 °C for 2 hours followed by annealing in 50 sccm N_2 at 400 °C for 2 hours to obtain Au/MgO. After the pretreatment, the catalyst was kept in N_2 and the temperature was decreased to 220 °C. IR spectra were taken with 50 sccm N_2 flow. Then the gas was switched to 50 sccm 7% CO/N_2. Temperature was increased to 360 °C by a ramping rate of 5 °C/min. At the same time, the IR spectra were measured every minute during the temperature ramping.

As a comparison, bare $Mg(OH)_2$ support was prepared the same way as the $Au/Mg(OH)_2$ catalyst but without adding the Au precursor. The fresh $Mg(OH)_2$ support was loaded in the cell and the same pretreatment was carried out. The same CO TPR experiment of $Au/Mg(OH)_2$ was taken on the $Mg(OH)_2$ support.

3.2.4 DFT Calculations

MgO supported Au nano-wire was chosen as our model catalyst. The ideal MgO(100) surface was represented by periodic slab models of four layers, repeated in a super cell

geometry with at least 2 nm vacuum spacing between them. A three layers thick and three atoms wide Au wire was added on one side of the MgO(100) slab as shown in Figure 3.1 from reference [36].

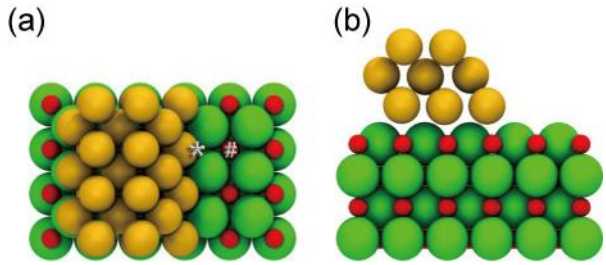

Figure 3.1 (a) Top view and (b) side view of the used Au/MgO interface model. * and # indicates the two sites in our micro-kinetic model.

DFT calculations with the plane-wave based Vienna ab initio simulation package VASP. We used the generalized-gradient approximation in the form of the exchange-correlation functional PW91. The total energies of all the PW91 optimized structures were further refined in a single point fashion at hybrid level in form of HSE06. The interaction between the atomic cores and electrons was described by the projector augmented wave (PAW) method.

3.3 Results

3.3.1 XRD results

Figure 3.2 showed the bulk phases of the fresh and used catalysts characterized by XRD. The bottom spectroscopy showed that the support has a bulk MgO phase with good crystallinity after the steam treatment at 450 °C under 20 % water vapor for 24 hours. After loading Au with DP method, the bulk phase of the support changed to $Mg(OH)_2$. Thus the

freshly prepared catalyst by using DP method is actually Au/$Mg(OH)_2$ catalyst. After running for the WGS reaction at 220 °C for over 210 hours, the bulk phase didn't show significant changes. In order to convert the support to MgO, annealing treatment at different temperatures (400 °C, 450 °C and 500 °C in 40 sccm Ar flow) were performed. Figure 3.3 showed the XRD results of the phase changes after annealing at different temperatures. From the XRD results, 400 °C is enough for fully transformation of the bulk phase of the support to MgO. Further annealing at higher temperature didn't show significant changes in the bulk phase. So 400 °C annealing was taken as the standard pretreatment to obtain the Au/MgO catalyst. However, compared with the steamed support before loading Au, the MgO peaks showed peak broadening after annealing. This may be due to the decomposition of the $Mg(OH)_2$ and the resulted MgO phase was not as crystalline as the fresh support. Also as shown in Figure 3.2, after exposure to the WGS gas mixture at 220 °C for 210 hours, the bulk phase didn't show much changes.

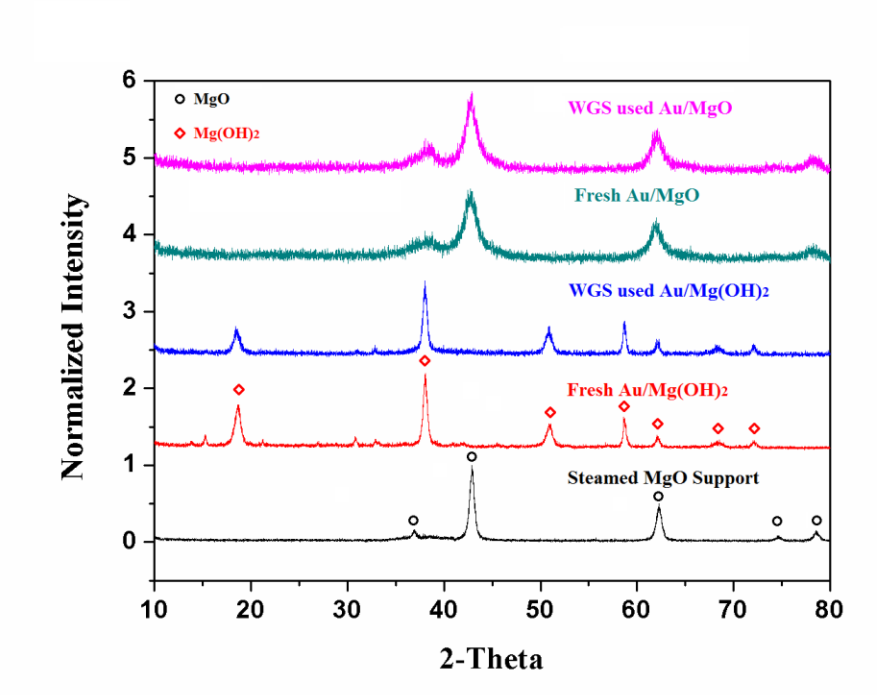

Figure 3.2 XRD on the Au/$Mg(OH)_2$ and Au/MgO

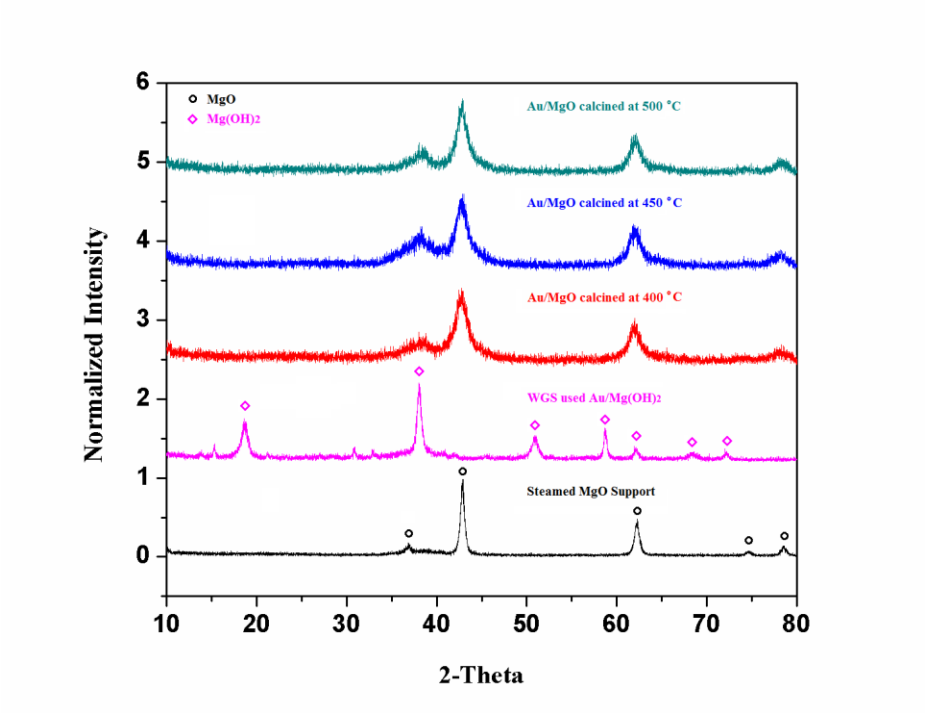

Figure 3.3 XRD on the Au/MgO catalysts after annealing at different temperatures

3.3.2 TEM results

The activity of supported Au catalysts is strongly dependent on the Au particle sizes. Thus it is critical to know the Au particle size distribution of the Au/MgO and Au/$Mg(OH)_2$ catalysts. HAADF-STEM analysis was performed on the used catalysts to better reveal the small and hidden Au particles. Figure 3.4 showed typical HAADF-STEM images that were used to measure the Au particle size distribution for Au/MgO and Au/$Mg(OH)_2$. Uniform Au particles were formed on the Au/$Mg(OH)_2$ catalyst. But after annealing treatment, the Au particles sintered and larger Au particles appeared. Statistics was performed on more than 300 Au nanoparticles for each catalyst and the number average Au particle sizes are 2.1±0.4 nm for Au/$Mg(OH)_2$ and 4.1±0.4 nm for Au/MgO after WGS reaction, respectively as shown in Figure 3.5. The Au particle morphology was checked by HRTEM. As shown in Figure 3.6, both catalysts show Au particles of similar cubo-octohedral shapes. Even after annealling at higher temperature (> 400 °C), gold particle on MgO remains the same structure as that on $Mg(OH)_2$ and only particle size increased.

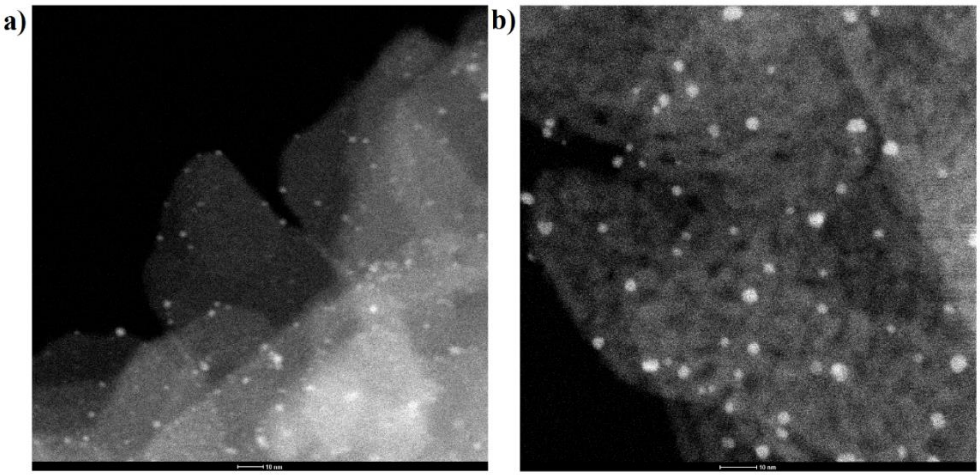

Figure 3.4 Typical HAADF-STEM images of a) Au/$Mg(OH)_2$ and b) Au/MgO catalysts, respectively, used to determine the Au particle size distributions.

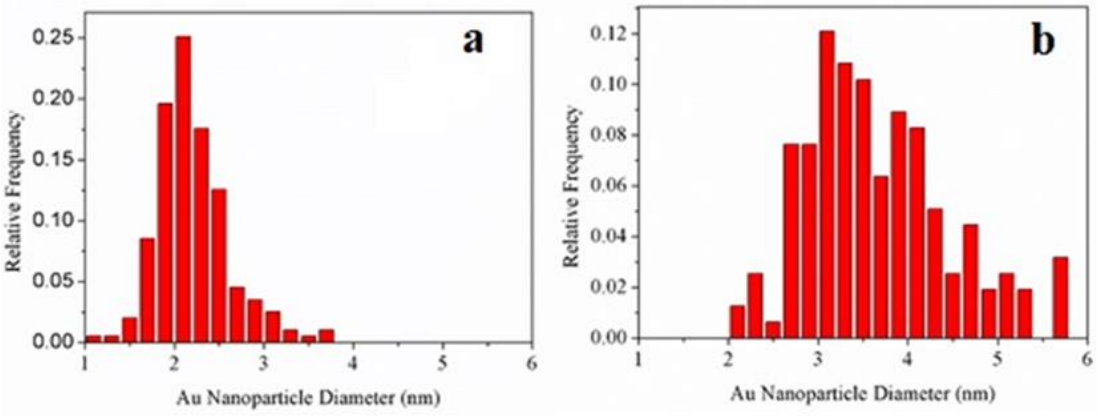

Figure 3.5 Au particle size distribution of a) Au/$Mg(OH)_2$ and b) Au/MgO

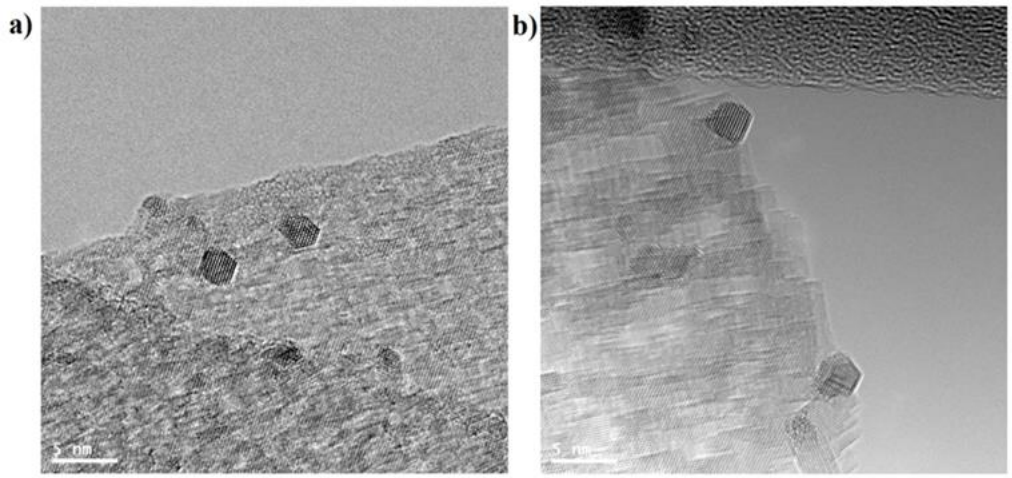

Figure 3.6 Typical HRTEM images for a) $Au/Mg(OH)_2$ and b) Au/MgO

3.3.3 WGS kinetics

Figure 3.7 showed the typical Arrhenius plot and reaction order plot of Au/MgO catalyst. The standard conditions for the rates reported were 220 ℃ and a feed composition of 6.8% CO, 8.5% CO_2, 21.9% H_2O, and 37.4% H_2. The Au loadings determined from AA are all around 2.5 wt%. The WGS reaction rates were normalized by total moles of Au. Table 3.1 showed WGS reaction rates per mole of Au at 220 °C over Au/MgO and $Au/Mg(OH)_2$ catalysts.

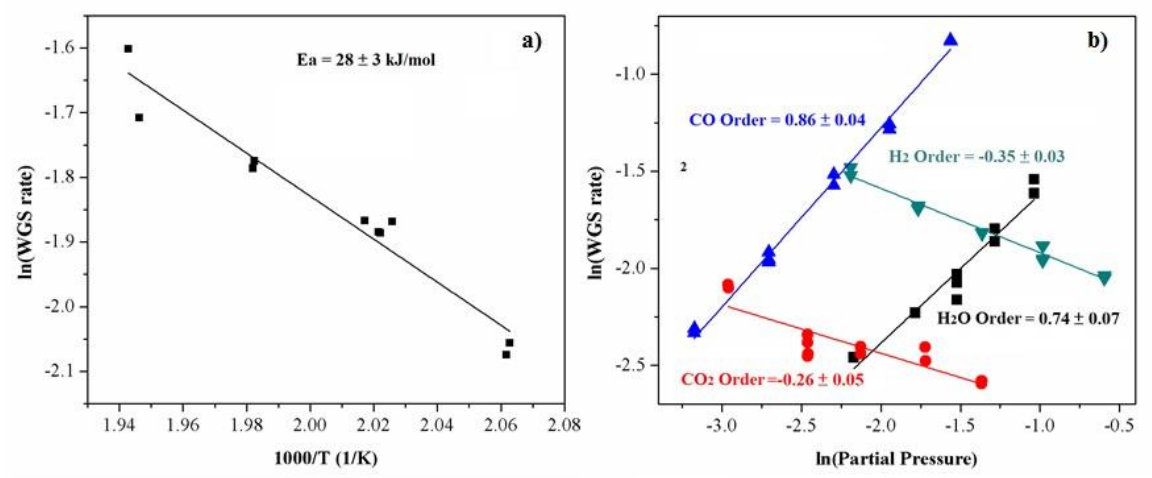

Figure 3.7 a) Arrhenius plot and order plots of Au/MgO, b) Apparent orders plot.

Table 3.1 WGS kinetics of Au/MgO and Au/$Mg(OH)_2$

Support	WGS Rate per mole of Au at 220°C/ 10^{-3} mol H_2 (mol metal)$^{-1}$ s^{-1}	Ea /kJ(mol)$^{-1}$	H_2O	CO_2	CO	H_2
$Mg(OH)_2$	1.5	29	1.00	-0.27	0.80	-0.31
MgO	1.6	28	0.74	-0.26	0.86	-0.35

Au/MgO and Au/$Mg(OH)_2$ showed similar WGS reaction rates per mole of Au at 220 °C. They also showed similar apparent reaction orders with respect to CO, CO_2 and H_2. However, Au/MgO has a lower H_2O order compared with Au/$Mg(OH)_2$ (~0.7 vs. ~1.0). The negative CO_2 and H_2 orders indicate the inhibitory effects of these gases. The CO order is close to 1, which implies a weak binding of CO on the surface.

KIE has been widely used to study the reaction mechanism. Due to the difference in mass of Deuterium (D) and Hydrogen (H) atoms, it will have different zero-point energy for D

and H. So by replacing H with D, the overall rate could be influenced if H bond is involved in the RDS. KIE experiment results are shown in Table 3.2. The KIE ratio was calculated by dividing the rate measured with H_2/H_2O by rates measured with D_2/D_2O. Au/MgO and $Au/Mg(OH)_2$ showed similar KIE ratio (~2.0). This implies a similar rate determining step on these two different catalytic system. The relatively high KIE ratio also implies the participation of hydroxyl groups in the rate-determining step (RDS).

Table 3.2 KIE experimental results of Au/MgO and $Au/Mg(OH)_2$

Sample	WGS Rate per mole of Au at 220 °C (10^{-3}/s) with H_2-H_2O	WGS Rate per mole of Au at 220 °C (10^{-3}/s) with D_2-D_2O	KIE Ratio (H_2/D_2)
Au/MgO	1.6	0.8	2.0±0.3
$Au/Mg(OH)_2$	1.5	0.8	2.0±0.1

3.3.4 *Operando* FTIR

Figure 3.8 showed the *operando* FTIR spectra collected at different time under the standard WGS reaction condition at 220 °C. A sharp peak at around 3700 cm^{-1} were observed and the intensity decreases with the stabilization time. The peak at 3770 cm^{-1} is assigned to O-H stretching of adsorbed hydroxyl group. The peaks at 2830 and 2730 cm^{-1} are assigned to C-H stretching of formate species. C-H peak area didn't change much during the stabilization. The peak at 1040 cm^{-1} is assigned to O-C-O stretching of carbonate species. During the stabilization, the O-H peak area decreased with time while the O-C-O peak area increased.

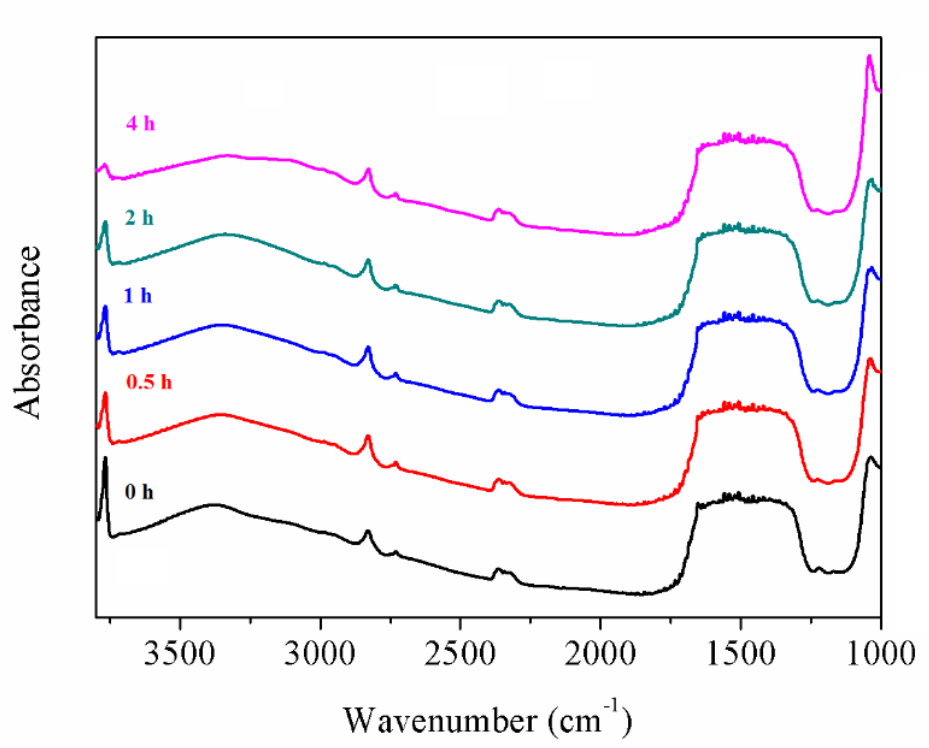

Figure 3.8 IR Spectroscopy of Au/MgO at different time at 220 °C

During the stabilization process, WGS rates per mole of Au were also measured. The WGS rates and the peak areas changes with respect to time are plotted in Figure 3.9. The WGS rates per mole of Au were plotted as the red dots. About 50% deactivation of the WGS rates were observed after 12 hours reaction. But most of the deactivation happened in the first 4 hours and the WGS rates tend to stabilize in the following 8 hours. IR peak area of the formate species showed no significant changes during the stabilization process. The IR peak areas show an initial drop for the hydroxyl group and an initial rise for the formate, but we are not able to get a rate value until 30 minutes on stream. The rate, OH area, and CH area for formate all show a similar trend after the 30 minute point, as is shown further in Figure 11 in the discussion section below.

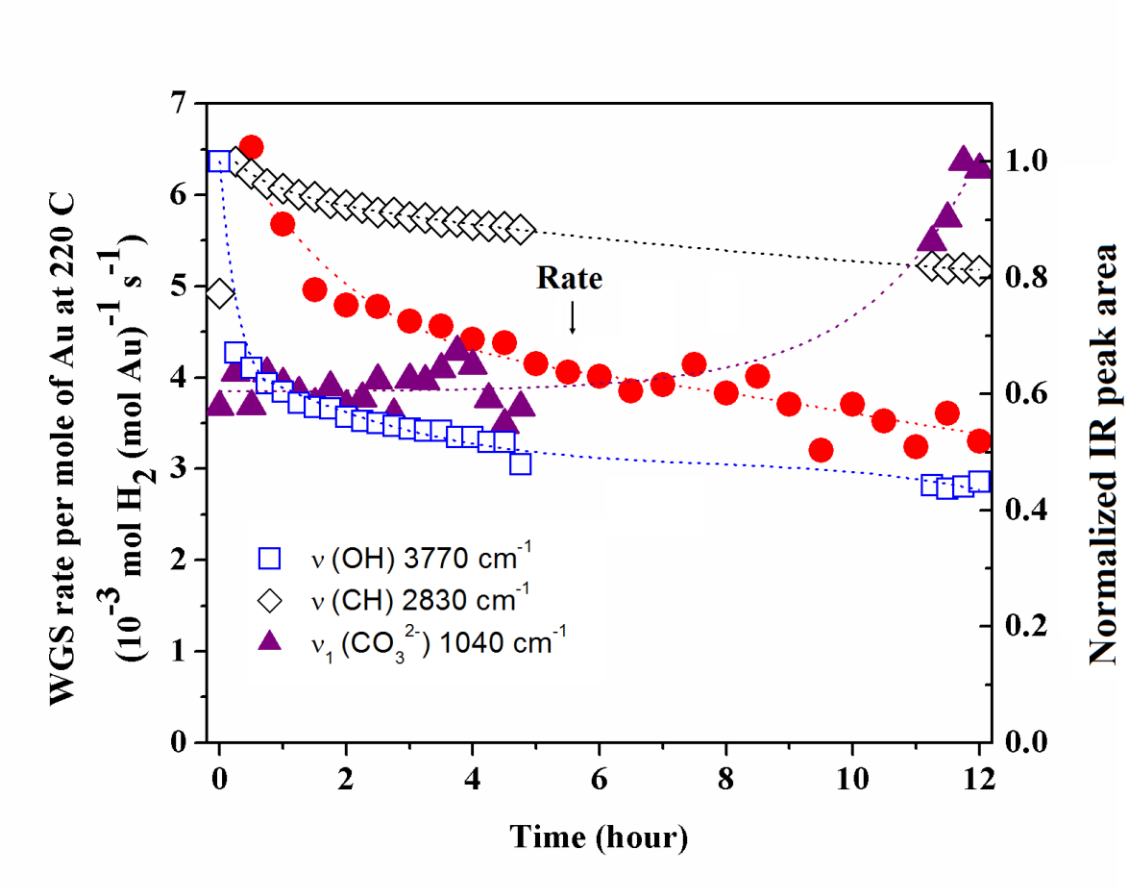

Figure 3.9 WGS rate and IR peak areas change during stabilization

3.3.5 CO Temperature-programmed Desorption FTIR

The IR spectra under different gas conditions are shown in Figure 3.10. For the Au/MgO catalyst, after reduction and annealing pretreatment, there are mainly two peaks. One peak is at around 3750 cm^{-1}, which is assigned to adsorbed hydroxyl group from H_2O dissociation [35]. The other is a broad peak at around 3600 cm^{-1} which is assigned to adsorbed molecular H_2O [35]. The hydroxyl group is strongly bound to the surface and can't be completely removed by just annealing at 400 °C (as shown in Figure A3.3).

However, the introduction of CO could partially reduce the IR peak area of the hydroxyl group. The IR spectra during the CO TPR process is shown in Figure 3.11. As shown in Figure 3.11a, as temperature increases from 220 °C to 360 °C, the 3750 cm^{-1} peak intensity gradually decreases. This implies that the hydroxyl group on the Au/MgO catalyst is reactive towards CO.

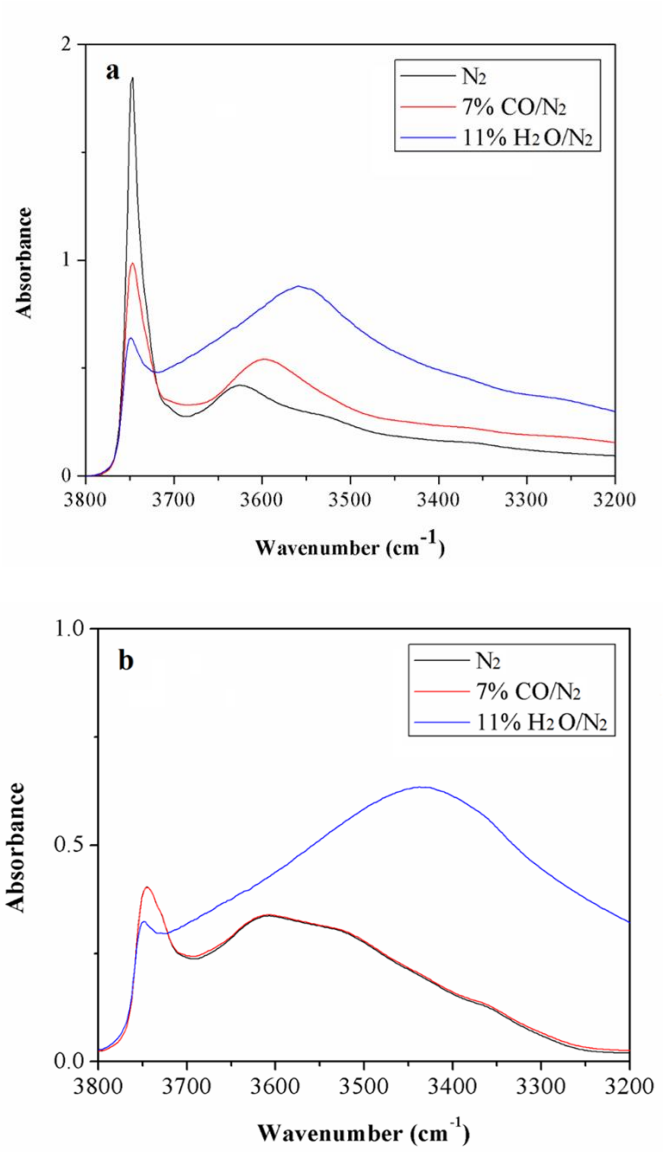

Figure 3.10 IR spectra under different gas compositions of a) Au/MgO, b) MgO support

As a comparison, CO TPR experiments were also performed on the MgO support. The IR spectra during the temperature ramping is shown as Figure 3.11b. We still observe the 3750 cm^{-1} and 3600 cm^{-1} peaks. However, on the MgO support, the 3750 cm^{-1} peak intensity is significantly lower than that of Au/MgO (although at the same amount of samples). Introduction of CO didn't change the hydroxyl group intensity on the MgO surface. Even during the temperature ramping process, there is no significantly change in the 3750 cm^{-1} peak intensity. On the contrary, the 3600 cm^{-1} peak assigned to adsorbed molecular H_2O decreased during the temperature ramping. This shows that the hydroxyl group on the MgO surface is not reactive towards CO. Also the hydroxyl group is more strongly bonded than the molecular H_2O on the surface.

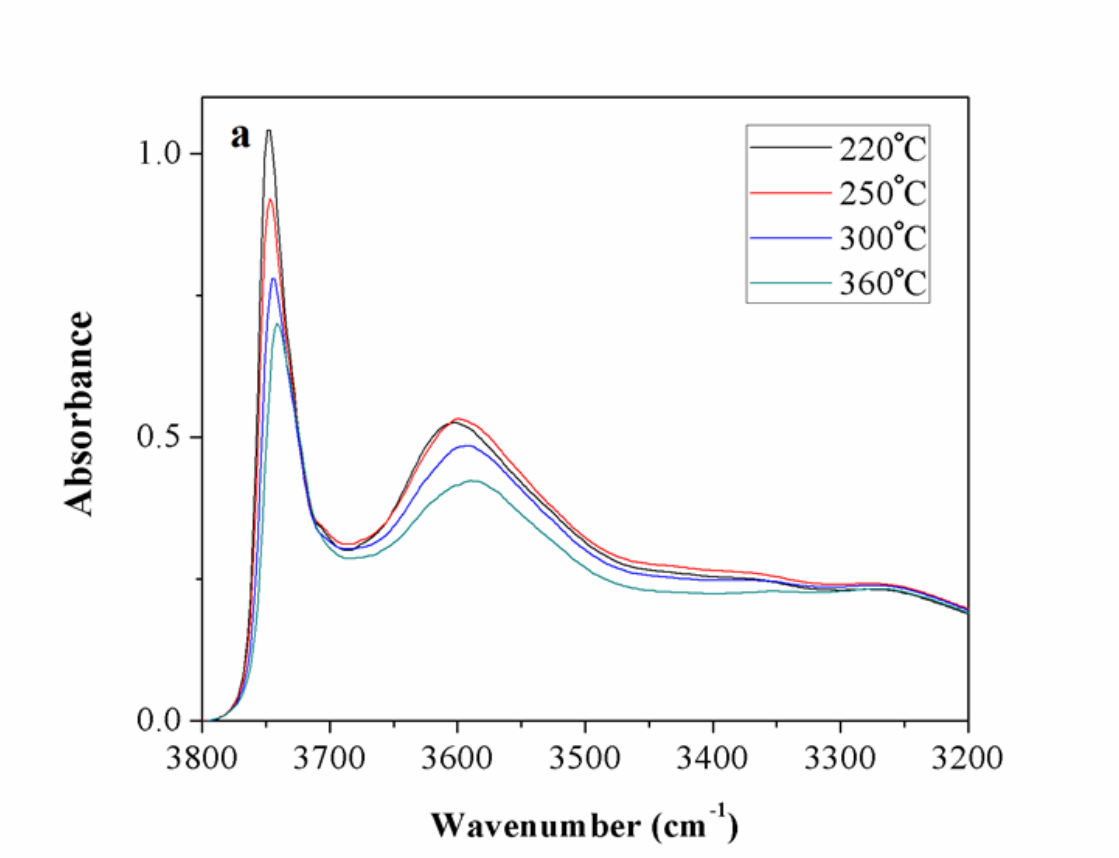

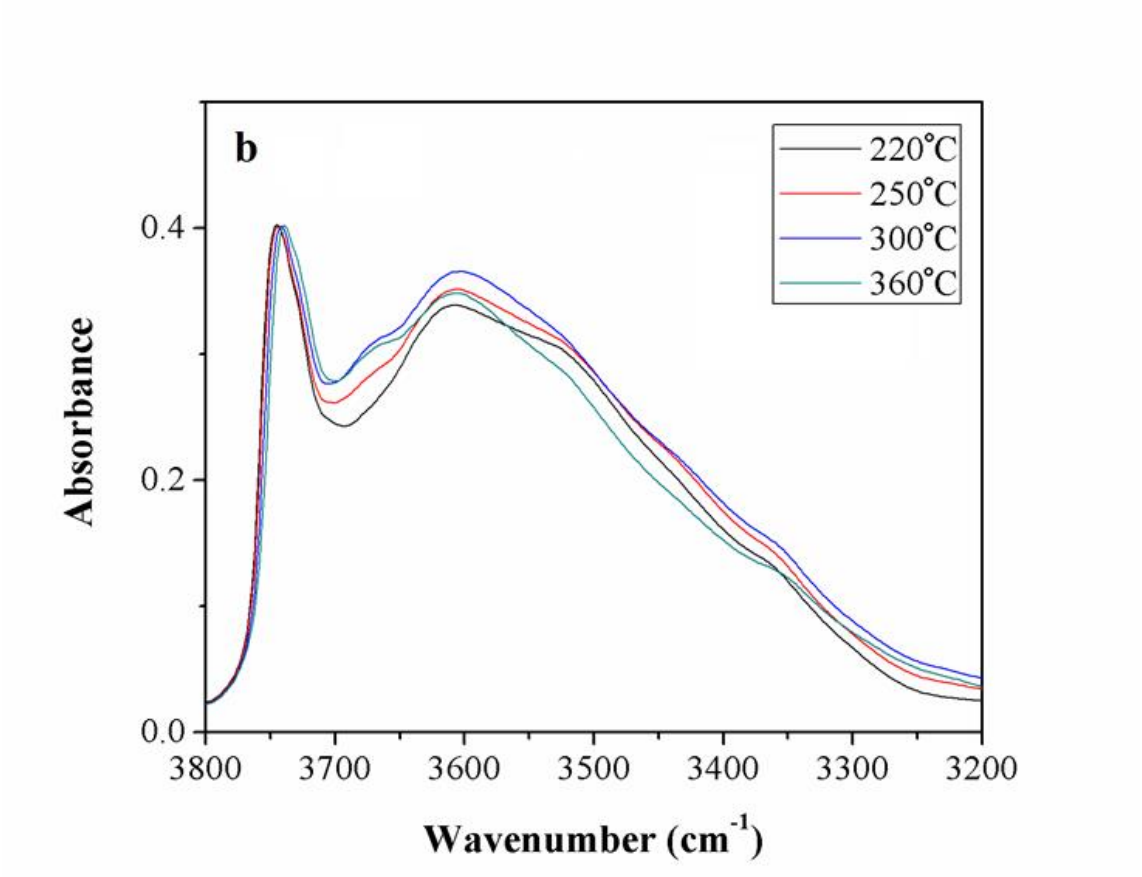

Figure 3.11 CO TPR FTIR spectra of a) Au/MgO, b) MgO support.

It is interesting to note that formate is also formed during the CO TPR experiment. Figures A3.4 and A3.5 show the IR spectra as a function of temperature. The major peak at around 2830 cm^{-1} is assigned to C-H stretching of bridge formate. The peaks at 2820 cm^{-1} is assigned to C-H stretching of unidentate formate. The peaks at 2755 and 2720 cm^{-1} are assigned to C-H stretching of bidentate formate.

The trends in the peak areas in the both the OH and CH stretching regions, fit by using Casa XPS, plotted versus the temperature are shown in Figure 3.12. For Au/MgO, the OH peak areas decreased by about 24% while that for CH (2775 to 2900 cm^{-1}) increased with temperature, with the biggest changes occurring at 300 ºC and above. For the MgO support

alone, no significant change was observed in the OH region, but the CH region a growth in area similar to that seen on Au/MgO occurred, but started at a 250 ºC rather than 300 ºC. Also from Figure 3.12, Au/MgO showed about 2 times higher initial peak area compared to the MgO support.

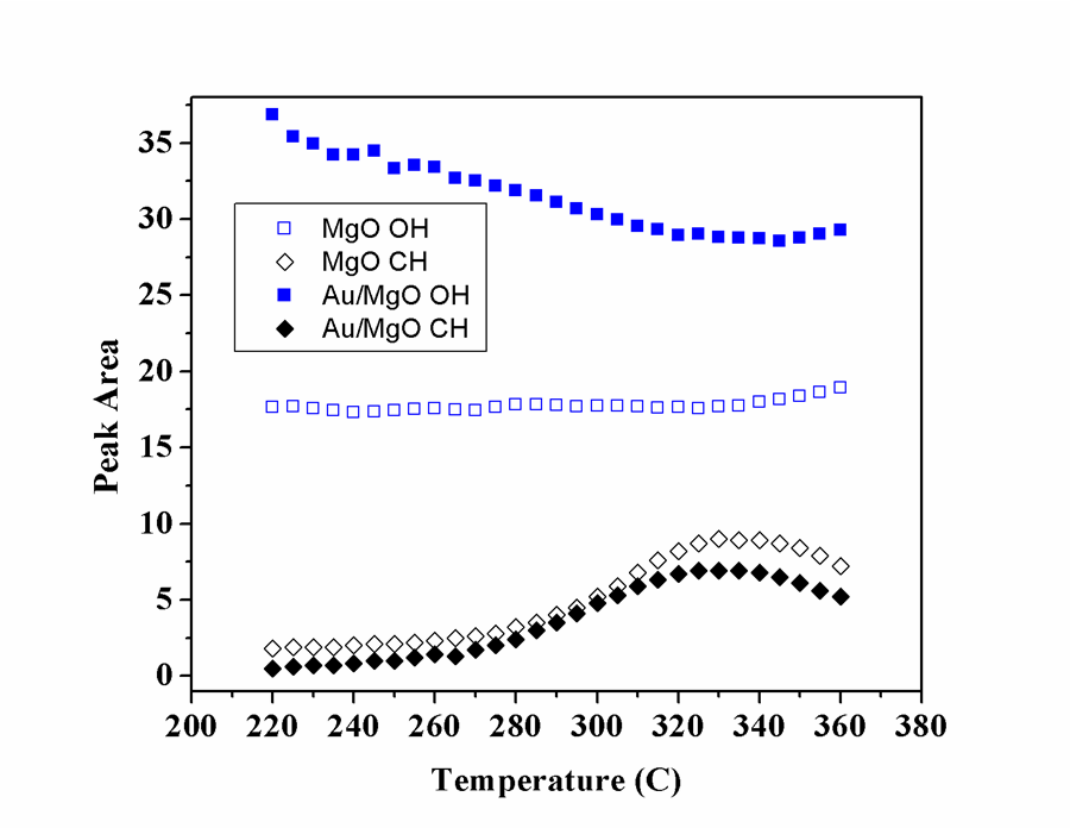

Figure 3.12 IR peak area changes in the OH and formate CH stretching regions during CO TPR

3.4 Discussion

3.4.1 Comparison of MgO and $Mg(OH)_2$ as supports for WGS

Deposition precipitation (DP) is a common method used for gold catalyst synthesis.

However, the deposition of Au on $Mg(OH)_2$ is very difficult as we always produced very low gold loadings (<0.5%), probably due to its very high PZC (point of zero charge). Here, we modified this method. Uniform particle size distribution was obtained on $Au/Mg(OH)_2$ with 2.1±0.4 nm. To synthesize Au/MgO directly, complicated procedures are required and expensive gold precursors are needed. We demonstrated direct conversion of $Au/Mg(OH)_2$ to Au/MgO with annealing at above 400 °C . Both the XRD (Figure 3.3) results have shown that MgO support can be obtained with the annealing pretreatment. However, usually gold catalysts tend to sinter easily. Under this severe annealing conditions, gold particle shape (Figure 3.6) didn't change while only the number average Au particle diameter increased from 2.1 to 4.1 nm.

3.4.2 Implication of WGS kinetics

Au/MgO showed similar WGS rate per mole of Au with $Au/Mg(OH)_2$ at 220 °C. However, from the HAADF-STEM results, the number average Au particle diameter of Au/MgO is about double times of the number average Au particle diameter of $Au/Mg(OH)_2$. Since the activity of supported Au catalysts is strongly dependent on the Au particle sizes. In order to fairly compare the WGS activity of the Au/MgO and $Au/Mg(OH)_2$ catalysts, WGS rates should be compared at the same Au particle sizes.

HRTEM revealed the Au nanoparticles possess a cubo-octohedral shape. From our previous results [13, 14], the Au atoms at the metal-support interfaces are proved to be the active sites. The WGS rates were correlated with the number average Au particle diameter (d) by $d^{-1.8}$ or $d^{-2.9}$ depending whether the perimeter Au atoms or corner Au atoms are the

dominant active sites (Figure A3.4). Based on these relations, the WGS rate per mole of Au at 220 °C of Au/MgO is estimated to be 4~8 times higher than that of Au/$Mg(OH)_2$ if Au/MgO has the same number average Au diameter as Au/$Mg(OH)_2$. So MgO is inferred to be a better support for WGS than $Mg(OH)_2$.

The apparent activation energy and apparent reaction orders could give us further information about the surface specie coverages. If a catalytic reaction follows a Langmuir-Hinshelwood type of mechanism, the intrinsic reaction rate is a direct function of the relative surface concentrations of the adsorbed species that are actively involved in the reaction mechanism. The measured apparent kinetic parameters (activation energy and reaction orders) are hence dependent on the relative surface concentrations of the adsorbed reactive species. A simple estimation of the relative surface concentrations by using apparent reaction order could be

$$\theta_A = 1 - 2n_A$$

Where θ_A is the relative surface coverage and n_A is the apparent reaction order of reactant A.

In the case of WGS reaction, the apparent CO and CO_2 orders can be used to gauge the relative size of the carbon pool while the apparent H_2O and H_2 orders yield similar information about the hydroxyl pool (generated due to adsorption and dissociation of water on the catalytic surface). Most importantly, since the measured reaction rate directly depends on the number of 'dominant' active sites on the catalyst surface, the apparent reaction orders are related to the relative surface concentrations over these dominant active sites.

Au/MgO and Au/$Mg(OH)_2$ almost showed the same kinetic parameters. This implies that

they shared similar WGS reaction mechanism. The only significant difference exists for the apparent reaction order with respect to H_2O. Au/MgO has a lower H_2O order compared with Au/$Mg(OH)_2$ (0.7 vs. 1.0). Based on our discussion above, this is an implication that the Au/MgO has a higher relative coverage of hydroxyl groups on the surface, which could be due to a higher H_2O affinity. Comparison with the WGS rates and H_2O orders of other oxide supported Au catalysts revealed that the lower H_2O order tends to increase the WGS rates (Figure A2.7). Since the H_2O order is closely related with hydroxyl group coverage on the surface, this implies the hydroxyl group may participate in the rate-determining step which influences the overall reaction rate. This is further proved by the *operando* FTIR results.

3.4.3 *Operando* FTIR

In order to directly observe the adsorption species changes during the WGS reaction, *operando* FTIR was performed on the Au/MgO catalyst. During the stabilization process of the FTIR experiment, the Au particles will sinter and surface species coverage will change. This will cause the WGS rate to decrease as time goes by. The IR peak area is direct reflection of the surface coverage of the corresponding adsorption species. *Operando* FTIR provides the advantage to measure WGS rates and IR spectroscopy at the same time. So the correlation between WGS rate and the IR peak areas will be useful to determine the critical adsorption species influencing the WGS catalytic process. Plots of the WGS rates vs. normalized IR peak areas measured at the same time produced the correlations in Figure 3.13. As shown, the WGS rate followed a positive linear correlation with both the peak

area due to the hydroxyl group and that due to formate. There is no corresponding correlation between the O-C-O peak area from carbonate, which implies that it is a spectator in this reaction. Another interesting feature of note is the weak adsorption of CO. Usually CO adsorbed on metallic Au will show a peak near 2100 cm^{-1}, but, as shown in Figure 3.7, no clear peak could be identified at that wavenumber. This is consistent with the results of the measurement of kinetics, where the apparent reaction order with respect to CO is high, indicating low coverage and weak adsorption of CO.

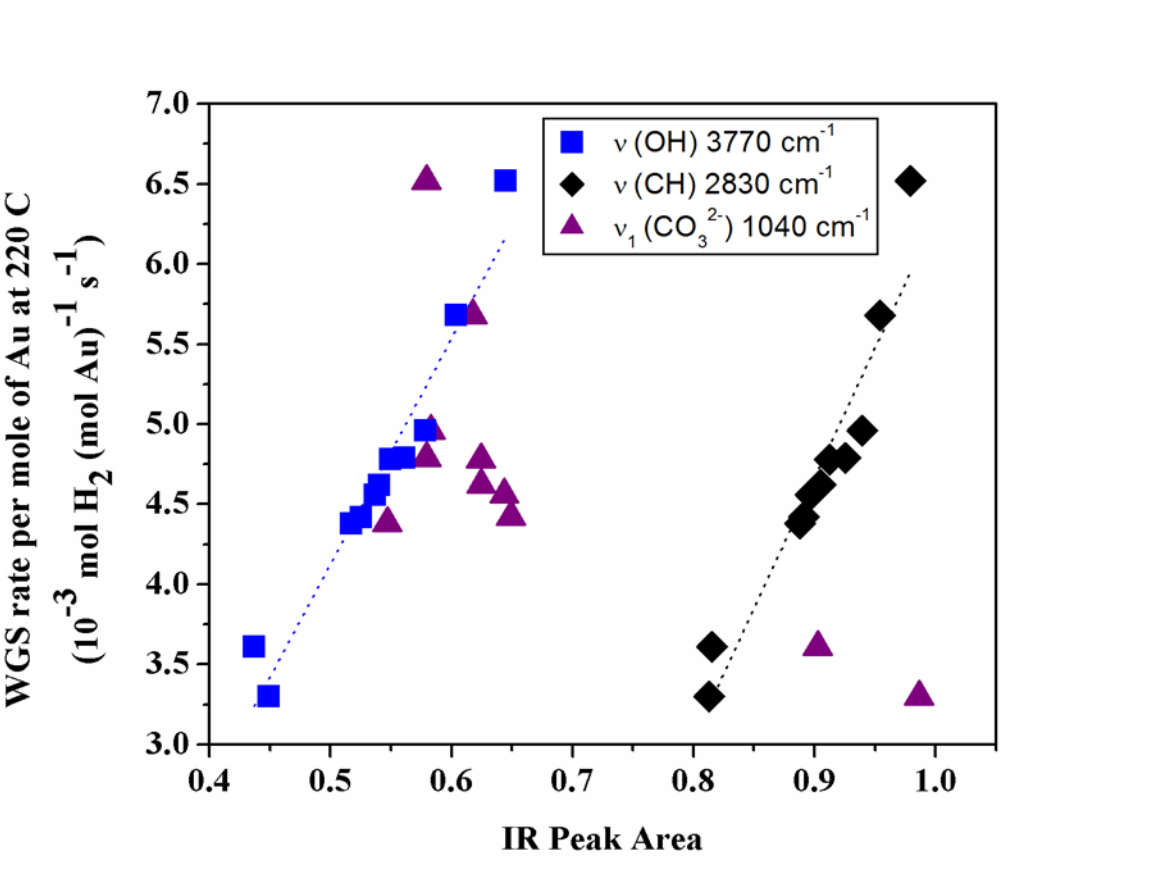

Figure 3.13 Correlation between WGS rates and IR peak areas

3.4.4 CO TPR experiments

To better understand the origins of the hydroxyl groups and their reactivity towards CO, CO TPR experiments were performed. Figure 3.10 showed the typical IR spectra for the Au/MgO catalyst and MgO support in 50 sccm N_2, 7% CO/N_2 and 11% H_2O/N_2 after annealing at 400 °C. Salvatore etc. has reported the IR spectra of hydroxyl groups on MgO powder [33] and they assigned the IR peak at 3750 cm^{-1} to the adsorbed hydroxyl groups from dissociated H_2O and the broad IR peak at 3600 cm^{-1} to the adsorbed molecular H_2O. The spectra reported in this work is a good match with their observation. As shown in Figure 3.10, even after annealing at 400 °C, there are still hydroxyl groups on the Au/MgO catalyst and MgO support. This implies that the hydroxyl groups are strongly bonded to the MgO surface.

However, the 3750 cm^{-1} peak intensity of Au/MgO in Figure 3.10a is significantly higher than that of MgO support as shown in Figure 3.10b. This result implies that the existence of the Au-MgO interface significantly enhances or stabilizes dissociative water adsorption. It is also interesting to observe that the 3750 cm^{-1} peak area is significantly decreased by introduction of CO gas over Au/MgO, while for MgO alone the peak intensity not affected at all (it overlaps with the IR spectra in N_2). This shows clearly that the hydroxyl group due to dissociated H_2O adsorption is only reactive to CO when the Au-MgO interface exists. Introduction of 50 sccm/min of 11% H_2O/N_2 at 220 °C significantly decreased the 3750 cm^{-1} peak and increased the 3600 cm^{-1} peak. This process is irreversible since, as shown in Figure A3.3, switching the gas back to 50 sccm/min of pure N_2 did not increase the 3750 cm^{-1} peak to its original intensity even when the temperature was ramped to 360 °C with a

ramping rate of 5 °C/min, in fact, the intensity changed very little as the temperature increased. The 3600 cm^{-1} peak, which is due to molecular H_2O adsorption, decreased as temperature increased, but the the observation that all the molecular water was not removed at 360 °C suggests that some water was strongly hydrogen bonded to the OH groups.

The CO TPR results shown in Figure 3.11 give further evidence for the reactivity of hydroxyl groups. On the Au/MgO catalyst, the intensity of 3750 cm^{-1} peak decreased with temperature in presence CO. However, on MgO support, the intensity of 3750 cm^{-1} peak didn't change with temperature. Quantification of the peak areas showed about 24% decrease for the Au/MgO but almost no change for the MgO support. This further supports the conclusion that in order for the hydroxyl group to react with CO, the Au-MgO interface is necessary. The quantification also showed that the area of the hydroxyl group peak for Ag/MgO was about two times higher than that for MgO for IR wafers of similar weight. This result is not straightforward to interpret, because the extinction coeffients for OH at the interface and OH on the MgO surface away from the interface are not known. It is not inconsistent, however, with the assumption that OH concentration is enhanced at the interface.

The CO TPR results here are in good accord with the *operando* FTIR results and the DFT calculation results discussed below. The presence of the Au-MgO interface appears to enhance H_2O dissociation, consistent with the finding from DFT that addition of Au reduces the energy barrier for H_2O dissociation from 1.12 eV (on MgO support) to almost 0 eV (at Au-MgO interface) [36]. Furthermore, it is these hydroxyl groups that are reactive towards CO. This provides an explanation for the correlation between the WGS rate and hydroxyl group peak area observed in *operando* FTIR experiments during catalyst

stabilization, where sintering is assumed to reduce the total number of interfacial sites.

The final remaining issue is role of formate. While the correlation of the fomate peak area with the WGS rate of reaction suggests that formate could be a rate determining intermediate, the CO TPR results speak strongly against that assumption. The rate measurements show clearly that Au is essential for a significant rate, but the IR measurements during the CO TPR measurements show that fomate is formed at least as readily on the bare MgO support as on the Au/MgO catalyst. Furthermore, formate appears on the catalyst only well above the temperature were rates were measured and grows to higher intensity with a further increase in temperature. That behavior suggests that the formate is a stable species, not an intermediate that is reactive at 220 ºC . Also from the DFT calculation results [36], the energy barrier of the formate formation over Au/MgO is 1.40 eV. While for the carboxyl formation step, the energy barrier is 0.57 eV. The theoretical results imply that the formate formation is more difficult than the carboxyl group. The formate formation step is not as competitive as the carboxyl formation step. Also as temperature increases, formate formation will be more favored.

3.4.5 DFT calculation

DFT calculations were performed to better understand the special chemistry generated at the metal oxide interface and to get a more profound understanding of the WGS mechanism over the Au/MgO catalyst. Details of these results are reported in reference [36], but the major conclusions are summarized here. It was found that, with the exception of H2O, all the species bind more strongly at the Au/MgO interface than on the clean Au(111) or

MgO(100) surfaces. CO tends to adsorb on the interface Au atoms. Most importantly, the H2O dissociation energy barrier is decreased from ~2eV on Au(111) to essentially zero at the Au-MgO interface. The adsorption of OH is also favored at the Au-MgO interface. The calculations show further that H adsorbed on surface oxygen forms a strong hydrogen bond to the dissociated OH group to give a co-adsorbed (H+OH)*# pair, where * and # indicate metal and oxide sites. The co-adsorbed pair is 0.53 eV more stable than infinitely separated OH and H groups. These findings are in accordance with the conclusions from CO TPD experiments that the hydroxyl group peak intensity is enhanced on Au/MgO catalyst than MgO support.

Generally, there are two types of reaction mechanisms for WGS, redox and associative. In the redox mechanism, the RDS is the reaction of adsorbed CO with O to form CO_2. The oxygen comes from either the support or adsorbed oxygen. While in the associative mechanism, the rate-determining step is either the adsorbed CO reacting with the adsorbed OH groups to form COOH or the decomposition of COOH, requiring either an empty site or reaction the neighboring adsorbed OH. Two important findings of computational and modeling studies [36] are 1) that COOH formation has a high degree of rate control and is, therefore, the rate determining step and 2) strong hydrogen bonding exists between adsorbed OH and its nearby adsorbed H neighbor as a result of water dissociation at the Au/MgO interface. We propose that this latter finding can account for the measured KIE since the hydrogen bonding in the (H+OH)*# pair must be broken to form the CO-OH bond. The presence of a KIE also rules out the redox mechanism because no bonds to hydrogen are made or broken in its rate determining step. The computed barriers for the full associative mechanism are reported in [36].

3.5 Conclusion

Au/MgO and Au/$Mg(OH)_2$ was successfully prepared by deposition precipitation method with urea. Au/MgO showed similar WGS kinetics with Au/$Mg(OH)_2$ except for a lower H_2O order. The lower H_2O order implies a difference of the H_2O affinity of the two different catalyst systems. WGS rates have a positive correlation with hydroxyl group coverage. The RDS on the Au/MgO system is identified as the carbonate formation. H_2O adsorption affinity influences the WGS rate by changing the hydroxyl pool on the surface in the RDS. Thus H_2O order and hydroxyl group surface coverage may be adopted as a potential descriptor for active WGS catalysts.

CHAPTER 4. THE ROLE OF PT NANOPARTICLES AS THE ACTIVE SITES FOR THE WATER-GAS SHIFT REACTION

4.1 Introduction

Water-gas shift reaction (WGS) is an important reaction in industry for producing high-purity hydrogen which can be utilized for ammonia synthesis and petrochemical hydro-processing as well as fuel cells. Since WGS is exothermic, it has higher equilibrium conversions at low temperatures, and thus it is desired to have catalysts with higher rates per unit volume to operate at low temperatures. The commercial low temperature catalyst is usually Cu-ZnO-Al_2O_3. However, this type of catalyst is hard to pretreat and easy to sinter during the reaction. In order to overcome these disadvantages, Pt supported on oxides have been identified as a class of active catalysts such as Pt/TiO_2, Pt/Al_2O_3, Pt/CeO_2 etc.[37-39] They have good stability under the harsh reducing environment of steam reforming gas conditions. On the other hand, the catalytic activity of supported Pt catalysts is strongly dependent on the support type. Therefore, they are also good model catalyst systems for studying the metal-support interaction and providing in-depth understanding of the fundamental catalytic processes.

It has been shown that Pt supported on a ‘reducible’ support (such as TiO_2) is more active than Pt on a ‘non-reducible’ support (such as Al_2O_3). [40, 41] This has been attributed to

the more oxygen vacancies on the reducible support which could facilitate the H_2O dissociation. [42, 43] However, usually multiple types of Pt species, including single Pt

atoms, Pt clusters and Pt nanoparticles coexist on the support. Thus, it is difficult to distinguish the activity of different Pt species, and the active sites of supported Pt are still under debate. Andreas Heyden etc have reported that increasing the support oxygen vacancies could promote the WGS activity and the Pt-support interfaces are the active sites. [44, 45] However, Maria Flytzani-Stephanopoulos et al. have claimed that single Pt atoms stabilized by Na are the active sites. [46, 47] Recently, Peter Stair et a1. reported the identification of Pt nanoparticles as the active sites for the CO oxidation and water-gas shift reaction by differentiating the reaction activity of different adsorbed CO species with infrared spectroscopy. [48] Ribeiro et a1. have utilized time-resolved IR spectra during transient WGS with $^{12}CO/^{13}CO$ and $^{12}CO_2/_{13CO2}$ to study the active sites of Pt/Al_2O_3.They reported that the active carbon containing intermediate species occupy less than 1% of the Pt surfaces and addition of Na increases the coverage to nearly 100% of the Pt surface.[56] These results give a more in-depth understanding of the active sites of the Pt catalysts.

Another advantage of supported Pt catalysts is that the activity could be significantly enhanced by adding a promoter. It has been extensively reported in the literature that Na promotes Pt catalysts. [49-51] However, the reason for the promotion is not fully understood yet. Burtron Davis et al. have reported that Na addition could change the C-H bond strength which will further influence the overall WGS activity. [51, 52] Dimitris Kondarides et a1. claimed that Na could change the CO adsorption strength at the Pt-support interfaces and at the same time induce more oxygen vacancies on TiO_2. [52, 53]

Both will contribute to the promotion of WGS activity. Richard Mallinson et al. have reported that strong metal-support interaction between Pt and NaOx provide highly active sites at the Pt-NaOx interfaces. [54] Fabio Ribeiro et a1. have reported that Pt remained metallic and CO adsorption properties were modified after Na addition by a combination of WGS kinetics and isotopic transient studies. [55, 56] Thus Na promotes the WGS activity by changing the local electronic properties, and the active sites should be metallic Pt. On the contrary, Maria Flytzani-Stephanopoulos et al. have reported that Na addition facilitates the formation of more single Pt atoms and the active sites are Pt(II)−O(OH)x species.[46, 47]

In this paper, we distinguish the active sites by comparison between some specially designed and prepared catalysts. We report a direct way to identify the active sites of Pt/TiO_2 for the water-gas shift reaction by controllable synthesis of Pt/TiO_2 catalyst without any single Pt atoms. The WGS kinetics of this catalyst are similar to that of the traditional Pt/TiO_2 (which have various Pt species including Pt nanoparticles and single Pt atoms). Thus it is a direct proof that the Pt nanoparticles are the dominant active sites for the water-gas shift reaction. The Na addition on the Pt nanoparticle catalyst showed similar promotion in the WGS rates and the effect of Na is discussed based on the WGS kinetics changes.

4.2 Experimental Methods

4.2.1 Catalyst Preparation

Two methods were utilized to prepare two types of Pt/TiO_2 catalysts with different Pt structures on the support. The first method is incipient wetness impregnation (IWI). Rutile TiO_2 was purchased from Sachtleben Chemie GmbH as the support. $Pt(NH_3)_4(NO_3)_2$ was purchased from Sigma Aldrich and used as the Pt precursor. A 10 mg Pt/ml solution was prepared by dissolving certain amount of Pt precursor in millipore water. The solution was added drop by drop to 1 g support until incipient wetness. The as-prepared catalyst was dried in vacuum at room temperature overnight. It was then reduced in 50 sccm 25% H_2/Ar at 300 °C for 2 hours (5 °C/min ramping). The catalyst is denoted as Pt/TiO_2 IWI.

Pt/TiO_2 with only Pt nanoparticles was prepared by an organic solvothermal method. Generally 0.16 mmol $Pt(acac)_2$ was dissolved in 10 ml oleylamine and 5 ml benzyl ether together with 1 mmol 1-tetradecanediol, 2.8-adamantanecarboxylic acid. The solution was reacted at 200 °C under Ar flow. The temperature was increased to 260 °C after 30 minutes and refluxed for 30 minutes. The solution was then cooled down to room temperature after the reaction. 40 ml iso-propanol and 20 ml ethanol were added to the solution and Pt nanoparticles were centrifuged. The resultant Pt nanoparticles were dispersed in hexane. Rutile support was immersed in the dispersion and sonicated for 30 minutes. Then the precipitates were centrifuged and dried. It was calcined at 185 °C to remove the residue ligands. The catalyst was annealed in 50 sccm O_2 at 400 °C for 2 hours (5 °C /min ramping) to remove the residue organic ligands. The catalyst is denoted at Pt/TiO_2 NP.

The Na promoted Pt/TiO_2 catalysts were prepared by using $NaNO_3$ as the precursor. A calculated amount of $NaNO_3$ was dissolved in millipore water and the solution was added drop by drop to the Pt/TiO_2 catalysts (Pt/TiO_2 IWI or Pt/TiO_2 NP) until incipient wetness. The catalysts were dried in vacuum at room temperature overnight. The dried catalysts were calcined at 250 °C for 2 hours in 50 sccm flow air. The catalysts were pretreated with the same reduction procedure as Pt/TiO_2 catalysts and tested at 280 °C for WGS kinetics.

4.2.2 WGS Kinetics Measurement

The WGS kinetics were measured in an automated setup with four independent parallel tubular plug flow reactor setup as mentioned before. For each run, about 300 mg of catalyst was loaded into the reactor. The catalysts were pretreated by reducing in 25%H_2/Ar at 300 °C for 2 hours with a ramping rate of 5 °C/min. The reduction flow rate was 50 sccm. The catalysts were stabilized at the standard WGS conditions (standard conditions, 6.8% CO, 21.9% H_2O, 8.5% CO_2, 37.4% H_2, and balance Ar) with a flow rate of 75.4 sccm at 300 ℃ for 20 hours until a stable conversion was observed. The temperature was lowered after stabilization to reach a conversion lower than 10% (differential reaction conditions). A more detailed procedure was described in our earlier work [13, 14]. The reaction rates were normalized by mass of catalyst, total moles of Pt, and exposed moles of Pt. The exposed amount of Pt was determined by CO chemisorption. The apparent activation energies were determined from an Arrhenius plot within a 30 ℃ temperature range around the test temperature. The reaction orders were determined by changing the partial pressure

of one reactant or product while maintaining the other partial pressures at the test temperature. The pressure ranges for apparent order determination are 4-21% CO, 5-25% CO_2, 11-34% H_2O and 14-55% H_2 at the test temperature. Less than 10% deactivation was observed during the five-day long kinetic measurement.

4.2.3 Catalyst Characterization

CO chemisorption was performed with a Micromeritics ASAP 2020 instrument to measure the Pt metallic surface area. Reduction pretreatment at 300°C was performed on the Pt catalysts prior to CO adsorption. The Pt/TiO_2 samples were characterized in 'Z-contrast' high-angle annular dark-field (HAADF) mode by using a probe aberration-corrected JEOL ARM200CF STEM equipped with a cold field emission gun and an Oxford XMAX100TLE windowless XEDS detector. *Operando* Fourier Transform Infrared Spectroscopy (FTIR) was performed on the Pt catalyst with a Bruker Vertex 70 FTIR. All spectra were collected at a resolution of 4 cm^{-1} and averaged over 100 scans for the background and 50 scans for the sample under steady state conditions. About 120 mg of Pt catalyst was sieved (<125 micrometer) and pressed into a pellet (~0.5 inch) and loaded into an IR cell. It was pretreated with the same method as was used for the WGS kinetics measurement. After that, the IR background spectra were taken with 50 sccm N_2 flow through the catalyst in the IR cell. 50 sccm $1\%CO/N_2$ was flowed through the IR cell and IR spectroscopy were taken at 100 °C to identify the adsorbed CO species.

4.3 Results

4.3.1 WGS Kinetics

Table 4.1 shows the WGS kinetics measured at 280 °C for different Pt/TiO_2 catalysts. The Pt/TiO_2 IWI catalyst showed very similar WGS kinetics with Pt/TiO_2 NP catalyst, which implies the same WGS reaction mechanism and active sites on the two catalysts. For the catalyst prepared by incipient wetness impregnation method, addition of Na caused an increase in apparent activation energy increase from 60 kJ/mol to 74 kJ/mol, which indicates changes in the active sites. At the same time, the apparent reaction order with respect to CO_2 decreased from -0.03 to -0.15 and apparent reaction order with respect to CO decreased from 0.32 to 0.14 Pt/TiO_2 NP catalyst showed similar trends with Na addition. The CO_2 order decreased from -0.02 to -0.20. The CO order decreases from 0.31 to 0.12. Both Na promoted Pt/TiO_2 catalyst showed similar changes in the apparent reaction orders with respect to CO and an increase in the apparent reaction order with respect to H_2. The changes in the apparent reaction orders indicate a change in the relative surface coverage of the reactive species. All these imply that the active sites have been modified after Na addition.

Table 4.1 WGS kinetics of the Pt/TiO_2 catalysts at 280 °C

Catalyst	Ea (kJ/mol)	H_2O	CO_2	CO	H_2
Pt/TiO_2 IWI	60	0.79	-0.03	0.32	-0.67
Pt-Na(1:10)/TiO_2 IWI	74	0.93	-0.15	0.14	-0.35
Pt/TiO_2 NP	62	0.61	-0.02	0.31	-0.65
Pt-Na(1:10)/TiO_2 NP	77	0.69	-0.20	0.12	-0.27

Table 4.2 shows the WGS rates per mole of Pt and turnover rates (TORs) at 300 °C on different Pt/TiO_2 catalysts. Pt/TiO_2 NP catalyst showed similar WGS rate per mole of Pt at 300 °C compared with Pt/TiO_2 IWI catalyst. Addition of Na promoted the WGS rates per mole of Pt for both catalysts to the same level. Both CO chemisorption and H_2 chemisorption were performed on the catalysts to determine the % Pt exposed. Both CO and H_2 chemisorption showed similar results as shown in Table 4.3. The WGS TOR was obtained by normalizing the WGS rate per mole of Pt by the CO chemisorption results. Pt/TiO_2 prepared by incipient wetness impregnation method showed lower WGS TOR compared with Pt/TiO_2 with only Pt nanoparticles. Na addition will promote the TOR of both Pt/TiO_2 catalysts by a factor about 3.

Table 4.2 WGS rates of the Pt/TiO_2 catalysts at 300 °C

Catalyst	WGS rate per mole of Pt at 300 °C /10^{-2}mol H_2 (mol Pt)$^{-1}$ s^{-1}	TOR /$10^{-2}s^{-1}$	%Pt Exposed
Pt/TiO_2 IWI	3.4	20	0.17
Pt-Na(1:10)/TiO_2 IWI	8.6	57	0.15
Pt/TiO_2 NP	4.3	61	0.07
Pt-Na(1:10)/TiO_2 NP	8.6	172	0.05

Table 4.3 % Pt Exposed determined by CO and H_2 chemisorption

Catalyst	CO Chemisorption	H_2 Chemisorption
Pt/TiO_2 IWI	0.17	0.12
Pt-Na(1:10)/TiO_2 IWI	0.15	0.19
Pt/TiO_2 NP	0.07	0.05
Pt-Na(1:10)/TiO_2 NP	0.05	0.09

4.3.2 STEM Characterization

Figure 4.1 and Figure 4.2 show the STEM images of the Pt/TiO_2 NP catalyst and Pt-Na(1:10)/TiO_2 NP catalyst respectively. For the Pt/TiO_2 catalyst prepared by incipient wetness impregnation, there are multiple types of Pt species on the support, including single Pt atoms, Pt clusters and Pt nanoparticles. A STEM image of the PtNa(1:10)/TiO_2 IWI catalyst was shown in Figure A4.1. Multiple single atom sites are found on this catalyst. However, no single Pt atoms or Pt clusters was observed on the Pt/TiO_2 NP catalyst. So this catalyst ruled out the participation of the single Pt atoms or Pt clusters as active sites for WGS reaction.

It has been reported that Na addition can promote the dispersion of Pt, thus, more single Pt atoms could form on the support. However, on the Pt/TiO_2 NP catalyst here, addition of Na didn't show further dispersion of the Pt species. Only Pt nanoparticles were observed and no other Pt species were observed. High resolution STEM showed a surface full of Na atoms. Contrast analysis showed no single Pt atoms. Based on the STEM results here, the Pt/TiO_2 and Pt-Na(1:10)/TiO_2 NP catalysts have only Pt nanoparticles on the support and can be used as model systems to study the active sites for the WGS reaction.

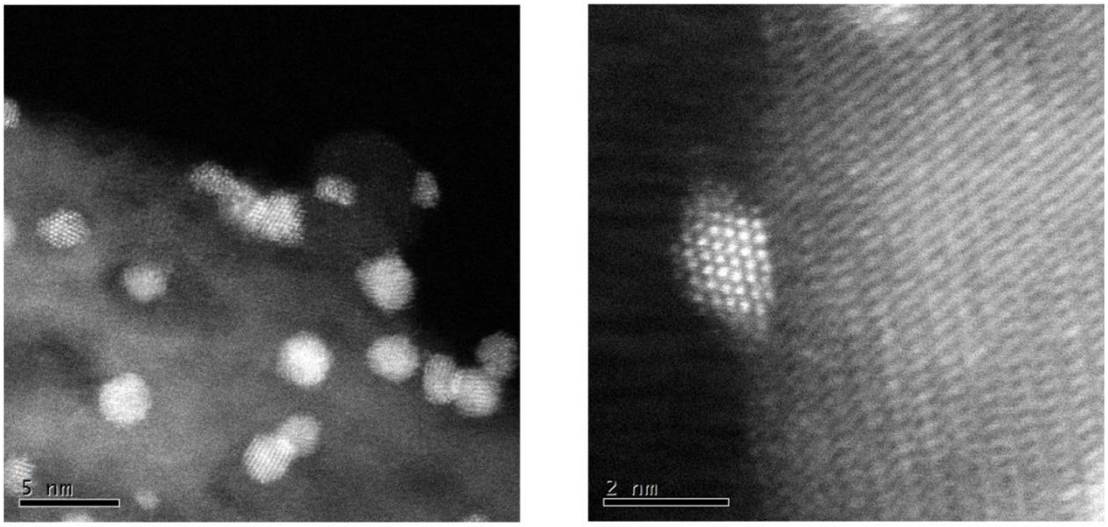

Figure 4.1 STEM images of Pt/TiO_2 NP catalyst

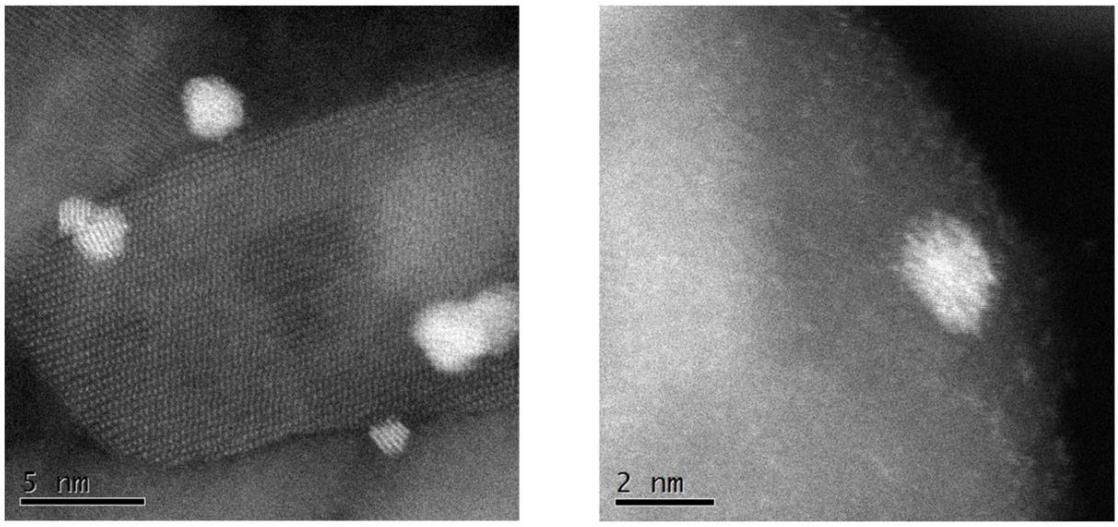

Figure 4.2 STEM images of $Pt\text{-}Na(1{:}10)/TiO_2$ NP catalyst

4.3.3 *Operando* FTIR Experiments

The FTIR results on the Pt/TiO_2 catalysts are shown in Figure 4.3. The Pt/TiO_2 IWI catalysts showed doublet peaks around 2079 cm^{-1} and 2087 cm^{-1}. The peak at higher

wavenumber is assigned to CO adsorbed on cationic single Pt atom while the peak at lower wavenumber is assigned to linearly adsorbed CO on metallic Pt atoms of Pt nanoparticles [48]. However, for the Pt/TiO_2 NP catalyst, only a single peak at around 2084 cm^{-1} was observed. This peak is assigned to CO linearly adsorbed on metallic Pt nanoparticles. No peak due to CO adsorbed on single Pt atoms was observed. This result further elucidates that the Pt/TiO_2 NP is free of single Pt atoms, which is consistent with the STEM results.

The FTIR results on the $Pt\text{-}Na/TiO_2$ catalysts are shown in Figure 4.4. After adding Na, there is a decrease in the intensity of the CO peak. This implies that some Pt is covered by Na. Also the IWI catalyst showed higher peak intensity than NP catalyst. Which is consistent with the CO chemisorption results that IWI catalysts have a higher Pt metallic surface area.

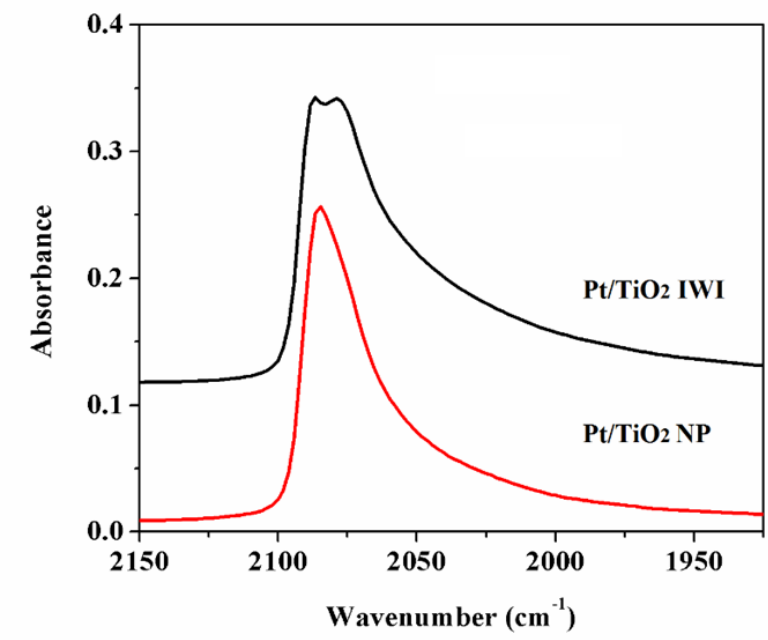

Figure 4.3 FTIR spectroscopy of Pt/TiO_2 catalysts under 1% CO/N_2

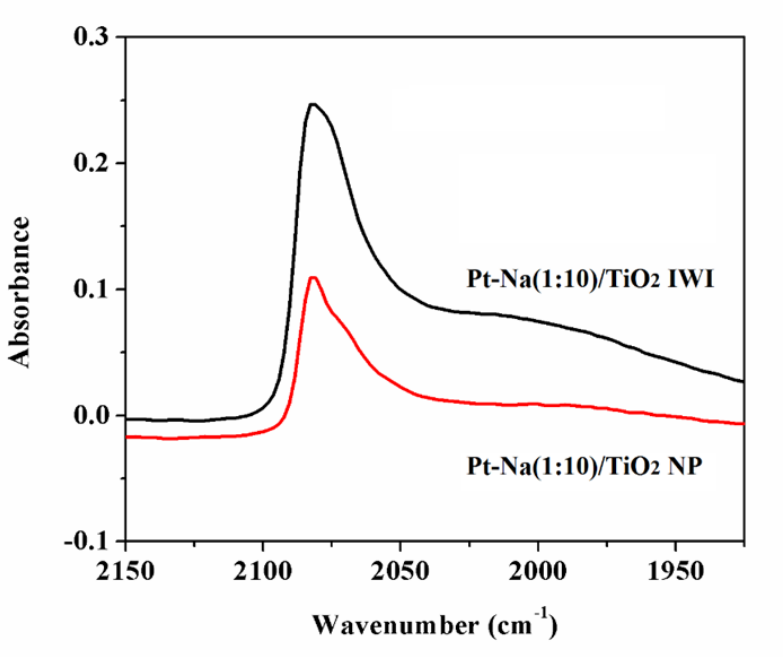

Figure 4.4 FTIR spectroscopy of Pt-Na/TiO_2 catalysts under 1% CO/N_2

4.4 Discussion

Pt/TiO_2 catalysts were prepared by two different methods. For the traditional Pt/TiO_2 catalyst prepared by incipient wetness impregnation, various Pt species exist on the support including single Pt atoms, Pt clusters and Pt nanoparticles (Figure A4.1). But for the Pt/TiO_2 catalyst prepared by loading Pt nanoparticles, STEM results confirmed that only Pt nanoparticles existed. Also from the *operando* FTIR results, the Pt/TiO_2 IWI catalyst showed both IR peaks due to CO adsorbed on single Pt atom and CO linearly adsorbed on metallic Pt nanoparticles. However, on Pt/TiO_2 NP catalyst, only a single CO adsorption peak due to CO adsorbed on metallic Pt nanoparticles was observed. Compared with the Pt/TiO_2 IWI catalyst, Pt/TiO_2 NP showed a blue shift about 5 cm^{-1} which may be due to a coverage effects. As all the Pt exists in nanoparticle forms, it may provide more sites for

CO binding and increases the surface CO coverage, causing a dipole-coupling effect and shifted the observed IR peak. Based on the STEM and FTIR results, two different types of Pt/TiO_2 catalysts were successfully prepared and the Pt nanoparticles were separated from the single Pt atoms and Pt clusters on the Pt/TiO_2 NP catalyst.

WGS kinetics (including the apparent activation energy and apparent reaction orders) are strongly dependent on the reaction mechanism and active sites. Although the Pt/TiO_2 catalysts were prepared by two different methods, both showed very similar WGS kinetics regardless of the different Pt species on the support. These prove that the two systems have similar WGS reaction mechanism and active sites. On the other hand, WGS TOR at 300 °C of Pt/TiO_2 IWI is lower than that of Pt/TiO_2 NP. The existence of single Pt atoms or Pt clusters on the Pt/TiO_2 IWI sample didn't change the kinetics and WGS rates by much. This implies that single Pt atoms are not active species for the water-gas shift reaction, and that Pt nanoparticles are the dominant species that catalyzes the water-gas shift reaction. On the Pt/TiO_2 NP catalyst, all the Pt atoms formed Pt nanoparticles. But for the Pt/TiO_2 IWI catalyst, part of the Pt atoms are in single Pt atoms forms. Thus the overall TOR will be an average between the TOR on metallic Pt atoms and single Pt atoms. So it is lower than the TOR of the Pt/TiO_2 NP catalyst, which is a direct measurement of the TOR on the Pt nanoparticles.

On the other hand, from STEM results, Na addition didn't bring further dispersion of the Pt nanoparticles. Although Na species are well dispersed on the rutile support, no Pt single atoms were observed based on the contrast. Na promotion effects were observed for both Pt/TiO_2 catalysts and the promotion ratios are similar. Also the changes in the WGS

kinetics are the same for both Na promoted Pt/TiO_2 catalysts. A decrease in the apparent reaction order with respect to CO is consistent with what we observe for other Na promoted Pt catalysts. Based on the Langmuir-Henshwood model, the higher the relative surface coverage, the lower the apparent reaction order. Since the CO order is closely related with the CO coverage and CO binding strength of the Pt active sites, it is inferred that the active sites have been modified by adding Na. The added Na will reside either on the TiO_2 support or on the Pt surface. The close contact between Pt and Na may modify the CO adsorption properties of Pt, which is reflected by the change in the CO order. On the contrary, the existence of Na on the Pt surface may inhibit the H_2 dissociation on the Pt surface, thus cause an increase in the H_2 order.

After Na addition, the *operando* FTIR spectroscopy was changed. For the Pt-Na(1:10)/TiO_2 IWI catalyst, it is hard to distinguish between the CO adsorbed on cationic Pt single atoms and CO adsorbed on metallic Pt nanoparticles. Pt-NaOx interfaces will change the CO adsorption and the peak may overlap with the CO adsorbed on cationic Pt atoms. For the Pt-Na(1:10)/TiO_2 NP catalyst, the IR peaks were decreased, implying NaOx formed on the surface, thus reducing the CO adsorption. Also based on the STEM results, for the Pt-Na(1:10)/TiO_2 NP catalyst, Pt particles should form the Pt-NaOx interfaces since no single Pt atoms were observed. However, on this catalyst, similar WGS TOR promotion and kinetics changes were observed compared with the IWI catalyst. This suggests that the Pt-NaOx interfaces are the key factor that influences the WGS kinetics and rate changes. Formation of single Pt atoms are not important in determining the WGS kinetics.

Maria Flytzani-Stephanopoulos et al. claimed that Na promoted the activity of supported Pt catalysts by increasing the dispersion of Pt, which causes a larger fraction of single Pt atoms. Thus they claimed that the single Pt atoms are the active sites for the water-gas shift reaction. However, from the results here, even when single Pt atoms or Pt clusters are absent from the Pt/TiO_2 catalysts, the Na still showed a promotion in the WGS reaction rate. The present study highlights the importance and indispensability of the Pt nanoparticles as active sites for the water-gas shift reaction and the Na modification of the active sites. The absence of the single Pt atoms doesn't significantly influence the WGS rates. The promotion of Na is not because of creation of more single Pt atoms. The interface between Pt nanoparticles with NaOx species is more important for increasing the activity.

4.5 Conclusion

Two different series of Pt/TiO_2 catalysts were prepared by different methods with different Pt species on the support. Single Pt atoms and Pt clusters were ruled out on one of the catalyst. However, the catalyst still showed similar WGS kinetics compared with normal Pt/TiO_2 catalyst with single Pt atoms. Thus it is inferred that the Pt nanoparticles are the active sites for the WGS reaction. Addition of Na changes the WGS kinetics significantly and this change was observed even without formation of single Pt atoms. Also Na can promote the WGS rate even without the existence of single Pt atoms. Thus we conclude that the Na promotes the WGS rate over Pt/TiO_2 catalyst by modifying the active sites. One likely explanation is the formation of Pt-NaOx interfaces and modification of the CO adsorption on Pt.

CHAPTER 5. EFFECT OF SODIUM ADDITION ON THE WATER-GAS SHIFT CATALYSIS OVER PLATINUM SUPPORTED ON MULTI-WALLED CARBON NANOTUBES

5.1 Introduction

Platinum-based catalysts have been studied as potential alternative for WGS [57]. The Pt based catalysts are often promoted using secondary metal promoters such as Re [58], Mo [59] or alkali metal. Na has been reported to show a substantial promotion in the WGS reaction rate over Pt/TiO_2 [54], Pt/CeO_2 [60] and Pt/Al_2O_3 [60, 61]. While the promotion in some cases has been attributed to the increased rate of formate decomposition [60], the increased reducibility of the sites created by Na at the metal/support interface is also suggested as a possible cause of increased reaction rate [54].

Recent studies by Zugic et al.[62, 63] suggest that Na can promote the WGS reaction rate over Pt supported on non-oxide supports such as multi-walled carbon nanotubes (MWCNT). The authors suggest that the active sites are formed by oxidized Pt bonded to Na ($Pt\text{-}Na_x\text{-}O_y\text{-}OH$). Similar active sites were proposed before for the Pt/Al_2O_3 catalysts [60]. Zugic et al. suggest that the promotion in the WGS rate is caused by the enhanced water dissociation due to the presence of Na.

In light of the study from Zhai et al. [46], our group investigated Na promotion over Pt/Al_2O_3 and Pt/TiO_2 [61] and found that Pt remains in metallic state under WGS reaction conditions. The similarity of kinetic parameters for Na promoted catalysts over various

oxide supports was used to suggest that chemically similar active sites are formed with addition of Na. In short, even though there is a disagreement in the published literature regarding the oxidation state of Pt under WGS, the aforementioned reports on oxides as well as the MWCNT supports suggest that Na creates a support-type effect and leads to the promotion in WGS rates.

In the present study, we have prepared a series of PtNa/MWCNT catalysts with increasing molar ratio of Na:Pt. Similar to the study performed by Pazmino et al. [61]. We have combined the kinetic measurements with *in situ* x-ray absorption to understand the role of Na. The central idea of this work is to extend the methodology used by our group before [61] to a non-oxide MWCNT support and contribute towards the understanding of alkali promotion over Pt for WGS. The catalyst structure has been investigated using TEM-EELS and density functional theory (DFT) calculations, with an ab-initio phase diagram approach. DFT calculations were also used to gain insights into the nature of promotion by Na. Based on our combined experimental and theoretical results we have proposed a possible mechanism to explain the promotion effect of Na on Pt for WGS reaction.

5.2 Experimental Methods

5.2.1 Catalyst Preparation

All the catalysts used in this study were prepared by sequential incipient wetness impregnation. The multi-walled carbon nanotubes were purchased from Cheap Tubes Inc. (BET area 240 $m^2 g^{-1}$). The Pt was loaded on the MWCNT support by the addition

of aqueous solution of tetrammineplatinum nitrate (Sigma Aldrich) in a drop-wise manner. The samples were dried overnight in vacuum at 60°C. The dried Pt containing-support was then loaded with Na using the aqueous solution of $NaNO_3$. These catalysts were dried again overnight in vacuum at 60°C. The dried catalysts were further calcined in air at 250°C (200 ml min^{-1}, 5°C min^{-1}) for 2 hours. The catalysts were then cooled to RT. The calcination was followed by reduction in pure H_2 (Praxair UHP grade) at 300°C. For reduction, the procedure used by Pazmino et al. [61] was followed. H_2 was introduced at room temperature and the temperature was ramped as follows: (1) from RT to 150 °C at 10 °C min^{-1}, stay at 150 °C for 30 min; (2) ramp to 200 °C at 2 °C min^{-1}, stay at 200 °C for 30 min; (3) ramp to 300 °C at 2 °C min^{-1}, stay at 300 °C for 2 hours; (4) purge with He at 300 °C for 30 min and cool in He to room temperature before exposing to air. By varying the amount of $NaNO_3$ in the solution catalysts with Na:Pt molar ratio of 2,10,17,30 and 45 (estimated by atomic absorption, explained in detail later) were prepared. These catalysts will be referred to as the 'as prepared' catalysts.

Some amounts of the as prepared catalysts with Na:Pt molar ratio of 17, 30 and 45 were washed with deionized water (200 ml) in a conical flask with a magnetic stirrer at RT for 30 minutes. The slurry was then centrifuged and the catalysts were again dried at 60°C in vacuum overnight. The washing was performed in order to remove excess Na (if any) and observe the effect on WGS kinetics.

The key difference between our synthesis method and the method used by Zugic et al. [62, 63] is the HNO_3 oxidative treatment used for the MWCNT support. While Zugic

at al. treated the MWCNT support with nitric acid to introduce oxygen functionalities on the surface, we used the MWCNT support as received.

5.2.2 WGS Kinetics Measurement

WGS reaction rates and apparent kinetic parameters were measured using a fully automated setup of fixed bed reactors the same as the previous description. The as prepared as well as the washed PtNa/MWCNT catalysts were reduced at 300°C (5°C/min) in presence of 25% H_2/Ar (50 sccm) for 2 hours. Following the reduction pretreatment, the catalysts were exposed to the WGS reaction mixture (standard conditions, 6.8% CO, 21.9% H_2O, 8.5% CO_2, 37.4% H_2, and balance Ar). The reactor temperatures were adjusted such that the CO conversions were < 10%, in order to achieve differential conditions. The apparent reaction orders were measured by varying the partial pressures of one component at a time over the range of 4–21% CO, 5–25% CO_2, 11–34% H_2O, and 14–55% H_2. The apparent activation energies were determined by changing the temperature in the span of 30°C around the test temperature for each catalyst. After the measurements were complete, the catalysts were passivated at room temperature in 30 sccm 2% O_2/Ar gas flow for 4hs before they were taken out from the reactors.

5.2.3 Catalyst Characterization

The sodium content of each catalyst was measured using the atomic absorption spectroscopy. The Perkin Elmer AAnalyst 300 instrument was used. About 20-25 mg of each catalyst was dissolved in the 5-6 ml of aqua regia and digested for 2 days in

capped Nalgene bottles. The digested mass was then diluted with distilled water to make total volume of ~50 ml. Na AAS standard from Sigma Aldrich was used to make calibration standards for the measurements. Since MWCNT support did not dissolve in aqua regia, the solutions were decanted carefully to separate them from the particles. These solutions were further diluted with deionized water to bring the expected Na level approximately below 1 ppm (to fall in the linear range of AAS for Na).

Moles of exposed platinum were measured using H_2 chemisorption at 35°C performed using Micromeritics ASAP 2020 instrument. The pretreatment described by Pazmino et al. [61] was followed. The catalysts were firstly evacuated at 300 °C, followed by reduction at 300 °C for 2 hours in H_2 and a second evacuation for 2 hours. H/Pt stoichiometry factor of 1 was used.

Transmission electron microscopy was performed using a FEI Titan 80-300 apparatus operating at 200 kV. The catalyst samples were dispersed in ethanol. The suspension was placed in an ultrasonic bath for about 5 min and a drop was deposited on a holey carbon film coated 200 mesh copper TEM grid.

In situ X-Ray Absorption experiments were performed at the insertion device beam line of the Materials Research Collaborative Access Team (MRCAT) at the Advanced Photon Source, Argonne National Laboratory. The catalysts were finely ground and pressed into a cylindrical sample holder in form of self-supporting wafers. The Pt L_{III} edge scans were taken under He flow, following the reduction pretreatment described above. The catalysts were then exposed to the WGS reaction mixture (7% CO, 7% H_2O, 8.5% CO_2, 37% H_2 and balance Ar) at 240°C. The EXAFS data were processed and analyzed using WINXAS97 software. A least-squares fit in R-space of the coordination

k^2-weighted Fourier transform data allowed the calculation of the nearest neighbor first-shell Pt–O and Pt–Pt parameters. The data with k^1 and k^3 weightings also resulted in satisfactory fits with negligible variation in the parameters. The information about the oxidation state of Pt after reduction pretreatment and under WGS conditions was obtained from the X-ray absorption near edge structure (XANES) data. The particle size of Pt clusters was estimated from the extended X-ray absorption fine structure (EXAFS) data using previously developed correlations.

5.2.4 DFT Calculations

All calculations were performed using Vienna Ab-Initio Simulation Package (VASP) code [64], with projector augmented wave (PAW) implementation [64] and PW91 functional [65].The Pt surface was modelled using 4 layered slabs with bottom two layers constrained at bulk atomic distances. Vacuum height of over 45 Å was used in all the calculations. The Brillouin zone was sampled using Monkhorst scheme where the *k* point grid was chosen based on the size of the unit cell for each of the tested structures. Electronic steps were converged till $1x10^{-4}$ while forces for ionic steps were converged till 0.02 eV/Å. Fermi smearing of 0.1 was used for the Pt calculations while Gaussian smearing was used for gas phase calculations. All gas phase calculations were done in 11Å x 12Å x 13Å boxes. To understand the interaction between Na and Pt, we modelled the promoted catalyst as an inverse NaOx film on Pt. We studied three different types of structures – Na, Na_2O and NaO on Pt (111). While the last structure is not stable in bulk oxide form, we still tested this structure since previous work on inverse oxide catalysts has shown that the cations in an oxide film in contact with a

transition metal surface can assume oxidation states that are not common in bulk oxides [66]. For each of these different NaOx species, multiple structures were investigated at different ratios of Na atoms to surface Pt atoms, and with different Moire patterns. This was done to sample a sufficiently large set of structures for each oxidation state to identify the most stable film structure of that state. The Pt surface was modelled with 4 layered slabs. As an example, the formation energy (*FE*) of the Na_2O film structures were calculated as shown,

$$FE = \frac{E_{film+Pt} - E_{Pt} - \#Na_2O(E_{Na_2O\ bulk})}{\#Na_2O}$$

where E_i is the DFT calculated energy of system i and $\#Na_2O$ is the number of Na_2O units in the film. $E_{Na_2O\ bulk}$ is the energy of bulk Na_2O on a per Na_2O basis. A similar expression can be used for Na metal, where instead of properties of bulk Na_2O, those of bulk Na metal can be used. For NaO, we used bulk Na_2O and bulk Na as references for calculation of formation energies. Figure 5.7 shows some example structures.

After identification of film structures with lowest formation energy for each oxidation state, we constructed a phase diagram to compare the structures with different oxidation states of Na on Pt (111). The methodology for construction of phase diagram is similar to what has been outlined by Reuter and Scheffler [67]. The free energy of formation of the films on a per surface Pt basis can be computed as,

$$\Delta G_{formation} = \frac{1}{\#Pt}\left[G_{film+Pt} - G_{Pt} - N_{Na}g_{Na,bulk} - N_O g_{O,gas}\right]$$

where G_i is the total free energy of system i and g_i is the partial molar free energy of system i, N_i is the number of atoms of i. With the entropy of solids negligible as compared to gases, we have

$$G = H - TS \approx E_{DFT} + E_{ZPE}$$

where E_{DFT} is DFT calculated energy of the system and E_{ZPE} is it's zero point energy. For gaseous O, writing g as chemical potential μ, we have,

$$g_o = \mu_o = \frac{1}{2}\mu_{O_2}$$

$$\mu(T,P) = \mu(T,p^0) + kTln\frac{p}{p^0}$$

$$\mu(T,p^0) = E_{DFT} + E_{ZPE} + \Delta H\left(T,p^0\right) - T\Delta S(T,p^0)$$

The enthalpy H and entropy S can be obtained from NIST database for p^0 of 1 atm. Thus, all quantities would be known in terms of the independent variables T and P. With this information, one can construct a phase diagram to identify the structure (oxidation state) with lowest free energy for a given T and oxygen partial pressure.

5.3 Results

5.3.1 WGS Kinetics

Figure 5.1 shows the variation in the WGS reaction rate per total moles of Pt at 250°C with the Na:Pt molar ratio for the as prepared catalysts. This rate increases monotonically from the monometallic Pt catalyst (3×10^{-3} mol H_2 (mol Pt)$^{-1}$ s^{-1}) to the catalyst with Na:Pt molar ratio of 17 (3.1×10^{-2} mol H_2 (mol Pt)$^{-1}$ s^{-1}). With further addition of Na, the WGS rate per total mol Pt decreased for the Na:Pt molar ratio of 30 and 45. In short, the WGS rate per total mol Pt at 250°C goes through a maximum with

increasing Na:Pt molar ratio. As said before, these molar ratios are estimated based on the amounts of Na measured using atomic absorption spectroscopy.

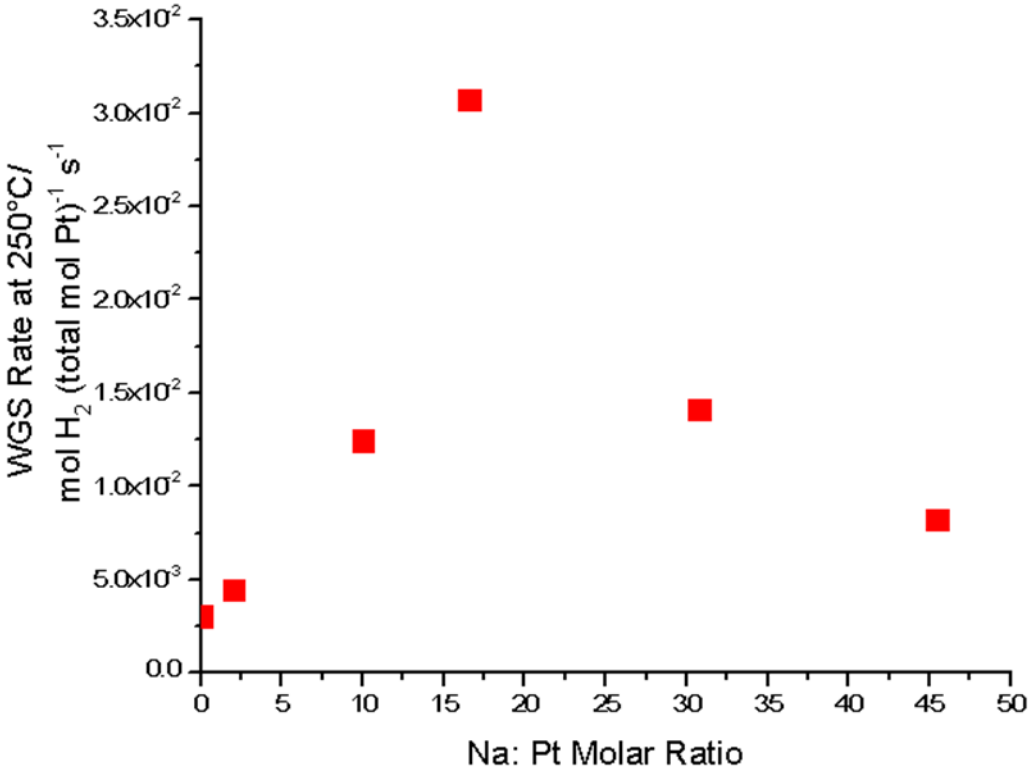

Figure 5.1 Variation of WGS rate per total moles of Pt at 250°C with the Na:Pt molar ratio for the as prepared PtNa/MWCNT catalysts

Figure 5.2 shows the variation of WGS turnover rates (TOR, estimated by normalizing the rates with moles of exposed Pt measured using H_2 chemisorption) with the Na:Pt ratio for the as prepared as well as washed catalysts. The WGS TOR increases initially with increasing Na:Pt ratio for the as prepared catalysts, and ultimately levels off. Compared to the monometallic Pt catalyst (7.5×10^{-3} mol H_2 (mol exposed Pt)$^{-1}$ s^{-1}), the WGS TOR is promoted 24-26 times for the Na:Pt molar ratios of 17 and higher. The Na loading decreased significantly after washing the catalysts with Na:Pt ratio 17 and higher (Na:Pt molar ratio decreased from 17, 30 and 45 to 2.5, 2.5 and 4

respectively) and the dispersion of Pt estimated using H_2 chemisorption increased simultaneously (Table 5.2). The WGS TOR at 250°C for all the washed catalysts was of the order of $\sim 2 \times 10^{-1}$ mol H_2 (mol surface Pt)$^{-1}$ s^{-1}, which was similar to the WGS TOR over fully promoted as prepared catalysts (with Na:Pt = 17 and higher).

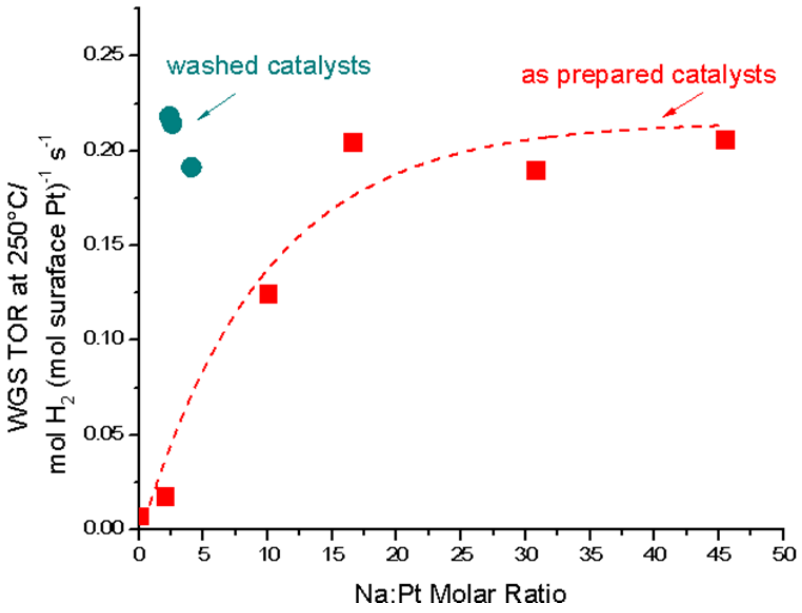

Figure 5.2 WGS TOR at 250°C plotted against the Na:Pt molar ratio for the as prepared and the washed PtNa/MWCNT catalysts

The WGS kinetic parameters for the as prepared and washed catalysts are listed in Table 5.1 and Table 5.2. Except for the monometallic Pt catalyst (270°C), all other catalysts were tested in the temperature range of 230-250°C. The WGS kinetic parameters (apparent activation energies and apparent reaction orders) for all the as prepared catalysts with Na:Pt ratio 17 and higher and all the washed catalysts are similar to each other within error. Compared to the monometallic Pt catalyst, the fully promoted as prepared and the washed catalysts exhibited lower apparent CO orders (0.1 vs. 0 to -0.1), lower apparent CO_2 orders (-0.06 vs. -0.2 to -0.3), higher apparent

H_2 orders (-0.4 vs. -0.2 to -0.15) and higher apparent activation energies (83 vs. 95-105 kJ mol^{-1}). For the catalysts with Na:Pt ratios 2 and 10, the apparent kinetic parameters have values in between that of the monometallic Pt catalyst and the fully promoted (and washed) PtNa catalysts.

Table 5.1 WGS kinetic data over as prepared PtNa/MWCNT catalysts

Catalyst	Rate at 250ºC/ 10^{-2} mol H_2 (mol Pt)$^{-1}$ s^{-1}	Pt dispersion/ %	TOR/ 10^{-2} s^{-1}	E_a/ kJ mol^{-1}	H_2O ±0.06	CO_2 ±0.04	CO ±0.04	H_2 ±0.04
4% Pt/MWNT	0.30	40	0.75	83±1	0.87	-0.09	0.1	-0.4
4% Pt/MWNT-2Na	0.45	25	1.8	87±1	0.89	-0.1	0.0	-0.3
4% Pt/MWNT-10Na	1.3	10	13	87±2	0.86	-0.2	0.0	-0.2
1.8% Pt/MWNT-17Na	3.0	15	20	95±1	0.87	-0.2	0.0	-0.15
1.9% Pt/MWNT-30Na	1.4	8	19	104±2	0.89	-0.2	0.0	-0.15
1.8% Pt/MWNT-45Na	0.83	4	21	105±3	0.86	-0.3	-0.1	-0.15

Table 5.2 WGS kinetic data for the washed PtNa/MWCNT catalysts

Catalyst	Rate at 250ºC/ 10^{-2} mol H_2 (mol Pt)$^{-1}$ s^{-1}	Pt dispersion /%	TOR/ 10^{-2} s^{-1}	E_a/ kJ mol^{-1}	H_2O ±0.06	CO_2 ±0.04	CO ±0.04	H_2 ±0.04
1.8% Pt/MWNT-2.5Na	2.9	13	21	95±2	0.96	-0.2	0.0	-0.2
1.9% Pt/MWNT-2.5Na	3.5	16	22	90±1	0.89	-0.2	0.0	-0.2
1.8% Pt/MWNT-4Na	1.5	8	19	100±2	0.81	-0.25	0.0	-0.2

5.3.2 Catalyst Characterization

The H_2 chemisorption results are shown in Table 5.1 and Table 5.2. For the as prepared catalysts, it can be seen that the % exposed measured using H_2 chemisorption, i.e. the fraction of moles of Pt exposed on the surface, decreases with increasing Na:Pt molar ratio. For the catalysts with Na:Pt molar ratios 30 and 45 catalysts, there is an increase in the moles of exposed Pt by ~2 times after washing. The stoichiometry factor of Pt/H=1 was used.

The average particle size for the as prepared catalysts with Na:Pt ratio of 17, 30 and 45 were estimated from the TEM images obtained post reaction . The average Pt particle sizes for these three catalysts are 2.9±0.6, 2.8±0.9 and 3.4±1.1 nm. The dispersions estimated based on the average particle sizes (= 1.08/particle size in nm) were about 32-37%. These dispersion values are significantly higher than the dispersions estimated from the H_2 chemisorption results, indicating partial coverage of the Pt by Na species.

The *in situ* Pt L_{III} XANES spectra for the Pt/MWCNT and the PtNa 1:30/MWCNT catalyst is shown in Figure 5.3 and Figure 5.4. The shapes of the spectra and the edge energies for both the catalysts after reduction at 240°C measured under He are similar to those for the metallic Pt foil. When the catalysts were exposed to WGS (spectra in blue), an increase in the edge energy was observed, with a simultaneous increase in the intensity beyond the edge. The difference spectra, or the ΔXANES data, for these catalysts is shown in Figure 5.5. These spectra are plotted from the difference computed by subtracting the spectra recorded in He at 240°C after reduction pretreatment from the spectra recorded under WGS conditions at 240°C [9]. The shape of ΔXANES for the Na-promoted catalyst is identical to that of the monometallic catalyst. However, the

intensity of the ΔXANES spectrum for the PtNa 1:30/MWCNT catalyst is about 1.3 times higher than the intensity for the ΔXANES spectrum for the monometallic Pt catalyst.

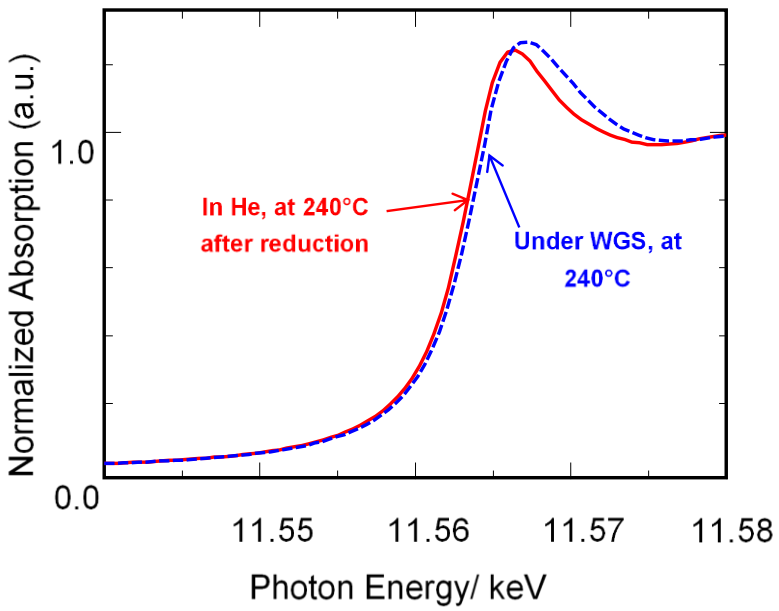

Figure 5.3 In situ XANES spectra for the monometallic Pt/MWCNT catalyst

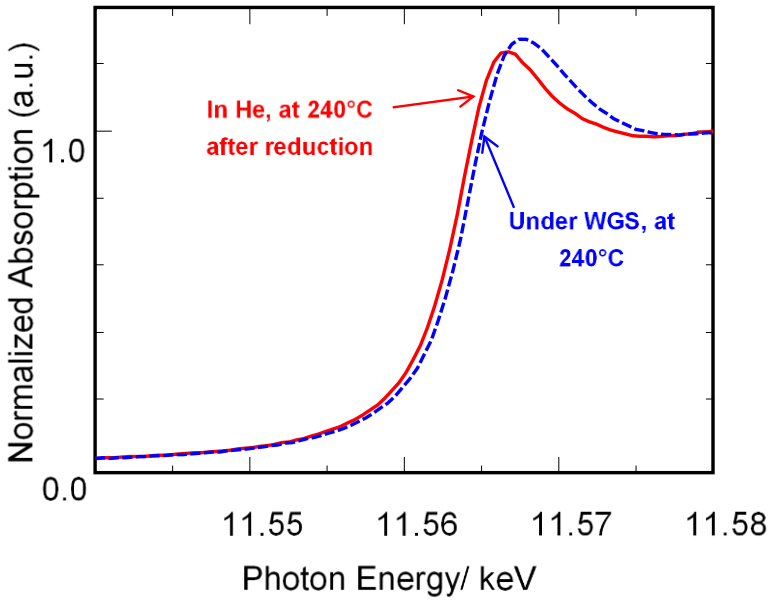

Figure 5.4 In situ XANES spectra for the PtNa 1:30/MWCNT catalyst

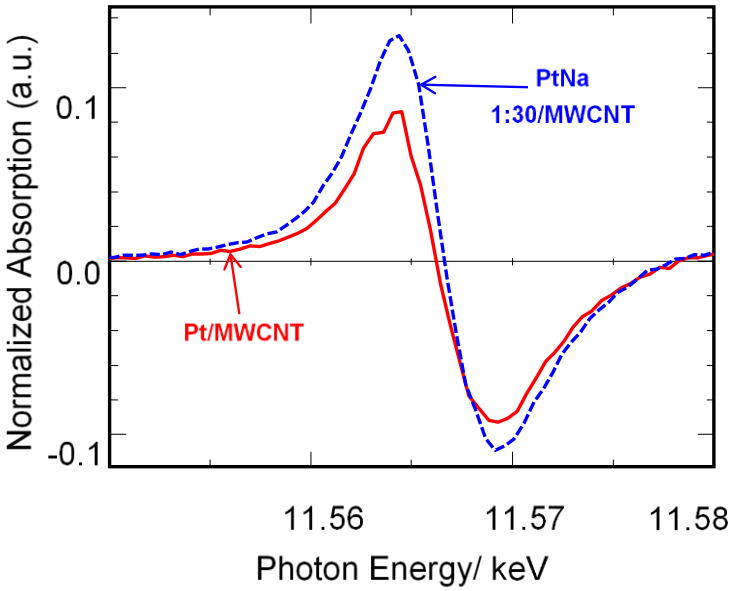

Figure 5.5 In situ Pt LIII edge ΔXANES spectra for the monometallic Pt/MWCNT and the PtNa 1:30/MWCNT catalyst

The details of the *in situ* EXAFS fit parameters are given in Table 5.3. For the air exposed catalysts i.e. prior to reduction, Pt-Pt and Pt-O coordination was observed, with Pt-Pt coordination number consistently higher than the Pt-O coordination number. This structure is consistent with the metallic Pt core oxidized on the surface. The catalysts after reduction do not exhibit any Pt-O coordination, suggesting that Pt is fully reduced. The *in situ* (under WGS conditions at 240°C) Pt L_{III} edge EXAFS spectra for the Pt/MWCNT catalyst and the PtNa 1:30/MWCNT catalyst are shown in Figure 5.6. The peak positions for the spectra for both the catalysts are identical to that of Pt foil. However, the magnitudes of the peaks are much smaller compared to the Pt foil, suggesting the presence of Pt nanoparticles. There was no Pt-O (platinum-oxygen) coordination observed for both these catalysts, confirming that Pt stays reduced (metallic) under WGS. The average coordination numbers obtained from the EXAFS fits (Table A5.1) were used to estimate the average particle sizes of Pt clusters using previously developed correlation [68]. The average particle sizes estimated from EXAFS for the as prepared as well as the washed catalysts all fall within the range of 3.0 to 4.5 nm under WGS conditions. With a higher Na loading, there is an increase in the average particles size estimated from EXAFS for the as prepared catalysts. The washing does not affect the average particle size significantly. Additionally, no Pt-Na coordination was observed with the EXAFS fits.

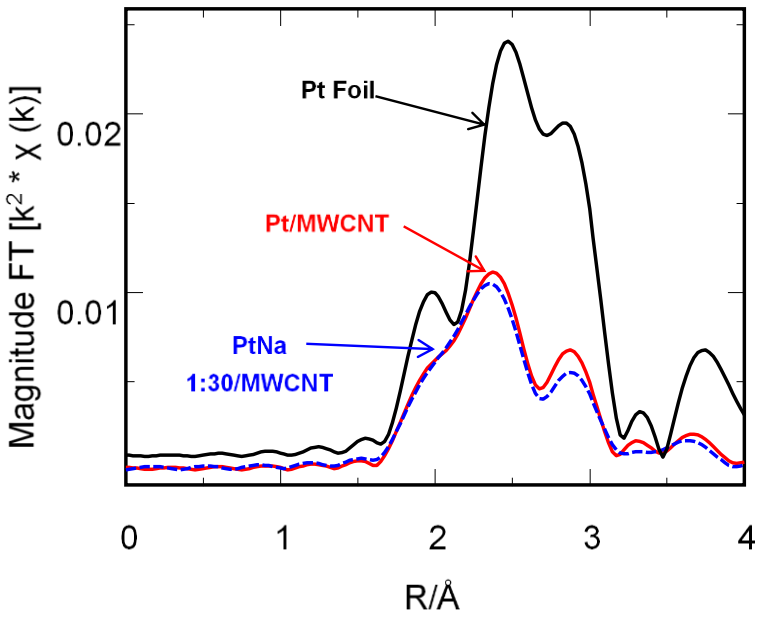

Figure 5.6 In situ Pt LIII edge EXAFS spectra for the monometallic Pt/MWCNT and the PtNa 1:30/MWCNT catalyst

5.3.3 DFT Calculation

5.3.3.1 Phase Diagram

Multiple film structures were sampled with different orientations on underlying Pt metal substrate. Since the oxidation state of the Na in contact with Pt is not experimentally confirmed, multiple oxidation states were tested, Na_2O, NaO and Na. Figure 5.8 shows some of the structures that we tested. The formation energies for all the Na_2O structures are shown in Figure 5.9a, with the lowest energy structure highlighted. The formation energy of about -0.22 eV per Na_2O indicates that this structure is quite stable on Pt (111). This structure was used in the construction of phase diagram. A similar approach was used for NaO and Na films as well, where phase

diagrams were constructed with the structure having lowest formation energy. For NaO, we tested two types of linkages shown in Figure 5.7 – one with O-Na-Pt linkage and another with Na-O-Pt linkage. In general, we found the second type of linkage to be significantly more stable than the first one. Figure 5.9b shows the phase diagram of all three types of Na structures on Pt that we tested for low oxygen partial pressure representative of the reducing environment of WGS. Under experimental conditions of low temperature, it is the oxide form of Na_2O on Pt which is found to be most stable. The phase diagram shows metallic Na to be stable at very high temperatures. At these temperatures one might need to consider possible vaporization of Na, but our region of interest in this case is only the low temperature region, where Na_2O is found to be the most stable. Unsurprisingly, NaO on Pt is never as stable as the other two structures. The free energy of formation of the oxide on a per surface Pt atom basis at temperatures of 250^0C is found to be about -0.9 eV, indicating that the oxide structure is very stable on Pt. These results are in agreement with EELS images showing regions of Na signals are always associated with O signals. The high stability of the oxide structure on Pt hints at the possibility that even after washing the catalyst samples in water, the Na oxide in contact with the Pt does not get washed away, which may explain the high activity of the washed samples. EELS results for washed samples are in close agreement, showing presence of Na oxide on the samples even after washing.

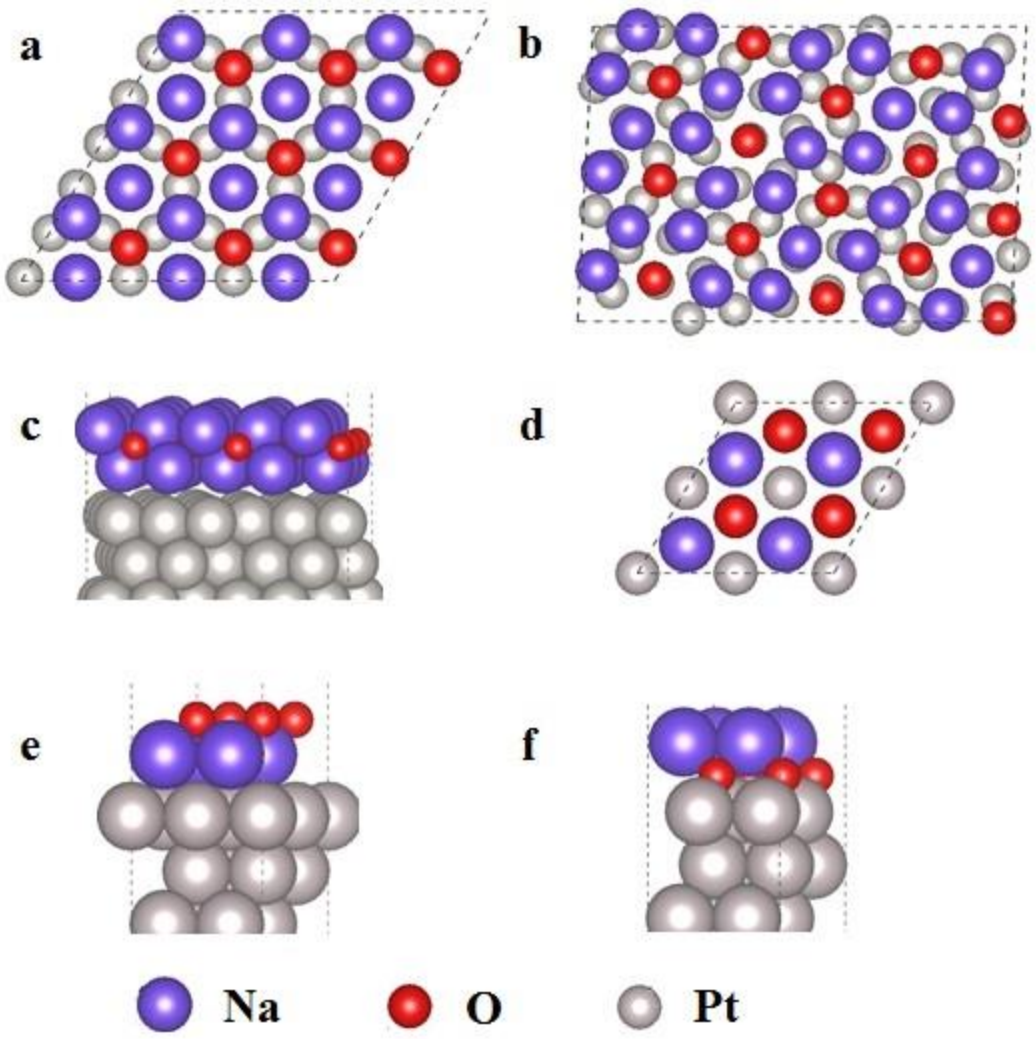

Figure 5.7 Example inverse catalyst structures – Pt: grey, Na: blue, O: red- (a) a pseudomorphic Na_2O film (b) a non-pseudomorphic Na_2O film (c) side view of a typical Na_2O film (d) a pseudomorphic NaO film (e) NaO film with O pointing away from Pt (f) NaO film with O pointing towards Pt. Na films on Pt were similar to NaO films but without the O atoms

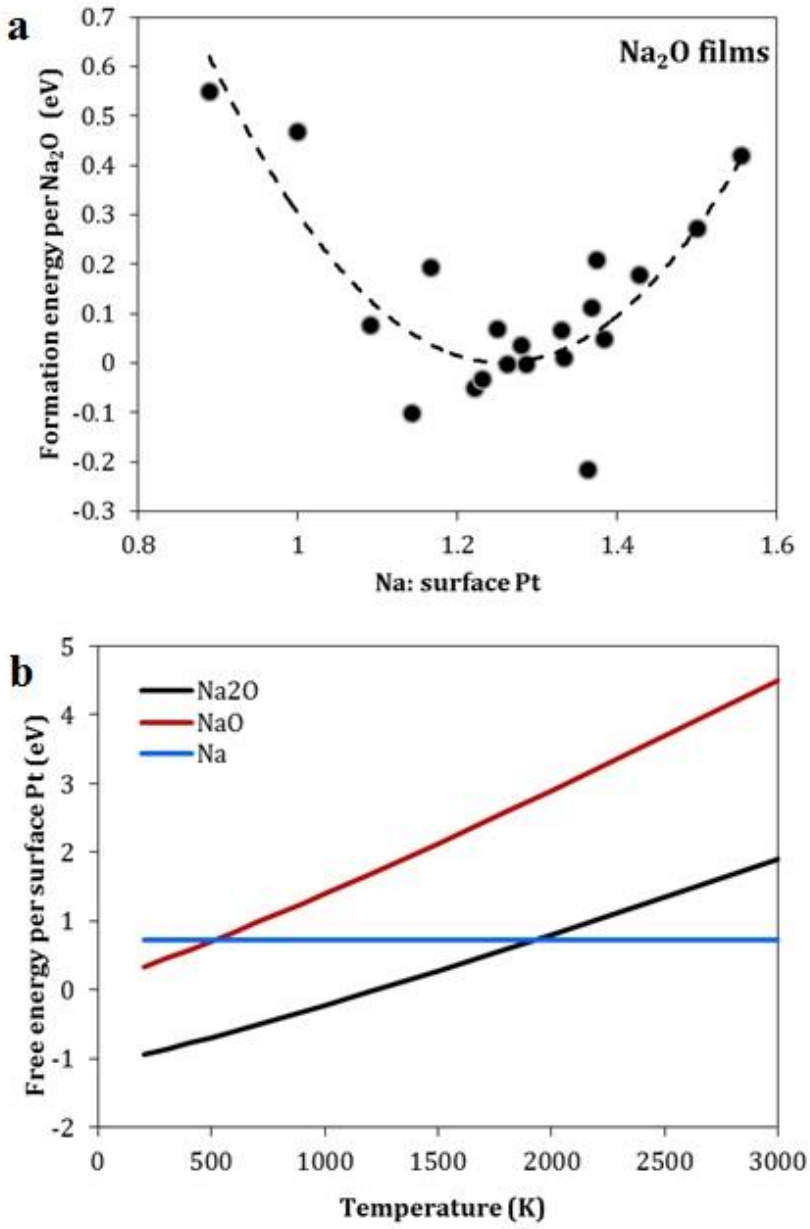

Figure 5.8 a) Formation energies of Na_2O films on Pt as a function of number of Na atoms per surface Pt atoms. Highlighted lowest energy structure used in the phase diagram b) Phase diagram for the different types of inverse Na structures on Pt at partial pressures of oxygen p/p0 = 0.02, to represent the reducing conditions of WGS

5.3.3.2 Adsorption energy calculations

While we do not have complete information about the structure of the active site of the catalyst, these results confirm that Na in contact with the Pt is in the form of an oxide. It is possibly participation of the Na oxide in the WGS reaction mechanism that results in promotion of activity. To this end, we performed adsorption calculations on the most stable inverse Na_2O film on Pt, for common WGS intermediates like H_2O, CO and OH. Interestingly, we found that when H_2O is placed on the oxide in such a configuration that allows for H bonding between H_2O and oxygen of the oxide (Figure 5.10), it dissociates spontaneously. While the structure of the catalyst may not be necessarily in the form of an extended oxide film on Pt, this result indicates that the water dissociation barrier on the oxide in the real catalyst would most probably be significantly lower than that on pure Pt. However, the calculated adsorption energy of CO on the oxide (5.40 eV) was found to be more than 7 eV weaker than on pure Pt (111) (-1.83 eV). Similarly, adsorption energy of OH on the oxide film (5.54 eV) was about 4.7 eV weaker than on pure Pt (0.81 eV). On the basis of these calculations, we can claim that it is not just the oxide in contact with Pt which is involved in the reaction. There is most probably direct participation of metallic Pt as well. Therefore, the active site is most probably interface sites between oxide and Pt, where the Pt adsorbs CO and the oxide facilitates easy dissociation of water.

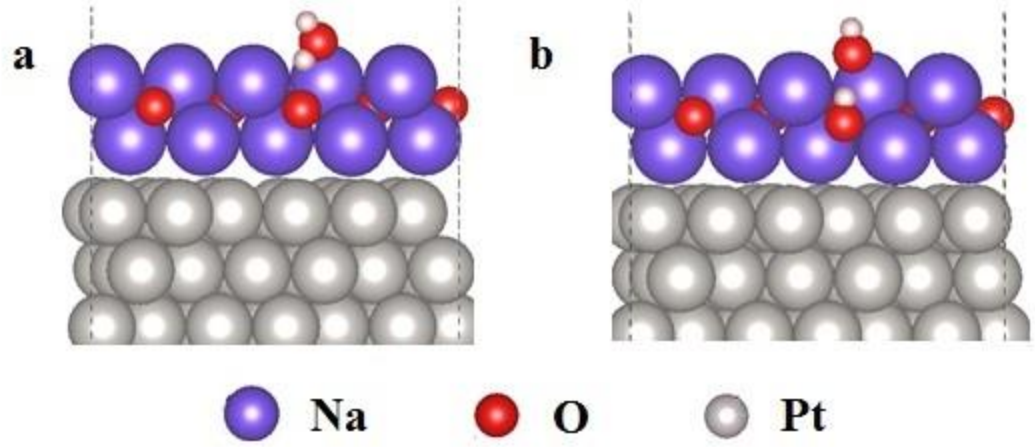

Figure 5.9 Spontaneous dissociation of water on Na_2O on Pt a) water molecule before relaxation b) after relaxation

5.4 Discussion

5.4.1 Promotion in the WGS rate over the as prepared catalysts

In accord with the previously reported results [10], we also observed a promotion in the WGS rates per total mol of Pt with addition of Na. The WGS rate per mol Pt at 250°C increased by a factor of 10 with addition of Na (1:17 ratio), as compared to the monometallic Pt catalyst. However, for the as prepared catalysts, the WGS rate per total mol Pt forms a volcano-like curve with increasing Na weight loading. When this rate is normalized by the moles of exposed Pt measured using H_2 chemisorption (to compute the WGS turnover rate), it first increases monotonically from monometallic Pt catalyst up to the PtNa 1:17/MWCNT catalyst. This TOR further becomes constant for the Na:Pt 17 and higher. This suggests that the decrease in the WGS rate per total moles of

Pt at 250°C was due to a decrease in the available Pt surface sites with increasing Na loading. For this to happen, we believe that Na must cover Pt surface at higher weight loadings.

The argument of Na covering the Pt surface can be supported with the H_2 chemisorption, TEM and the EXAFS data over the as prepared catalyst. The Pt % exposed computed for the catalysts with Na:Pt 17, 30 and 45 from the H_2 chemisorption are 15%, 8% and 4% respectively. The average particle sizes measured using TEM for these catalysts were similar to each other and the % exposed computed using these particles sizes were in the range of 33-35%. The average particle sizes computed using the EXAFS data measured under WGS conditions are 3.5 nm, 3.5 nm and 4.5 nm for the catalysts with Na:Pt molar ratio of 17, 30 and 45 respectively. Although the TEM and EXAFS data suggests that for the Na:Pt 45 catalyst, there is an increase in the average particle size, this increase is not commensurate with a 4 times lower Pt dispersion compared to the Na:Pt 17 catalyst, measured using H_2 chemisorption. Moreover, the apparent kinetic parameters measured over these catalysts in the range of 230-250°C (activation energies and reaction orders) are all similar to each other within error. This suggests that the differences in the WGS rates per total mol Pt could solely be due to the differences in the available active sites on the surface.

Based on these results, we envision that the active sites for the Na promoted catalysts are formed by decoration of Pt particles with Na. Although, our attempts to perform elemental mapping of Na using electron energy loss spectroscopy failed due to the incompatibility of Na for this method, our chemisorption and TEM/EXAFS results point towards such covering by Na. For the fully promoted catalysts, the WGS rate per

total mol Pt appears to be proportional to the available Pt surface area measured using H_2 chemisorption. DFT results also show that the formation energy of Na oxide is very favorable on Pt (111). Based on Figure 5.9a, the most stable Na_2O film on Pt is -0.22 eV more stable compared to bulk Na_2O. We propose that Na promotes the WGS rate through a support-type effect i.e. Na acts as a better support for water activation by directly sitting over the Pt particle surface (discussed later in detail). Thus, when the Na loading is increased beyond a point where the available Pt surface area per mol Pt is compromised, there is a decrease in the WGS rate per total mol Pt, while the TOR computed from H_2 chemisorption still remains constant. We imagine Na to be nucleating at specific sites over the Pt surface, forming Na islands. These islands must grow in size with further addition of Na in order to explain the loss in the Pt surface area that is not accounted by growth in the average Pt particle size.

We make a note that it is possible that not all the Na is selectively located over the Pt surface. A sizable fraction of Na could still be located on the MWCNT surface. In absence of any spectroscopic evidence for location of Na, our model currently relies on the aforementioned chemisorption and TEM/EXAFS results.

5.4.2 Effect of washing

We have established that excess Na leads to the growth of Na islands over Pt thereby decreasing the Pt surface area available. In order to remove this excess Na, the catalysts beyond the point of maximum (Na:Pt 17,30 and 45) in the Figure 1 were washed with deionized water at RT for 30 mins. The Na:Pt molar ratios estimated from the atomic absorption of Na were 2.5, 2.5 and 4 respectively for the three washed catalysts. If the

argument of Na covering Pt was to be true, the washing procedure should lead to an increase in the surface area measured using H_2 chemisorption. The particle sizes under WGS conditions for the washed catalysts estimated from EXAFS were 3.5 nm, 3.0 nm and 4.0 nm respectively (these correspond to the as prepared Na:Pt 17, 30 and 45 catalysts after washing respectively). This suggests that there is no or a slight decrease in the particle sizes estimated for the as prepared catalyst (3.5 nm, 3.5 nm and 4.5 nm for Na:Pt 17,30 and 45 as prepared). However, the Pt dispersions for the Na:Pt 30 and Na:Pt 45 catalysts increased from 8% and 4% (as prepared) to 16% and 8% (post washing) respectively. The WGS rates per total mol Pt at 250°C for these catalysts also increased by 2.4 and 1.8 times respectively. The dispersion from H_2 chemisorption (and the particle size from EXAFS) for the Na:Pt 17 catalyst did not change appreciably after washing. Also, the WGS rate per total mol of Pt at 250°C before washing (3.0×10^{-2} mol H_2 (mol Pt)$^{-1}$ s^{-1}) is similar to the rate measured post washing (2.9×10^{-2} mol H_2 (mol Pt)$^{-1}$ s^{-1}). These results further confirm that the WGS rate is proportional to the exposed Pt surface area for the Na promoted catalysts.

However, it can be seen that for the molar ratio of Na:Pt ~2, the as prepared catalyst exhibited WGS TOR at 250°C (1.8×10^{-2} mol H_2 (mol surface Pt)$^{-1}$ s^{-1}) that is an order of magnitude lower compared to the washed catalyst with similar Na:Pt molar ratio of ~2.5 (2.1×10^{-1} mol H_2 (mol Pt)$^{-1}$ s^{-1}). We reiterate that we do not have any spectroscopic evidence for determining the exact location of Na. Thus, we invoke our Na island formation theory to explain the TOR for the washed catalysts that is similar to the as prepared catalysts with Na:Pt 17 and higher, with significantly lower Na loading. Na was deposited on the Pt/MWCNT using incipient wetness impregnation of

the aqueous solution of $NaNO_3$. With a limited movement for the Na ions in the solution that is added in drop-wise manner to the support, we believe that Na nucleates on the specific sites over the Pt surface in form of islands that grow in size with increase in Na content. As Na loading increases, excess Na may reside on MWCNT and block the Pt surfaces, which are over-promoted and can't get contact with the gas molecules. However, during the washing process, the entire catalyst mass was suspended into 200 ml deionized water. This may remove the excess Na on MWCNT and over-promoted sites. Only the Na that is in close contact with Pt as in the lower loading samples is left. Also, the washing procedure must allow enough freedom for all the Na ions that are now solvated, to move freely along the Pt surface. When the stirring is stopped, the Na ions must have settled down in a highly dispersed manner, probably creating much smaller Na domains over the Pt surface compared to the as prepared catalyst. In short, washing must lead to a more efficient re-distribution of Na over the Pt surface, creating more number of interface sites between Pt and Na support-type sites for a given Na loading. The similarity of WGS apparent kinetic parameters for the washed catalysts and the fully promoted as prepared catalysts supports this argument i.e. active sites of similar chemical nature (as the fully promoted as prepared catalysts), but more in number are created by uncovering over promoted sites. The similar washing experiments were performed by Zhai et a. over $PtNa/SiO_2$ and $PtNa/Al_2O_3$. The authors suggest that the washing only removes the Na associated with the support and the Na associated with Pt remains unaffected. Negative formation energies of the oxide film on Pt, as computed using DFT, also hints at the strong interaction between the Pt and sodium oxide. Perhaps it is strong enough that washing does not cause the Na_2O in

contact with Pt to be lost. This argument was supported by the absence of any change in the WGS rate after the washing procedure. However, we have seen significant (more than 2 times) increase in the WGS rate per total mol Pt for the as prepared PtNa catalysts with lower than maximum rate. This suggests part of that Na associated with Pt (cause for loss in Pt surface area) was removed during the washing procedure performed over PtNa/MWCNT catalysts.

5.4.3 Cause of promotion due to Na

Our group has investigated the effect of Na addition over Pt supported on Al_2O_3 and TiO_2 (rutile and P25) before [9]. Compared to the monometallic Pt, the WGS TOR (rate normalized by H_2 chemisorption) was promoted 100 times for the Al_2O_3 support and 4-6 times for rutile and P25 supports. The addition of Na modified the apparent kinetic parameters for catalysts with all the supports. The apparent activation energies were reported to increase by 15-20 kJ mol^{-1} compared to the unpromoted catalyst. Compared to the unpromoted catalysts, there was an increase in H_2O and H_2 orders and decrease in the CO and CO_2 orders measured around 230°C. The comparisons of the kinetic parameters measured over these supports with the parameters over Pt/MWCNT and PtNa 1:17/MWCNT are shown in Table 5.3. Similar trends in the apparent kinetic parameters were observed for the PtNa/MWCNT catalyst. Moreover, for all the Na-promoted Pt catalysts, the apparent activation energies higher than their Na-free counterparts, The H_2O orders lie between 0.9 and 1, the CO_2 orders are close to -0.2 (more negative compared to the unpromoted catalysts), CO orders between 0 and -0.1 (also, more negative compared to the unpromoted catalysts) and H_2 orders close to -0.2

were observed. This suggests that overall, independent of the underlying support, (Al_2O_3, TiO_2, ZrO_2 or MWCNT), addition of Na leads to the formation of active sites of similar chemical nature over the supported Pt catalysts. Thus, we believe that Na leads to a support-type effect, when it is located in the proximity of the Pt sites.

The increase in the H_2O order suggests that the coverage of the hydroxyl species (generated due to water dissociation) decreases with Na addition. This is consistent with the DFT calculated trend in OH binding energy where we see that OH binds more weakly to the oxide as compared to pure Pt. The more negative CO_2 order compared to the monometallic Pt catalysts could be attributed to formation of carbonates over the Na sites i.e. the increased the sticking probability or possible re-adsorption of CO_2 to the alkaline surface. The more negative CO order for the Na-promoted catalysts suggests that the relative coverage of CO increases with addition of Na. This also suggests that sites with a relatively higher binding affinity are created with addition of Na. This implication drawn from the CO orders is further supported by the ΔXANES data (discussed later). Thus, we suggest that Na not only leads to a support-type effect but also causes electronic modification of the Pt sites (possibly through the donation of electrons), which leads to a stronger binding and consequently, higher relative coverage of CO on the active sites.

DFT calculations for water adsorption on the inverse sodium oxide on Pt shows spontaneous dissociation of water. This hints at the possibility that the promotion effect is brought about by lowering of water dissociation barrier. However, CO adsorption on the oxide films is weaker than that on pure Pt. The DFT calculations were done on model structures to get insights into the real system and don’t necessarily replicate the

actual active sites of the experimental catalysts. However, based on these calculations, we can speculate that while the oxide can lower water dissociation barrier, metallic CO sites are required to adsorb CO. Therefore, the active site would probably have bifunctional attributes from the oxide as well as the Pt. In summary, the promotion in the WGS rate is the trade-off between the number of Pt sites that are modified by Na and the Pt surface sites that remain available as a conduit for CO activation after these Na islands are formed. We envision that hydroxyl species that are formed on the Na support-type sites could diffuse to Pt sites where the CO is activated. This would explain the proportionality of WGS rate per total moles of Pt to the Pt surface area.

Table 5.3 The comparison of WGS kinetic data over supported Pt on different supports and their Na-promoted counterparts

Catalyst	TOR at 250°C/ 10^{-2} s^{-1}	E_a/ $kJmol^{-1}$	H_2O ±0.05	CO_2 ±0.05	CO ±0.05	H_2 ±0.05	Reference
4% Pt/MWNT	0.75	83±1	0.87	-0.1	0.1	-0.4	This work
1.8% Pt/MWNT-17Na	20	95±2	0.87	-0.2	0.0	-0.15	This work
0.82% Pt/Al_2O_3	0.70	65±2	0.7	0.2	0.1	-0.3	Pazmino et al. [9]
0.82% Pt/Al_2O_3-30Na	60	87±2	0.9	-0.2	0.0	-0.2	Pazmino et al. [9]
1% Pt/P25	19	60±2	0.63	0.0	0.2	-0.6	Pazmino et al. [9]
1% Pt/P25-34Na	72	77±3	0.86	-0.2	0.1	-0.4	Pazmino et al.[9]
5.9% Pt/m-ZrO_2[a]	7.2	72±4	0.63	0.0	0.12	-0.45	Xie et al.[18]
2% Pt/t-ZrO_2[b]	34	93±3	0.80	-0.2	-0.15	-0.2	Xie et al. [18]

5.4.4 Working state of Pt: in situ XAS

The XAS experiments performed after the reduction pretreatment and under the WGS reaction conditions at 240°C were used to study the oxidation state and the coordination environment of Pt. From the XANES data obtained after the reduction and also during the WGS, the unpromoted Pt was in a reduced or metallic state under WGS. This was interpreted on the basis of similar edge energy to the metallic Pt foil. For the Na promoted catalysts as well, the Pt was observed to be in metallic state during WGS. This result is in accordance with what was observed by Pazmino et al. over the $PtNa/Al_2O_3$ catalysts. The EXAFS data further corroborates the observation of metallic Pt under WGS conditions. The absence of Pt-O coordination suggests that Pt stayed in the reduced state under WGS. The identical shapes and positions of the peaks for Na-promoted catalyst to the unpromoted Pt suggests that Na addition does not lead to formation of oxidized Pt. These results contradict the claims made by Zugic et al., where oxidized Pt was suggested as the active site for WGS over PtNa/MWCNT. The difference could arise from the different catalysts synthesis procedures used. As mentioned before, Zugic et al. subjected their MWCNT procedure to an oxidation process with HNO_3 to introduce oxygen functionalities, while we used the MWCNT support as delivered. However, the apparent activation energy reported for PtNa/MWCNT by Zugic et al. in presence of products in feed stream (105±10 kJ mol^{-1}) is similar to what we measured (90-105 kJ mol^{-1}), which could suggest similar chemical nature of active sites.

There was no Pt-Na coordination observed in the EXAFS. The absence of this coordination could be because of the lower signal to noise ratio for this scatter as

compared to the Pt-Pt scatter. In other words, the number of Pt-Na bonds must be significantly smaller than the average number of Pt-Pt bonds, for them to be detected using XAS.

The ΔXANES spectra have been used before to study the adsorption component of the local bonding states or the modifications that occurred after adsorption of a certain adsorbates. The adsorption of CO is known to cause a shift towards leading edge in the XANES spectrum for metallic Pt. The intensity of the difference spectrum is proportional to the amount of adsorbate (CO), normalized by the moles of Pt exposed on the surface. Despite the identical shapes of ΔXANES for the Pt/MWCNT and PtNa 1:30/MWCNT catalysts, the intensity for the Na–promoted catalyst is 1.3 times higher. The EXAFS data shows that both these catalysts have similar average Pt particle sizes under WGS (~3 nm). Thus, it is concluded that more CO is adsorbed on the Na-promoted catalyst as compared to the monometallic Pt. This result supports the claim of higher CO coverage made before for the Na-promoted catalysts, based on the lower apparent CO order compared to the monometallic catalyst.

5.5 Conclusions

A series of catalysts with increasing Na:Pt molar ratio, supported on MWCNT was synthesized and tested for the WGS reaction. The addition of Na causes modifications to the apparent kinetic parameters (increase in H_2O order, H_2 order and apparent activation energy, decrease in CO and CO_2 orders) that are similar to the modifications previously reported for Na-promoted Pt/Al_2O_3, Pt/TiO_2 and Pt/ZrO_2 catalysts. The independence of apparent kinetic parameters on the underlying parent support for Pt

suggests that Na leads to a support-type effect of its own and also enhances the binding of CO with Pt, which is confirmed with the *in situ* ΔXANES experiments. The *in situ* XAS data (XANES and EXAFS) showed that Pt remained in the reduced or metallic state under the WGS reaction conditions. The lower dispersion values obtained from H_2 chemisorption experiments compared to the TEM/EXAFS results suggest that Na covers Pt. The decrease in the WGS rate per total mol Pt at 250°C with increase in the Na weight loading is attributed to the loss of surface Pt due to coverage by Na. Thus, we suggest that Na forms islands over the Pt particles and leads to the aforementioned support-type effect. We propose that the washing procedure, without bringing about an appreciable change in the average Pt particle size, re-distributes the Na over the surface of Pt, creating the sites at the interface of Pt and Na support that are higher in number than (and similar in nature to) the as prepared catalysts. This leads to the WGS TOR for the washed catalysts at 250°C that is similar to the fully promoted as prepared catalysts at a significantly lower Na loading.

LIST OF REFERENCES

LIST OF REFERENCES

[1] C. Ratnasamy, J.P. Wagner. *Catalysis Reviews*, 2009, 51, 325–440.

[2] D.S Newsome, D.S, *Cat. Rev. - Sci. Eng.*, 1980, 21, 275-318.

[3] D.C. Grenoble, M.M., Estadt, D. F., Ollis. *J.Catal*, 1981. 67, 90-102.

[4] J. A. Rodriguez, *Catal. Today*, 160, 2011, 3–10.

[5] L. C. Grabow, A. A. Gokhale, S. T. Evans, J. A. Dumesic, M. Mavrikakis. *J. Phys. Chem. C*, 2008, 112, 4608–4617.

[6] W. Wang, S. Wang, X. Ma, J. Gong. *Chem. Soc. Rev.*, 2011, 40, 3703-3727.

[7] M. Haruta, N. Yamada, T. Kobayashi, S. Iijima. *J. Catal.*, 1989, 115, 301–309.

[8] D. Tibiletti, A. Amieiro-Fonseca, R. Burch, Y. Chen, J.M. Fisher, A. Goguet, C. Hardacre, P. Hu, D. Thompsett. *J. Phy. Chem., B*, 2005, 109, 22553–22559.

[9] T. Fujitani, I. Nakamura, T. Akita, M. Okumura, M. Haruta. *Angew. Chem. Int. Ed.* 2009, 48, 9515 –9518

[10] T.V.W. Janssens, B.S. Clausen, B. Hvrolbek, H. Falsig, C.H. Christensen, T. Bligaard, J.K. Norskov. *Top Catal.*, 2007, 44(1–2), 15–26.

[11] Q. Fu, H. Saltsburg. M. Flytzani-Stephanopoulos. *Science*, 2003, 301, 935-938.

[12] M. Valden, X. Lai, D. W. Goodman. *Science*, 281, 1647-1650

[13] W.D. Williams, M. Shekhar, W.S. Lee, V. Kispersky, W.N. Delgass, F.H. Ribeiro, S.M. Kim, E.A. Stach, J.T. Miller, L.F. Allard. *J. Am. Chem. Soc.* 2012, 132, 14018–14020

[14] M. Shekhar, J. Wang, W.S. Lee, W.D. Williams, S.M. Kim, E.A. Stach, J.T. Miller, W.N. Delgass, F.H. Ribeiro. *J. Am. Chem. Soc.*, 2012, 134, 4700–4708.

[15] D.C Meier, X.F. Lai, D.W. Goodman in: Surface Chemistry and Catalysis, A.F. Carley, P.R. Davies, G.J. Hutchings, M.S. Spencer. Kluwer Academic/Plenum, New York, 2002, 147.

[16] D. Andreeva, I. Ivanov, L. Ilieva, J.W. Sobczak, G. Avdeev, T. Tabakova. *Appl.Catal., A*, 2007, 333(2), 153–160.

[17] D. Andreeva, V. Idakiev, T. Tabakova, A. Andreev. *J. Catal.* 1996, 158, 354.

[18] F. Boccuzzi, A. Chiorino, M. Manzoli, D. Andreeva, T. Tabakova, L. Ilieva, V. Iadakiev. *Catal. Today*, 2002, 75, 169.

[19] A. Venugopal, M.S. Scurrell. *Appl. Catal., A* 2004, 258, 241-249.

[20] A. Venugopal, M.S. Scurrell. *Appl. Catal., A* 2003, 245, 137-147.

[21] J. Hua, Q. Zheng, Y. Zheng, K. Wei, X. Lin. *Catal. Lett.* 2005, 102, 99-108

[22] A.A. Herzing, C.J. Kiely, A.F. Carley, P. Landon, G.J. Hutchings. *Science*, 2009, 321, 1331-1335

[23] S. Carrettin, Y. Hao, A.G. Veronica, B.C. Gates, S. Trasobares, J.J. Calvino, A. Corma. *Chem. Eur. J.* 2007, 13, 7771.

[24] V. Aguilar-Guerrero, R.J. Lobo-Lapidus, B.C. Gates, *J. Phy. Chem C*, 2009, 113, 3259-3269.

[25] N. Lopez, T.V.W. Janssens, B.S. Clausen, Y. Xu, M. Mavrikakis, T. Bligaard, J.K. Norskov. *J. Catal.*, 2004, 223, 232-235.

[26] J.A. Rodriguez, *Catal. Today*, 2010, 160, 3–10.

[27] M. Flytzani-Stephanopoulos, B. C. Gates. *Annu. Rev. Chem. Biomol. Eng.*, 2012, 3, 545-574.

[28] M. Yang, S. Li, Y. Wang, J. A. Herron, Y. Xu, L. F. Allard, S. Lee, J. Huang, M. Mavrikakis, M. Flytzani-Stephanopoulos. *Science*, 2014, 346, 1498-1501.

[29] M. Amft, N. V. Skorodumova. *Physical Review B*, 2010, 81, 195443.

[30] C. Chizallet, G. Costentin, M. Che, F. Delbecq, P. Sautet. *J. Am. Chem. Soc.* 2007, 129, 6442 -6452.

[31] Z. Yan, S. Chinta, A. A. Mohamed, J. P. Fackler, Jr., D. W. Goodman. *J. Am. Chem. Soc.* 2005, 127, 1604 -1605.

[32] G. Mpourmpakis, D. G. Vlachos. *J. Phys. Chem. C* 2009, 113, 7329–7335.

[33] C. Milone, M. Trapani, R. Zanella, E. Piperopolulos, S. Galvagno. *Materials Research Bulletin*, 2010, 45, 1925–1933.

[34] V. J. Cybulskis P.E., Andrew D. Smeltz, Y. Zvinevich, R. Gounder, W. Nicholas Delgass, F. H. Ribeiro. *Chemical Engineering Education*, (2016) accepted.

[35] S. Coluccia, L. Marchese, S. Lavagnino, M. Anpoi. *Spectrochimica Acta*, 1987, 43A, 12, 1573-1576.

[36] Z. J. Zhao, Z. L. Li, Y. R. Cui, H. Y. Zhu, W. Schneider, W. N. Delgass, F. H. Ribeiro, J. Greeley, Importance of metal-oxide interfaces in water-gas shift chemistry: a combined DFT, microkinetic, and experimental study on Au/MgO, submitted.

[37] A.A. Phatak, N. Koryabkina, S. Rai, J.L. Ratts, W. Ruettinger, R.J. Farrauto, G.E. Blau, W.N. Delgass, F.H. Ribeiro, *Catal. Today*, 2007, 123, 224-234.

[38] O. Thinon, K. Rachedi, F. Diehl, P. Avenier, Yves Schuurman, *Top Catal*, 2009, 52, 1940-1945.

[39] C.M. Kalamaras, P. Panagiotopoulou, D.I. Kondarides, A.M. Efstathiou, *J. Catal.*, 2009, 264, 117-129.

[40] P. Panagiotopoulou, D.I. Kondarides, *Catal. Today*, 2006, 112, 49-52.

[41] S.S. Kim, H.H. Lee, S.C. Hong, *Appl. Catal. A*, 2012, 423-424, 100-107.

[42] S.C. Ammal, A. Heyden, *J. Catal.*, 2013, 306, 78-90.

[43] S.C. Ammal, A. Heyden, *ACS Catal*. 2014, 4, 3654−3662.

[44] S. Aranifard, S.C. Ammal, A. Heyden, *J. Catal.*, 2014, 309, 314-324.

[45] D. Tibiletti, F.C.Meunier, A. Goguet, D.Reid, R.Burch, M.Boaro, M. Vicario, A. Trovarelli, *J. Catal.*, 2006, 244, 183-191.

[46] Y.P. Zhai, D. Pierre, R. Si, W.L. Deng, P. Ferrin, A.U.Nilekar,G.W. Peng,J.A.Herron,D.C. Bell, H. Saltsburg,M. Mavrikakis, M. Flytzani-Stephanopoulos, *Science*, 2010, 329, 1633–1636.

[47] M. Yang,J.L. Liu, S. Lee, B. Zugic,J. Huang, L.F. Allard, M. Flytzani-Stephanopoulos, *J. Am. Chem. Soc*. 2015, 137, 3470−3473.

[48] K.L. Ding, A. Gulec, A. M. Johnson, N. M. Schweitzer, G. D. Stucky, L. D. Marks, P. C. Stair, *Science*, 2015, 350, 189-192.

[49] H. Xie,J.L. Lu, M. Shekhar, J.W. Elam, W. N. Delgass, F.H. Ribeiro, E. Weitz, K.R. Poeppelmeier, *ACS Catal.* 2013, 3, 61−73.

[50] J.M. Pigos, C.J.Brooks, G. Jacobs, B.H. Davis, *Appl. Catal. A*, 2007, 328, 14-26.

[51] H.N. Evin, G. Jacobs, J. Ruiz-Martinez, G.A. Thomas, B.H. Davis, *Catal. Lett*, 2008, 120, 166–178.

[52] P. Panagiotopoulou, D.I. Kondarides, *J. Catal.*, 2008, 260, 141-149.

[53] P. Panagiotopoulou, D.I. Kondarides, *J. Catal.*, 2009, 267, 57-66.

[54] X. Zhu, M. Shen, L.L. Lobban, R.G. Mallinson, *J. Catal.*. 2011, 278, 123–132.

[55] J.H. Pazmiño, M. Shekhar, W.D. Williams, M.C. Akatay, J.T. Miller, W.N. Delgass, F.H. Ribeiro, *J. Catal.*, 2012, 286, 279-286.

[56] V.J. Cybulskis, J. Wang, J.H. Pazmiño, F.H. Ribeiro, W.N. Delgass, *J. Catal.*, 2016, 339, 163-172.

[57] K.G. Azzam, I.V. Babich, K. Seshan, L. Lefferts, *J. Catal.*. 2007, 251, 153–162.

[58] K.G. Azzam, I.V. Babich, K. Seshan, L. Lefferts, *Appl. Catal., B,* 2008, 80, 129–140.

[59] W.D. Williams, L. Bollmann, J.T. Miller, W.N. Delgass, F.H. Ribeiro, *Appl. Catal., B* 2012, 125, 206–214.

[60] H.N. Evin, G. Jacobs, J. Ruiz-Martinez, U.M. Graham, A. Dozier, G. Thomas, et al., *Catal. Lett.* 2008, 122, 9–19.

[61] J.H. Pazmiño, M. Shekhar, W. Damion Williams, M. Cem Akatay, J.T. Miller, W. Nicholas Delgass, et al., *J. Catal.*. 2012, 286, 279–286.

[62] B. Zugic, D.C. Bell, M. Flytzani-Stephanopoulos, *Appl. Catal., B,* 2014, 144, 243–251.

[63] B. Zugic, S. Zhang, D.C. Bell, F. Tao, M. Flytzani-Stephanopoulos, *J. Am. Chem. Soc.* 2014, 136, 3238–3245.

[64] G. Kresse, J. Furthmüller, *Phys. Rev. B* 1996, 54, 11169–11186.

[65] G, Kresse, D. Joubert, *Phys. Rev. B* 1999, 59, 1758–1775.

[66] H. Xie, J. Lu, M. Shekhar, J.W. Elam, W.N. Delgass, F.H. Ribeiro, et al., *ACS Catal*. 2013, 3, 61–73.

[67] Reuter, K. and Scheffler, M. PRB, 2001, 65, 035406

[68] J. T. Miller, A. J. Kropf, Y. Zha, J. R. Regalbuto, L. Delannoy, C. Louis, E. Bus, J.A. van Bokhoven, *J. Catal.* 2006, 240, 222-234.

APPENDICES

Appendix A Appendix for Chapter 2

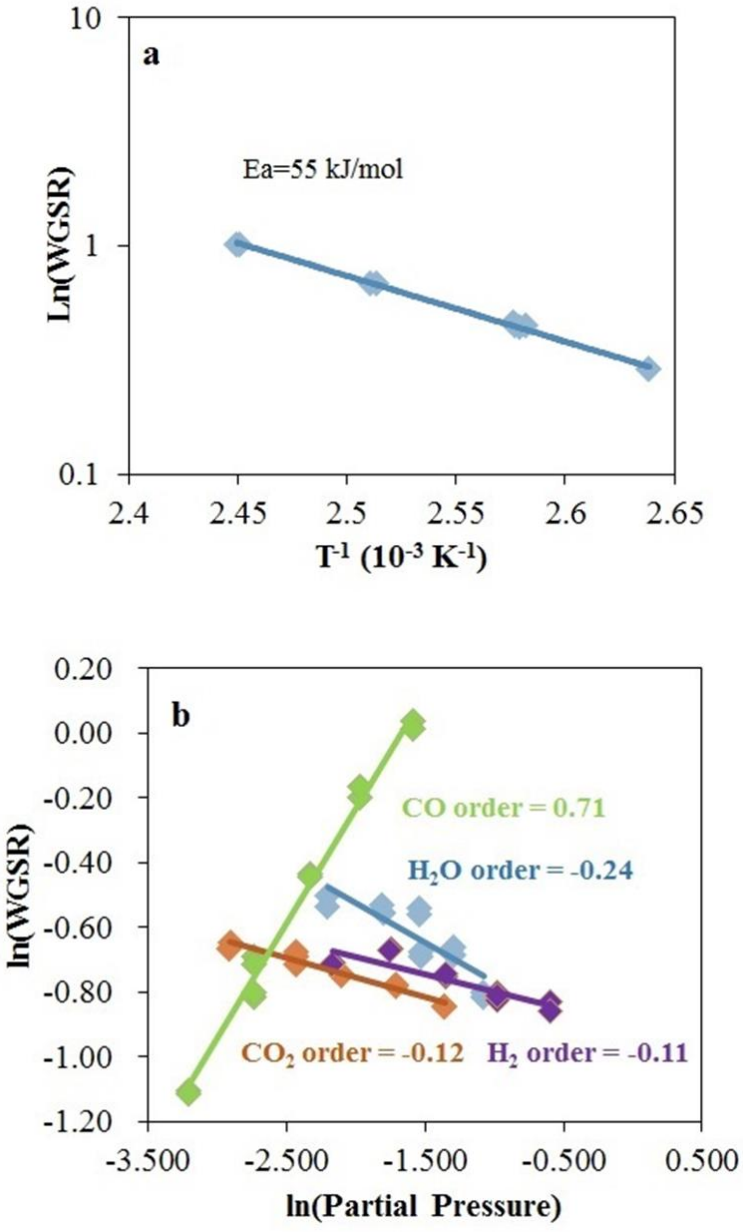

Figure A2.1 a) Typical Arrhenius plot to determine the apparent activation energy b) Typical plots to determine the apparent reaction orders.

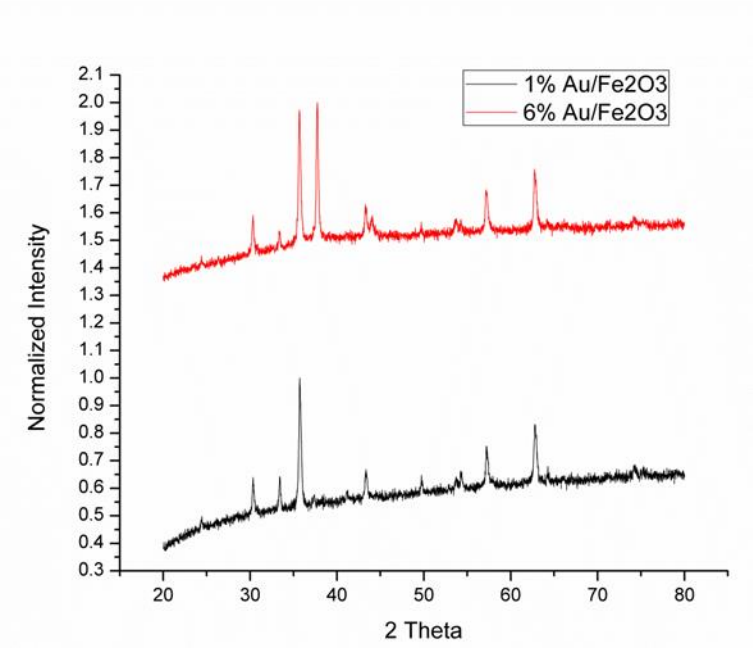

Figure A2.2 XRD of 1.0% and 6.2% Au/Fe_2O_3 samples.

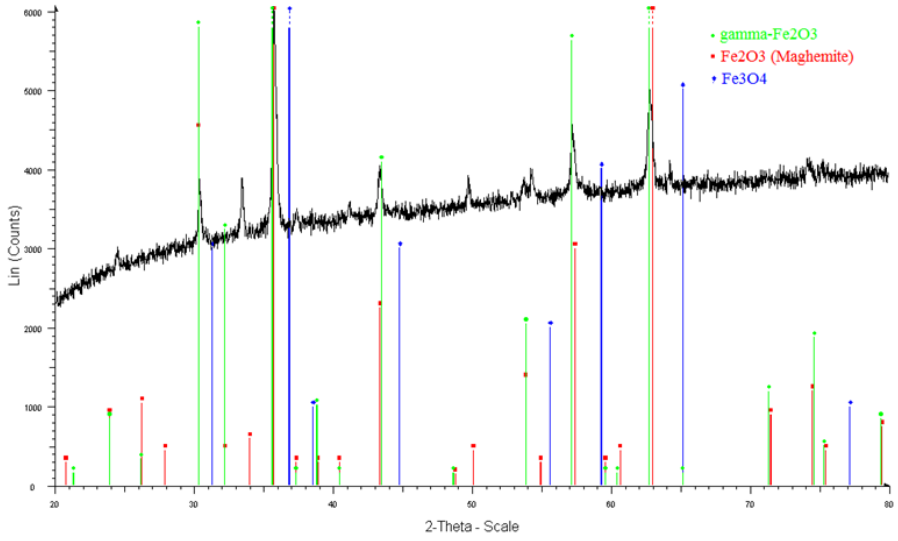

Figure A2.3 XRD peak assignment for the 1.0% Au/Fe_2O_3

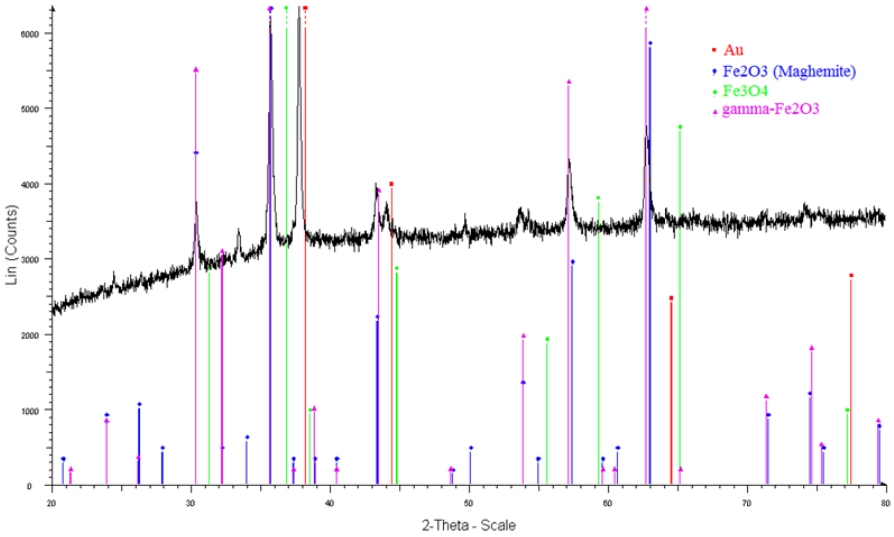

Figure A2.4 XRD peak assignment for the 6.2% Au/Fe_2O_3

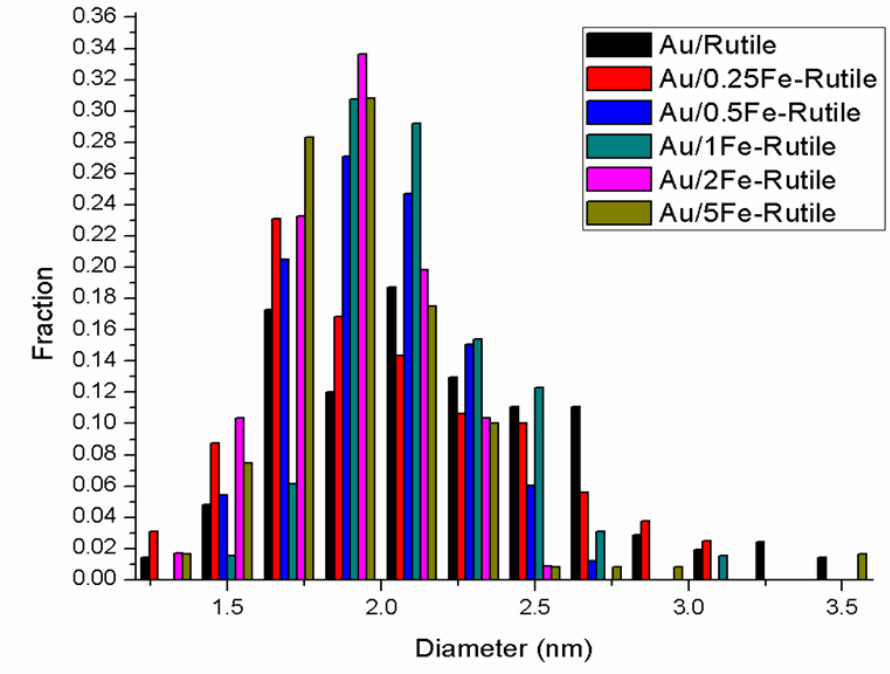

Figure A2.5 Au particle size distributions of Au/Fe-rutile samples

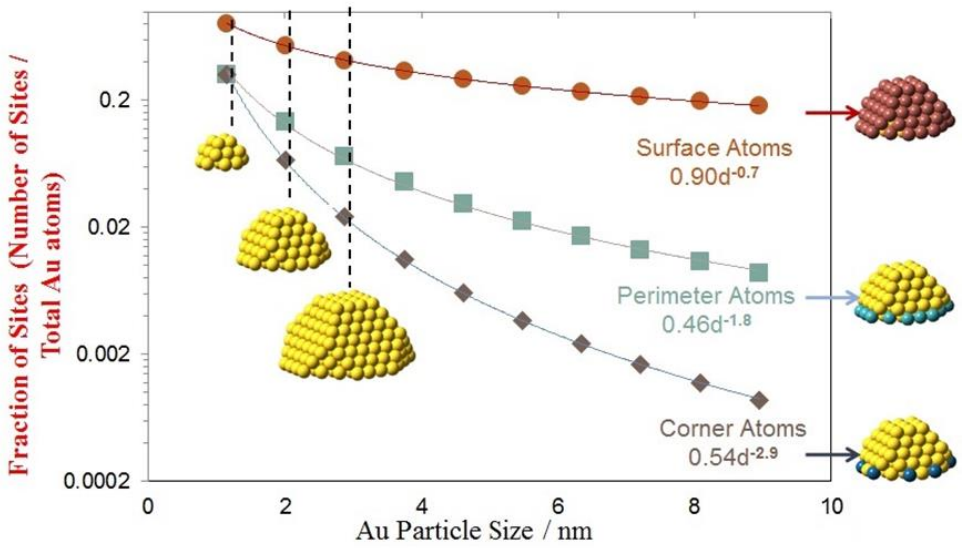

Figure A2.6 Cubo-octohedral model of the Au particles [13, 14]

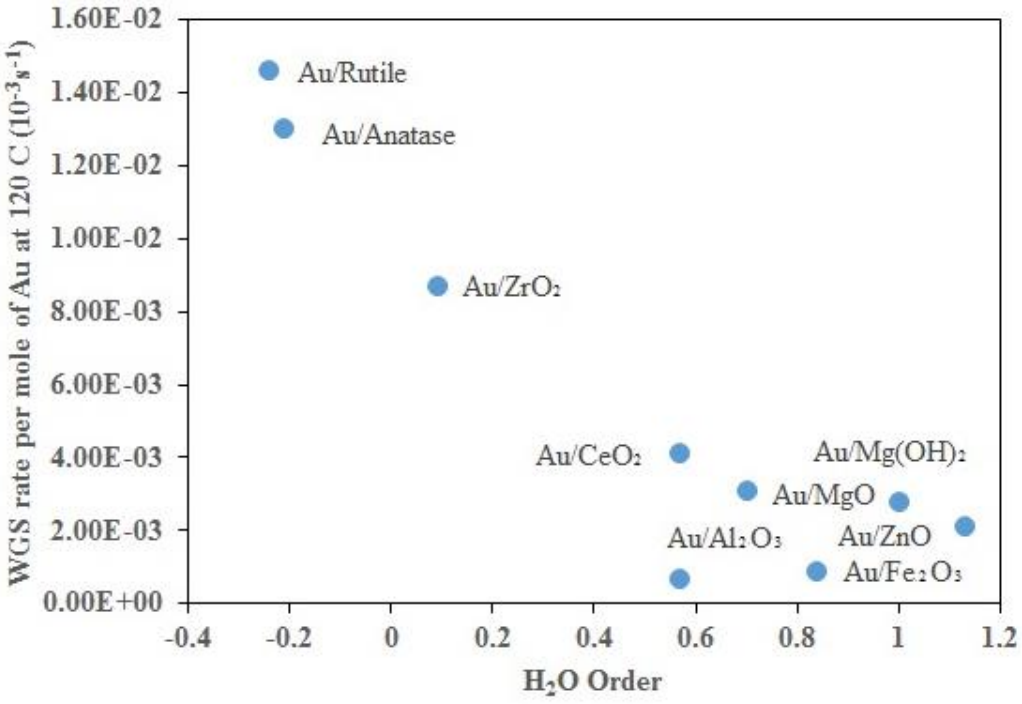

Figure A2.7 Comparison of WGS rates and apparent order with respect to H_2O between different supported Au catalysts

Appendix B Appendix for Chapter 3

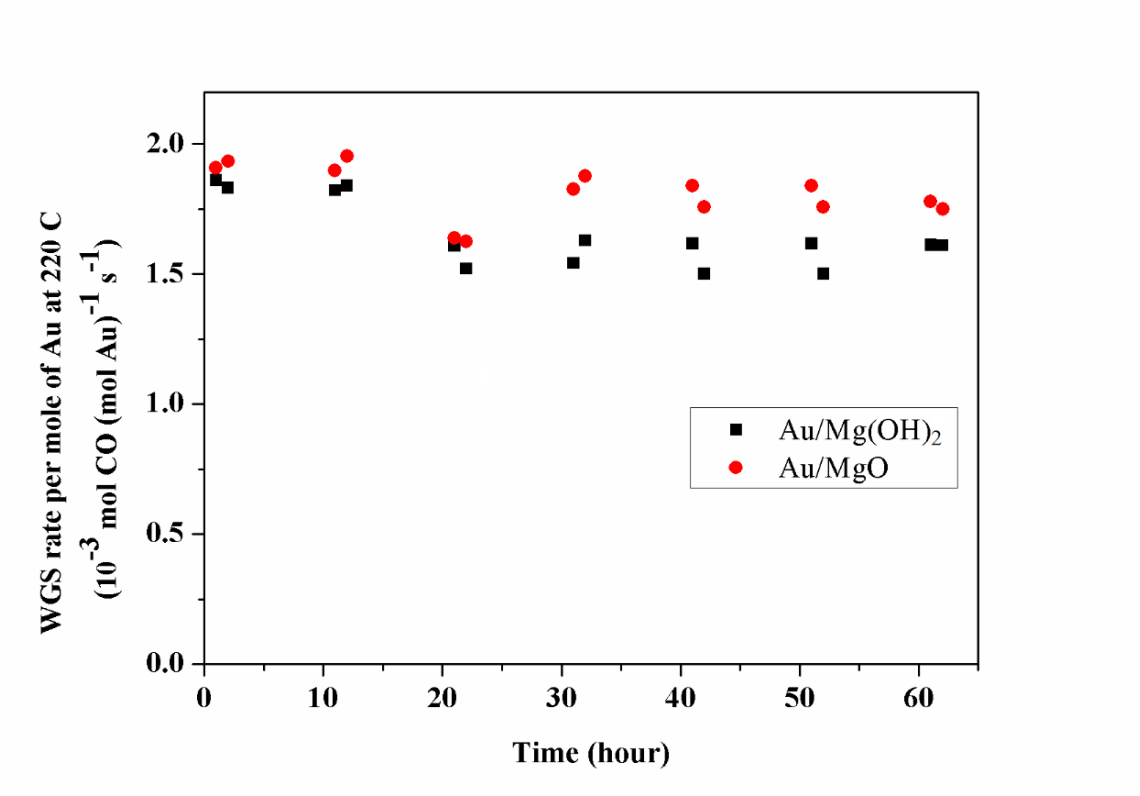

Figure A3.1 Deactivation plot during the WGS kinetics measurement

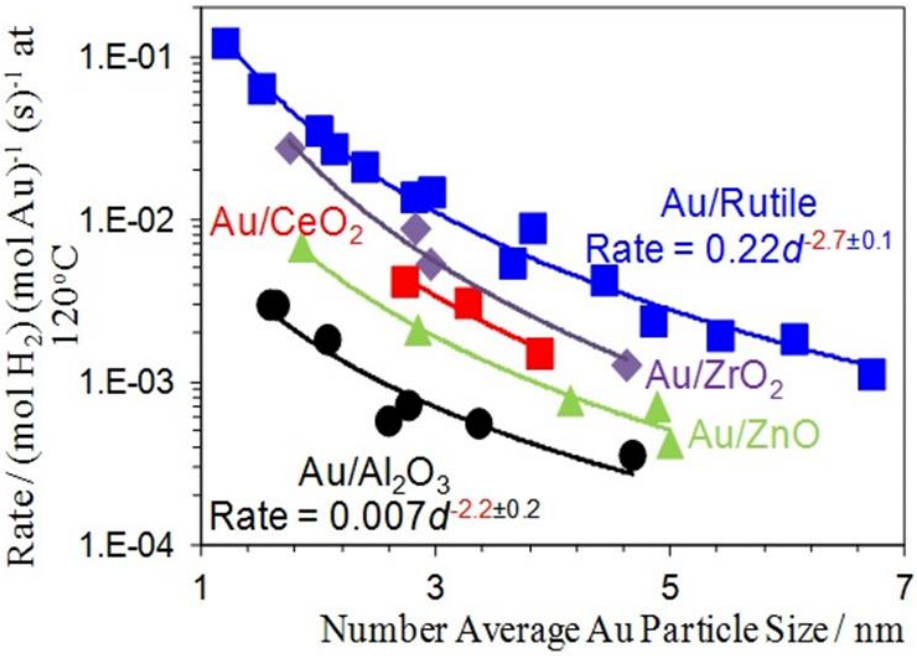

Figure A3.2 WGS rates dependence on the average Au particle sizes for different supports [13, 14]

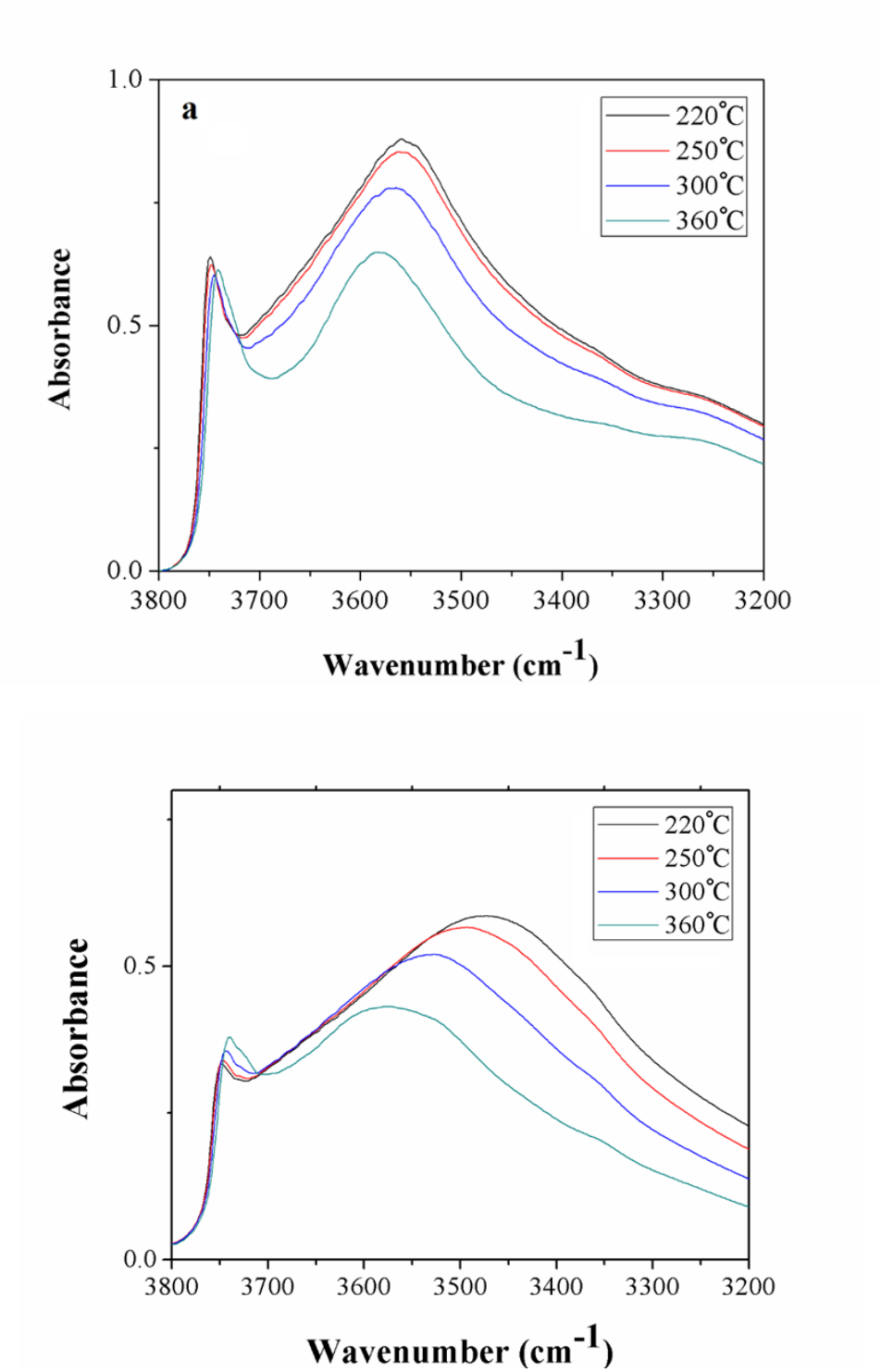

Figure A3.3 N_2 TPD after exposure to 11% H_2O/N_2 a) Au/MgO b) MgO Support

Table A3.1 Calculated binding energies (eV) of CO, H_2O, H, OH and COOHon the Au/MgO(001) interface, clean Au(111), and clean MgO(100).The reference states are CO(g), H_2O(g), 1/2H_2(g), H2O(g) – 1/2 H_2(g), and CO(g) + H2O(g) – 1/2 H_2(g), respectively.

	Au / MgO			Au(111)		MgO(100)	
	Site	PW91	HSE06	site	PW91	site	PW91
CO	Au-top	-0.64	-0.55	bridge	-0.40	Mg-top	-0.14
	Au-bridge	-0.70	-0.36				
H_2O	O-top	-0.44	-0.41	top	-0.10	Mg-top	-0.42
OH	Au-Au-Mg	-0.20	-0.13	top	1.24	hollow	1.83
	Au-Mg-Mg	0.21	0.32				
COOH	Au-Mg(O)	-0.87	-0.71	top	-0.15	O-top	0.58
	Au-Mg(OH)	-0.61	-0.45				
H	Au-bridge	-0.21	-0.18	fcc	0.02	O-top	1.87
	O-top	0.29	0.29				

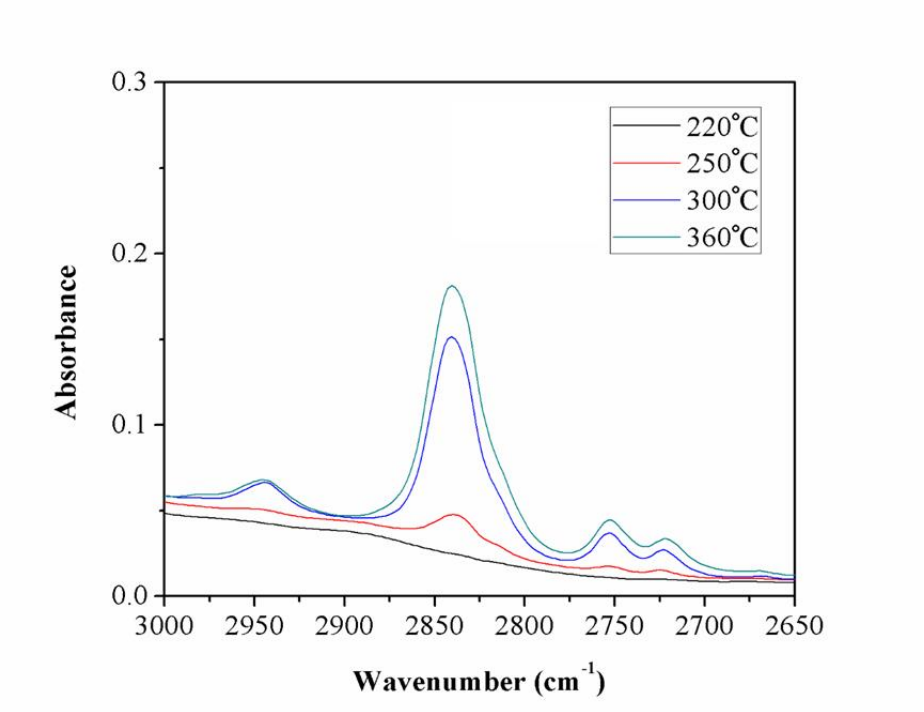

Figure A3.4 C-H stretching region for formate peaks during the CO-TPR on Au/MgO

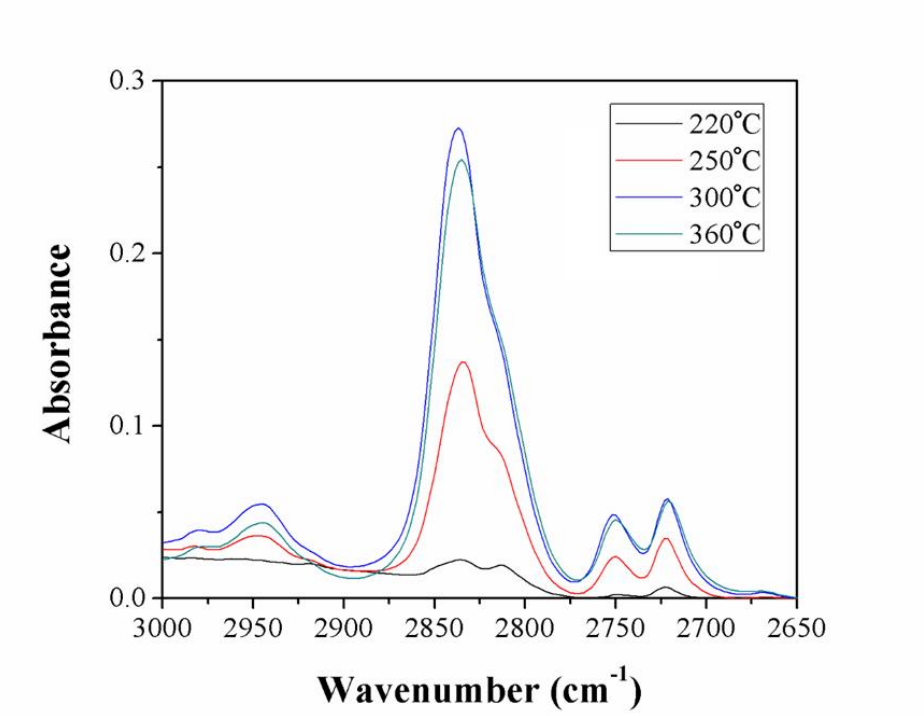

Figure A3.5 CH stretching region for sormate peaks during the CO-TPR on MgO

Appendix C Appendix for Chapter 4

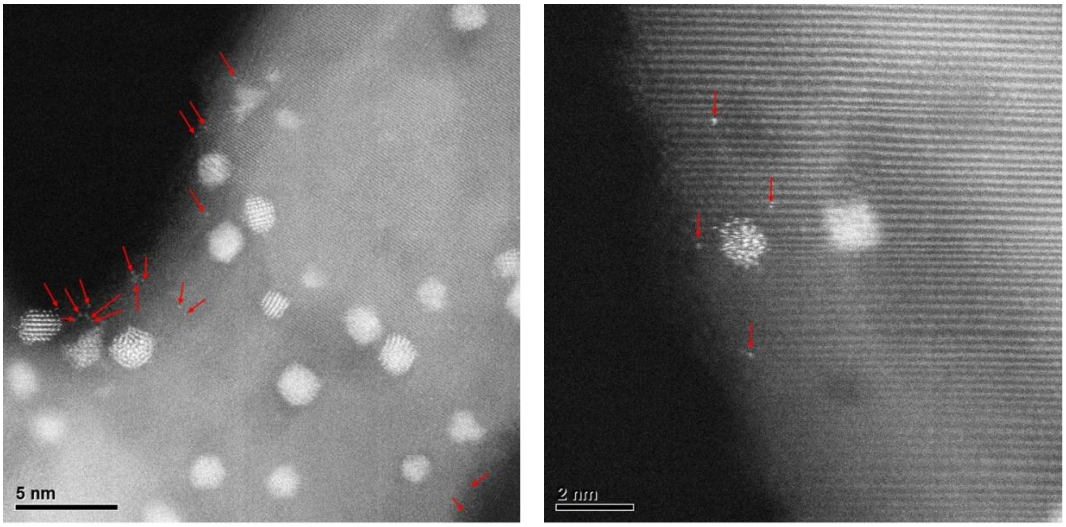

Figure A4.1 STEM images of PtNa(1:10)/TiO_2 IWI, single Pt atoms are shown by the red arrows.

Appendix D Appendix for Chapter 5

Table A5.1 In situ Pt LIII edge EXAFS data over as prepared and washed PtNa/MWCNT catalysts. The WGS conditions under which the scans were taken were 7% CO, 7% H_2O, 8.5% CO_2, 37% H_2 and balance Ar at 240°C

Catalyst	Treatment	Scatter	N	R/Å	$\Delta\sigma^2$ ($x10^3$)	Eo/eV	Particle Size/nm
4% Pt/MWCNT	Air RT	Pt-O	2.1	2.06	1.0	1.4	
		Pt-Pt	3.9	2.71	1.0	-5.3	
	He 240°C	Pt-Pt	8.1	2.71	4.0	-2.5	
	WGS 240°C	Pt-Pt	7.9	2.72	3.5	-2.3	3.0
	He 240°C	Pt-Pt	8.5	2.75	3.5	-1.4	3.5
4% PtNa 1:10/MWCNT	H_2 300°C	Pt-Pt	10.0	2.74	4.0	-3.4	5.5
	WGS 240°C	Pt-Pt	9.5	2.75	3.5	-3.5	5.0
1.7% PtNa 1:2.5/MWCNT (after washing the 1:17 catalyst)	Air RT	Pt-O	1.9	2.06	1.0	3.4	
		Pt-Pt	5.1	2.73	1.0	-2.6	
	H_2 300°C	Pt-Pt	7.6	2.72	4.0	-2.9	
	He 240°C	Pt-Pt	7.6	2.71	3.5	-2.2	3.0
	WGS 240°C	Pt-Pt	8.4	2.74	3.5	-1.7	3.5
1.7% PtNa 1:17/MWCNT	H_2 300°C	Pt-Pt	9.1	2.71	4.0	-2.3	4.0
	WGS 240°C	Pt-Pt	8.2	2.74	3.5	-2.9	3.5
1.9% PtNa 1:2.5/MWCNT (after washing the 1:30 catalyst)	Air RT	Pt-O	2.0	2.05	1.0	1.0	
		Pt-Pt	4.6	2.71	1.0	-5.1	
	H_2 300°C	Pt-Pt	7.6	2.72	4.0	-2.6	
	He 240°C	Pt-Pt	7.5	2.71	3.5	-2.5	2.5
	WGS 240°C	Pt-Pt	7.9	2.74	3.5	-1.7	3.0
1.9% PtNa 1:30/MWCNT	H_2 300°C	Pt-Pt	9.2	2.72	4.0	-4.2	4.0

	WGS 240°C	Pt-Pt	8.5	2.73	3.5	-4.0	3.5
1.7% PtNa 1:4/MWCNT (after washing the 1:45 catalyst)	Air RT	Pt-O	1.6	2.04	1.0	-3.3	
		Pt-Pt	5.5	2.72	1.0	-0.5	
	H_2 300°C	Pt-Pt	7.9	2.71	4.0	-2.5	3.0
	He 240°C	Pt-Pt	8.6	2.70	3.5	-2.8	3.5
	WGS 240°C	Pt-Pt	8.9	2.72	3.5	-1.7	4.0
1.7% PtNa 1:45/MWCNT	H_2 300°C	Pt-Pt	10.0	2.72	4.0	-2.0	5.5
	WGS 240°C	Pt-Pt	9.4	2.73	3.5	-2.4	4.5

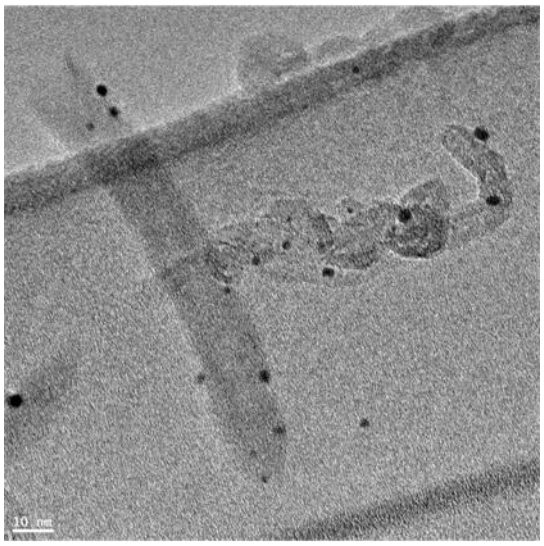

Figure A5.1 Representative TEM images for the as prepared PtNa/MCNT catalysts with Na:Pt 17

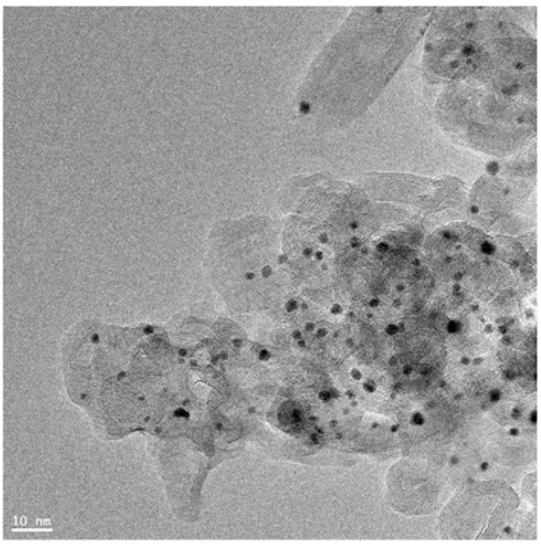

Figure A5.2 Representative TEM images for the as prepared PtNa/MCNT catalysts with Na:Pt 30

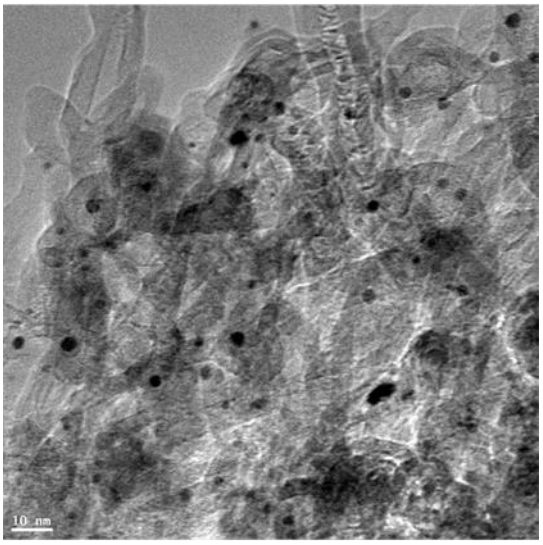

Figure A5.3 Representative TEM images for the as prepared PtNa/MCNT catalysts with Na:Pt 45

VITA

VITA

Education

Bachelor of Science, 2010
Beijing University of Aeronautics and Astronautics, Beijing, China
Doctor of Philosophy, 2016
Purdue University, West Lafayette, Indiana, USA

Experience

Research Assistant, Advisor: Prof. W. Nicholas Delgass and Prof. Fabio H. Ribeiro
School of Chemical Engineering, Purdue University 2011-present
Project: Oxide supported Au for water-gas shift reaction

- Prepared and supported Au catalysts on various oxide supports.
- Determined the water-gas shift reaction kinetics of various catalysts with a high-through put reactor system.
- Promote the catalytic activity of Au/rutile to 4 times of commercial Cu-ZnO-Al_2O_3 catalysts with Fe. Identify the modification of active sites by Fe.
- Identify the participation of hydroxyl groups in the WGS rate determining step over Au/MgO.
- Study the dopant effects on supported Au catalysts.

Project: Alkali promotion on Pt catalysts for water-gas shift reaction

- Promote the WGS rates by more than 20 times over supported Pt catalysts with alkali addition.
- Identify the active sites of alkali promoted Pt catalysts by characterization methods including X-ray Absorption and STEM.

Project: Pt bimetallic catalysts for water-gas shift reaction

- Promote Pt catalyst activity to a factor of 10 by Co addition. Identify the Pt-CoOx interface as the active sites by selective leaching.
- Study the effects of different treatment on the activity of Pt3Re bimetallic catalysts.

Project: Noble metal on tungsten carbide for water-gas shift reaction

- Prepared noble metal supported on tungsten carbide catalysts by incipient wetness impregnation method.
- Observed promotion of noble metal on tungsten carbide activity towards water-gas shift reaction.

Research Assistant, Advisor: Prof. Yadong Li
State Key Lab of New Ceramics and Fine Processing, Tsinghua University, China, 2010-2011
Project: Bimetallic Noble Metal Nanoparticle Synthesis and Their Catalytic Application

- Synthesized bimetallic alloy nanocrystals in oleylamine and used surfactants to adjust the final sizes and morphologies. Developed a method to synthesize PdSn hollow nanocrystals which showed better performance towards CO oxidation.

Awards and Honors

- KOKES Award for the 24th North American Catalysis Society (NACS) meeting 2015
- Eastman Travel Grant 2015
- Beijing Outstanding Bachelor Graduate (Selected from all the universities in Beijing) 2010
- Beihang University Gold Medal (10 out of all graduating bachelors in Beihang University) 2010
- First Prize, Scholarship for Outstanding Academics (three times, 2%) 2009,2008,2007
- Scholarship supported by Guanghua Committee (two times, 10/3000) 2009,2007
- First Prize, Schlumberger Scholarship in School of Advanced Engineering (5%) 2008

Conference Presentations

- Y. Cui, K. D. Sabnis, F. G. Sollberger, C. Wang, J. T. Miller, W. N. Delgass, F. H. Ribeiro, 24th North American Catalysis Society Meeting,Water-Gas Shift Catalysis over PtCo Bimetallic Catalysts, Pittsburgh, PA, Jun 2015
- Y. Cui, Z.L. Li, K. D. Sabnis, V. J. Cybulskis, Z. J. Zhao, C. W. Han, V. Ortalan, J. Greeley, W. N. Delgass, F. H. Ribeiro, 2015 AIChE Annual Meeting, Au/MgO Catalysts for the Water Gas Shift Reaction, Salt-Lake City, Nov. 2015
- Y. Cui, K. D. Sabnis, V. J. Cybulskis, Z.L. Li, M. C. Akatay, W. N. Delgass, F. H. Ribeiro, 2014 AIChE Annual Meeting, Fe Promoted Au/Rutile for the Water-Gas Shift Reaction, Atlanta, GA, Nov 2014